2008

The viability of a thermoelectric fuel conditioning system for a diesel engine utilizing biodiesel

Timothy Schriefer

The Viability of a Thermoelectric Fuel Conditioning System for a Diesel Engine Utilizing Biodiesel

By

Timothy Schriefer

A thesis submitted in partial fulfillment of the Requirement for Master of Science in Mechanical Engineering

Approved by:

Department of Mechanical Engineering Committee

Dr. Margaret Bailey – Thesis Advisor _____

Dr. Robert Stevens _____

Dr. Agamemnon Crassidis _____

Dr. Edward Hensel- Dept Representative _____

Rochester Institute of Technology

Rochester, NY 14623

June 2008

I. Permission of Duplication

Permission Granted

The Viability of a Thermoelectric Fuel Conditioning System for a Diesel Engine Utilizing Biodiesel

I, *Timothy J. Schriefer Jr.*, hereby grant permission to the Wallace Library of the Rochester Institute of Technology to reproduce my thesis in whole or in part. Any reproduction will be for personal, research, or educational purposes and will not be for commercial use or profit.

Date: _____ Signature: _____

II. Acknowledgements

I would first like to acknowledge the Rochester Institute of Technology for providing the environment to develop mentally and academically to the point where this undertaking was possible. I would also specifically like to thank Dr. Steve Weinstein for his help with the development of the mathematical model, and Dr. Agamemnon Crassidis for his help with the control laws. Sean Ashman also deserves thanks for his help proofreading the entirety of this thesis.

I must also sincerely thank Dr. Margaret Bailey for her help and guidance throughout the entirety of this project and for the funding to pursue this research. Dr. Bailey also deserves my heartfelt thanks for the guidance she provided on various scholastic issues outside of the scope of this thesis.

Finally, I would like to thank my family for the support they provided both financially and mentally to me throughout the entirety of my education. I would have no hope of being where I am today without their assistance and guidance.

III. Abstract:

Certain internal combustion engines, which run on hydrocarbon fuels, experience difficulty upon engine start-up in extreme cold weather. As ambient temperature decreases below the fuel cloud point and beyond, paraffin form in the fuel and eventually clog the fuel filter causing the engine to fail to start. This problem becomes more pronounced when the engine in question is a Diesel and the fuel utilized is biodiesel. As an alternative fuel source, biodiesel has many advantages; however, its cold weather performance is worse than even conventional diesel fuel. As biodiesel becomes more integrated into the world's energy usage scenario, one of the systems within a Diesel engine that requires further investigation is its fuel conditioning system.

This thesis describes research aimed at the development of a fuel conditioning system that utilizes several emerging technologies while decreasing the amount of electrical energy required for operation. The system utilizes a eutectic - thermoelectric (E-TE) combination which consists of a eutectic compound based latent heat storage device with adjacent thermoelectric elements to transfer waste heat stored in the eutectic reservoir into the fuel filter, thus diminishing the amount of electrical energy typically required for the fuel conditioning process. Simulations of the E-TE system are conducted while operating within three different modes (start-up, heat storage, and electrical energy generation) depending on fuel and ambient temperature conditions, while a supervisory controller distinguishes between desired operational status.

The research activities and findings reported contained herein include development of E-TE system models which each consist of several components. The first of which is a set of control laws, implemented in Simulink®, which control system performance using various temperature related variables. The second component is a supervisory control law, implemented in Matlab®, which controls the switching between various modes of operation. With system model developed, the viability of the system is examined.

IV. Table of Contents:

V. List of Figures:

VI. List of Tables:

VII. Nomenclature

A	Filter surface area [m^2]
$A_n, B_n, C_n,$	Mathematical Variables
$C1n, C2n, G$	
C	*Specific heat generic [J/(kgK)]*
C_f	Specific heat of the fuel [J/(kgK)]
C_{te}	Effective specific heat of the thermoelectric elements [J/(kgK)]
E_0	Energy of the fuel slug [J]
E_{te}	Energy of the thermoelectric model [J]
g	Gravity [m/s^2]
H	Height of the fuel filter [m]
h	"Convection" coefficient [$W/(Km^2)$]
h_0	Convection coefficient of the fuel [W/(Km)]
h_{0i}	Enthalpy of incoming flow for the fuel slug model [J/kg]
h_{0e}	Enthalpy of outgoing flow for the fuel slug model [J/kg]
h_{tei}	Enthalpy of incoming flow for the thermoelectric model [J/kg]
h_{tee}	Enthalpy of outgoing flow for the thermoelectric model [J/kg]
I	Current [amps]
J_0	Bessel function of the first kind 0 order
k_f	Thermal conductivity of the fuel [W/(mK)]
k_{te}	Thermal conductivity of the thermoelectric elements [W/(mK)]
k_{teeff}	Effective Thermal Conductivity of the thermoelectric elements [W/(mK)]
m_o	Mass of fuel in the fuel slug [kg]

m_{te}	Effective mass of the thermoelectric elements [kg]
$\dot{m}$	Mass flow rate for the fuel [kg/s]
$\dot{m}_i$	Mass flow rate for the incoming fuel [kg/s]
$\dot{m}_o$	Mass flow rate for the outgoing fuel [kg/s]
Q_{TE}	*Alpha model incoming* Heat [W/m^2]
Q_{ND}	Non dimensional Heat term
Q_c	Heat transferred to cold side of the thermoelectric elements [W]
Q_h	Heat transferred to hot side of the thermoelectric elements [W]
Q_k	Heat conducted through the thermoelectric elements [W]
$\dot{Q}_0$	Heat power added in fuel slug model [W]
$\dot{Q}_{te}$	Heat power added in thermoelectric model [W]
R	Filter Outer Radius (***alpha*** model) [m]
r	Radius [m]
r_1	Radius from the center of the inside of the fuel filter to the filter wall [m]
r_2	Radius from the center of the fuel filter to the outside of the filter wall [m]
R_{te}	Total electrical resistance of the thermoelectric elements [ohms]
S	Seebeck coefficient [V/K]
S_{eff}	Effective Seebeck coefficient for all elements [V/K]
T	Temperature [°C]
T_0	Temperature of the fuel slug [°C]
T_{0i}	Initial temperature of the fuel slug [°C]
T_1	Temperature at the inner filter wall [°C]
T_2	Temperature at the outer filter wall [°C]

T_i	Initial Fuel Temperature [°C]
T_E	Temperature of the Eutectic Reservoir [°C]
T_M	Melting Temperature of the Fuel [°C]
T_g	Goal Temperature [°C]
t	Time [s]
U_0	Internal energy of the fuel slug [J]
U_{te}	Internal energy of the thermoelectric elements [J]
V	Volume generic [m^3]
V_{0i}	Velocity of incoming flow [m/s]
V_{0e}	Velocity of outgoing flow [m/s]
V_{tei}	Velocity of incoming flow [m/s]
V_{tee}	Velocity of outgoing flow [m/s]
$\dot{W}_0$	Work removed in fuel slug model [W]
$\dot{W}_{te}$	Work removed in thermoelectric model [W]
Y_0	Bessel Function of the Second Kind 0 Order
Z_C	Thermoelectric figure of merit
z_{0i}	Height of incoming flow for fuel slug model [m]
z_{0e}	Height of outgoing flow for fuel slug model [m]
z_{tei}	Height of incoming flow for fuel slug model [m]
z_{tee}	Height of outgoing flow for fuel slug model [m]
α	Thermal Diffusivity [m^2/s]
δ_n	Eigenvalues
γ	Non-dimensionalization Constant
$_c$	Carnot efficiency

γ	Material efficiency
	Efficiency
σ	Electrical conductivity [S/m]
π	Mathematical Constant pi
π_p	Peltier Coefficient [W/amps]
	Density generic [kg/m^3]
τ	Non dimensional Time Constant

Note: A bar above the symbol indicates a non-dimensionalized version of the above symbols

1. Introduction:

This section provides an overview into the driving force behind this research as well as an overview of some of the critical technology that is pertinent to the research. It concludes with a review of some of the current research being undertaken in key technologies such as thermoelectrics, biodiesel, and eutectic compounds. The introduction section of this document contains the motivation, statement of work, background information on pertinent technologies, and a literature review of current applicable research.

1.1. Motivation

The pursuit of a thermoelectric based fuel conditioning system for an engine has several beneficial aspects. The system should be able to reduce the operating cost of the vehicle by reducing electrical power and fuel consumption required to run the vehicle.

First, if viable, the use of a thermoelectric and latent heat storage system may allow for a vehicle used in a cold weather environment to forgo the external power supply. The ability to no longer be tethered to an external power supply not only reduces the operating cost of the vehicle but also is more convenient for the vehicle operator. Furthermore, the ability to restart without an external power supply will yield fuel savings for the vehicle since it will not need to remain running when there is not a power supply available.

Also, as the power consumption usage of a vehicle continues to increase due to the increased usage of electronic, computers, and amenities, far more of a vehicle's fuel consumption is due to the alternator. The thermoelectric fuel conditioning system can

alleviate this problem in two separate ways. First, since power is no longer being drawn from the battery to power resistance heaters, the vehicle's electrical power consumption is less severe. Second, the thermoelectric elements while mainly focused on providing an efficient means of heat transfer within the conditioning system can also be used to generate power from the excess heat the car produces once the latent heat storage device is charged.

This dual purpose approach to the use of thermoelectrics is beneficial for several reasons. The most important reason to utilize thermoelectrics in a dual purpose role is to improve the economic viability of the system. While thermoelectric efficiency has increased, a thermoelectric device still typically exhibits too low of an efficiency to be economically viable on its own. However, when power generation is an additional use for the fuel conditioning system, its cost impact beyond the fuel conditioning system itself should be lessened.

When the benefits of a thermoelectric fuel conditioning device are coupled with the increased focus on clean energy and non-reliance on foreign energy sources, the thermoelectric solution begins to look more beneficial. Since one of the most viable alternative energy solutions is the use of fuel that is produced through the transesterification of a fatty acid, commonly referred to as biodiesel, the need for fuel conditioning is much more widespread. While it is commonplace in the coldest environments for a fuel conditioning systems use even with gasoline as a fuel, the region requiring some sort of conditioning is larger for diesel fuel, and both of these areas are significantly smaller than the region that will require fuel conditioning if biodiesel use is to be more widespread.

Thus the development of a thermoelectric fuel conditioning system is economically and environmentally beneficial.

1.2. Statement of Work

The purpose of the thesis is to test the viability of the E-TE fuel conditioning system. This will be accomplished through the creation of a mathematical model which will allow for the power consumption characteristics of the system to be studied.

This thesis involves several steps in the design of a thermoelectrically driven latent heat storage device used in the fuel conditioning subsystem in a diesel engine running on biodiesel. Currently, resistive heating elements and engine block heaters are necessary for an internal combustion engine to be used in cold northern weather in North America. This problem is more severe for diesel engines, especially those running on biodiesel. Therefore, the system will be designed in the context of a Diesel engine utilizing biodiesel as a fuel.

The research consists of many activities, the first of which is a comprehensive literature review on three main topics of interest. The first and largest portion of the literature review focuses on thermoelectrics for both generation and heat transfer purposes. The next portion spotlights on latent heat storage devices, specifically eutectic compounds. Then, various control schemes are examined for potential use as the control system for the thermoelectric elements. In addition, a literature review is undertaken to determine the best finite elements to be utilized for the modeling of the system. The final and least comprehensive portion of the literature review involves biodiesel and its cold weather properties.

The next two portions of the thesis will develop concurrently and will consist of modeling a thermoelectric heat transfer and electrical generation system and its corresponding control system. Models will be constructed utilizing Simulink® and Matlab®.

The final step in the thesis process is the writing of the thesis paper itself which will contain the literature review, system design, information on the modeling processes, and the design of the experimental setup. Then the thesis discusses the development of the model and control laws. The thesis also discusses the overall results of the project and the path for finishing the work in the future should the system merit further work.

1.3. Background

This section provides an overview of the technology that is under examination in this thesis. It begins with an overview of thermoelectrics. Alternative fuels are then discussed, followed by a discussion of eutectic compounds. Finally, control laws are discussed.

1.3.1. Thermoelectrics

Thermoelectric elements are constructed by connecting two dissimilar materials at a junction. For the purposes of using the thermoelectric effects this was initially done with metal alloys and eventually has moved on to include the use of tailored semiconductors [1]. Typically thermoelectric elements are connected electrically in series, but thermally in parallel to form a thermoelectric module [1]. A sample thermoelectric module is shown in Figure 1.

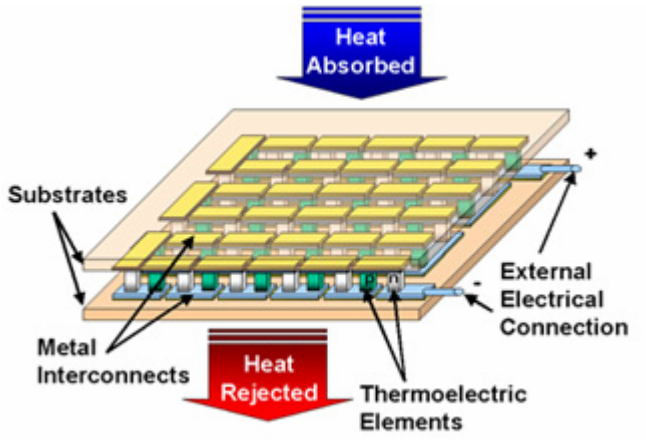

Figure 1: Thermoelectric Module [2]

There are three distinct effects associated with thermoelectrics. The first effect, known as the Seebeck effect, was discovered by Thomas Johann Seebeck in 1821 [3]. If the two sides of the element are maintained at different temperatures, T_1 and T_2, a voltage

will develop between the two proportional to the temperature difference [1]. The proportionality constant is called the Seebeck coefficient, labeled S or α (α in this document), and is typically measured in microvolts per degree Kelvin.

The second thermoelectric effect, known as the Peltier effect, was discovered by Jean Peltier in 1834 [3]. It states that if a current is supplied to the element, a rate of heating Q will occur at one junction and a rate of cooling –Q will occur at the other, meaning that one junction heats and the other cools [1]. The rate is governed by the ratio of current to heat rate and is measured by the Peltier coefficient π (π_p in this document), which is typically measured in watts per ampere [1].

The final thermoelectric effect is the Thomson effect, discovered by William Thomson Lord Kelvin in 1854 [3]. This deals with the rate of generation of reversible heat due to the passage of current along a portion of conductor [1]. The Thomson effect is generally not of primary importance.

In addition to the primary thermoelectric effects there also exist thermomagentic effects called the Nernst and Ettinghausen effects; however they are unimportant to the current research [1].

The first two thermoelectric effects lead to two different applications: thermoelectric electricity generation and thermoelectric cooling or heating. Thermoelectric generation is based on the Seebeck effect. Thermoelectric generators are heat engines and as such are subject to the laws of thermodynamics. The efficiency of a thermoelectric generator, φ, is the ratio of the electrical energy supplied to the load divided by the heat absorbed at the hot junction of the element [1].

Thermoelectric cooling or refrigeration is based upon the Peltier effect. The efficiency of thermoelectric cooling is characterized by the coefficient of performance. The coefficient of performance is the heat absorbed at the cold junction divided by the electrical power input to the system [1].

A third application exists although it is not typically used. If the current supplied to the thermoelectric element is reversed, in regards to the current supplied for thermoelectric cooling, the devices will augment the heat transfer occurring between the cold junction from the hot junction. This application is critical in the scope of this work, as the main phase of operation uses the thermoelectric elements as a heat pump.

Thermoelectric elements are constructed out of a variety of materials. The ideal thermoelectric material will generally have a high electrical conductivity combined with a low thermal conductivity. Current thermoelectric materials can be subdivided into three operating temperature ranges. Bismuth alloys containing antimony, tellurium, and selenium are the low temperature materials and are usable to approximately 450 K [1]. The second group of materials in the intermediate range is usable up to 850 K and consists mainly of lead telluride alloys [1]. The high temperature range materials tend to be silicon germanium alloys and operate up to around 1300 K [1]. In this research the low temperature group is utilized.

New thermoelectric materials are an area of significant research. One current research area involves improving the figure of merit, a measure of the performance of a thermoelectric material, using phonon glass-electronic crystals [1]. The crystals typically, skutterudites and clathrates, have thermal conductivity similar to glass but conduct electricity similar to crystals [2]. Another area of current research involves

improving economical considerations of thermoelectric materials. More economical materials are to be used in applications such as waste heat recovery where watts generated per first cost are more important than generation efficiency [1]. Candidate materials include magnesium tin alloys and ytterbium aluminum alloys [1].

1.3.2. Alternative Fuels

There are various alternative fuels currently being utilized and developed for use in vehicle, power generation, and heating applications. In general, to be considered an alternative fuel the fuel must not be one of the conventional fuels such as petroleum, coal, natural gas, or nuclear materials. Often when speaking of alternative fuels it is implied that the fuel is also renewable and not a non-traditional derivative of the conventional fuels such as shale oil. In this thesis, these distinctions are not recognized.

The main alternative fuels currently in existence are hydrogen, methanol, biomass, and biodiesel [4]. Alternative fuels offer environmental, economic, and national security related benefits. When considering alternative fuels it is important to consider how efficiently the fuel can be obtained. This requires taking into account costs associated with the extraction process and other processes such as transportation and storage. For example, while hydrogen is environmentally friendly it is not an efficient fuel to obtain as significant energy must be put forth to extract it through eletrolysis or the cracking of hydrocarbons. Hydrogen has a net energy gain of less than 100%. Conversely biodiesel is the most efficient net energy gain fuel at 220% [5]. The net energy gain of a fuel is ratio of the energy the fuel contains compared to what is required

to create it. This high net energy gain makes biodiesel an attractive renewable alternative fuel.

Biodiesel is an alternative fuel derived from vegetable oil that produces a fuel chemically similar to diesel fuel, hence the name. Biodiesel is produced through the transesterification of ester chains and as mentioned previously produces a compound chemically similar to diesel fuel and glycerin. Essentially the transesterification process removes the glycerin molecule from the triglyceride molecules that make up vegetable oils [6]. The process is accomplished by replacing the glycerin molecule with an alcohol molecule, using a strong base such as sodium hydroxide or potassium hydroxide as a catalyst [6].

The typical vegetable oils utilized for biodiesel production include soybean oil, rapeseed oil (canola), palm oil, and coconut oil [6]. Additionally the National Renewable Energy Laboratory has found several species of algae that consume carbon dioxide and will yield oil [7]. Algae offer the highest oil per acre yield of any potential oil producing crop. It should also be noted that biodiesel is often produced utilizing used cooking oil from the restaurant industry.

The alcohols typically used in the production of biodiesel are methanol and ethanol. Ethanol is an attractive choice as it is itself a alternative fuel; however it produces a less than ideal form of biodiesel when compared to biodiesel created with methanol as the alcohol. Methanol is typically derived from coal or natural gas, which are generally non-renewable fuels, though it can be made from wood [6]. Methanol is also more dangerous than ethanol as it is poisonous, whereas ethanol is the alcohol consumed by humans. Methanol may cause the decay of natural rubber parts in the

engine because leftover alcohol may remain in the biodiesel after the transesterification process.

Biodiesel is more desirable than diesel fuel due to its renewable nature. It also has additional benefits over traditional diesel fuel including being catorgized as a carbon neutral fuel. This classification implies it produces no net carbon dioxide, or that all the carbon dioxide released during combustion is carbon dioxide that has been removed from the atmosphere by the plants grown to create the biodiesel. Additionally, biodiesel reduces engine emissions of pollutants, especially sulfur oxides as there is no sulfur contained in or added to biodiesel [8]. Polycyclcic aromatic hydrocarbons (PCH's) and soot emissions are also reduced. Biodiesel is also better for an engine due to its increased lubricity, and is completely biodegradable, further minimizing its environmental impact [8].

However, biodiesel possesses some drawbacks to its application as vehicle fuel. As mentioned above, depending upon the alcohols used it can dissolve natural rubber parts in the engine. This is solved by utilizing non-natural rubber elastomers in the engine such as silicone. Biodiesel also contains approximately 12% less energy per unit mass than traditional diesel fuel, though this is offset by its increased combustion efficiency, meaning it burns more completely than traditional diesel fuel, and can be further offset by alcohol remaining in the fuel [6]. Another problem which can afflict both traditional diesel and biodiesel in hot humid climates is bacteria growth [6]. This can happen when the vehicle is inactive for extended periods of time. Bacteria can clog the fuel system and disable the vehicle, however adding biocide to the fuel will quickly kill the bacteria and solve operational problems[6]. The preventive solution is to store

the fuel in a cool dark place and keep the tank near full to minimize oxygen in the fuel tank, which will in turn minimize chances of a significant bacteria problem.

One of the most significant problems with utilizing biodiesel is its cold weather properties. Any hydrocarbon based fuel will gel and clog the fuel filter if the ambient temperature becomes cold enough. Biodiesel has the potential to cloud and clog the fuel filter at temperatures as high as 16 °C, though this generally occurs with biodiesel made from used cooking oil [6]. The temperature at which the clogging will occur is correlated with the cloud point of the fuel. Conversely, diesel fuel will generally begin to cloud around -7 °C [6]. In addition to the point where the fuel clouds and the point where the fuel clogs, there is another point, referred to as the pour point, where the fuel will completely gel and cease to flow through the fuel system. In diesel fuel, the pour point falls between -29 °C and -23 °C [6]. The pour point associated with biodiesel is significantly higher and can vary widely. As with diesel fuel, biodiesel can have winterizing agents added to the fuel to depress the cloud and pour points. Finally, it should be noted that the true point where the engine will cease operation is somewhere between the cloud point and the pour point. This temperature point is referred to as the cold filter plugging point (CFPP). The use of the low temperature flow test (LTFT) will estimate the CFPP as the LTFT is nearly equivalent to the CFPP for predicting operability in North America [9].

1.3.3. Eutectic Compounds

Some applications, including the application explored in this thesis, require the storage of thermal energy, which can be accomplished through the use of a material with a high specific heat such as oil. The downside of this storage method is to store large

amounts of thermal energy, a large mass of storage material is required or high temperatures will result.

An alternative to traditional thermal storage is to use a phase change material (PCM). PCMs use the thermal energy required to change a material's phase, such as the energy to change ice to liquid water, in order to reduce the temperature required to store a given amount of heat with a given mass of PCM. PCMs almost without exception, utilize the liquid-solid phase change to store the energy. Even though the liquid-gas phase offers a more impressive latent heat, the disadvantages of storing a gas, such as pressure and volume, outweigh the benefits [10]. PCMs can be grouped into two categories, salts and organic compounds including those which utilize fatty acids [10].

A specific category of organic compound that utilizes fatty acids is called a eutectic compound. Eutectic compounds are blends of various organic fatty acids and are called eutectic compounds due to the ability to tune the eutectic point, or melting point, of a given compound to a desired temperature. This tuning is accomplished by blending the various fatty acids that comprise the compound in varying amounts. This makes eutectic compounds very desirable for applications where the point where the large heat storage occurs is important. An application where PCMs are commonly used is within desert home heating, where heat is stored during the day by melting a solid PCM and is released back into the house during the night when the PCM moves from a liquid back to a solid.. This thesis utilizes a eutectic compound to provide a constant temperature heat reservoir from which the heat is transferred to and from the fuel filter during the startup and storage Phases of operation.

1.3.4. Control Laws

Control laws can be utilized to improve the transient response of a system by increasing the speed of the response, minimizing error in the response, and decreasing undesirable behavior such as overshoot. Closed loop control systems are the most common, where the input to the system plant is based upon some version of the error signal. The error signal of the control law is simply the difference between the desired response and the current response.

A basic control law used throughout this research is proportional integral derivative control (PID), which is a combination of three simple controls. The proportional controller, as its name implies, is proportional to the error signal. By increasing the proportional gain the system response speed increases, while conversely decreasing the proportional gain will slow the systems response [11]. However, occasionally proportional control will allow a system response to reache equilibrium while still produceicing an error referred to as steady state error [11].

To address steady state error, integral control action is added. The integral controller bases its control on the integral of the error signal. The manner in which an integral controller solves steady state error is by producing an increasing control signal as long as the error signal is nonzero [11]. However, due to the nature of the integral control it lags somewhat behind system response. This tends to lead integral controllers to produce oscillations in the response [11]. The solution to the response oscillation is to allow the system to know that the error is approaching zero, which is accomplished through the use of derivative control action [11].

Derivative control action is based on the derivative of the error signal, and allows the system to react to changes in the rate of change of error [11]. The primary use of derivative control is to damp out oscillations in the system response. Derivative control should not be utilized absent of other control schemes as it can fail to produce a response with error present so long as the error remains constant [11].

The combination of the three controls yields a PID controller, where the proportional portion can be utilized to improve system response speed, the integral portion addresses steady state error, and the derivative portion addresses oscillations. The PID controller control signal is the sum of each type of controller, with the amount of each control type being determined using the gain for the given control. However, PID control laws depend on exact knowledge of the plant parameters that are being modeled to be controlled. Thus, if errors exist in the plant model the control law may produce an undesirable or inadequate response. The solution to this problem is the use of a more robust control law.

Robust control laws manage to maintain adequate performance in the face of plant inaccuracies [12]. Two types of robust control are adaptive control and sliding mode control. Adaptive control changes the system parameters while operating to allow the system to meet the setpoint. Sliding mode control forces the system response to a line in the phase plane. Depending on the specifics of the sliding mode design it can deal with a certain range of values for each model parameter.

1.4. Literature Review

This section of the thesis will review past relevant research that has been undertaken in the fields applicable to this thesis. The review is broken down by topic

with Section 1.4.1 covering thermoelectrics, Section 1.4.2 covering eutectic compounds, and Section 1.4.3 covering biodiesel. Throughout this section, the past work undertaken will be tied to the research detailed herein, in order to highlight the development of the system.

1.4.1. Thermoelectric Devices

A frequent topic of research is the use of thermoelectric devices in the automotive industry. Bobi et al. [13] suggest that there are three main areas to consider the use of thermoelectric devices in the context of the automotive industry. First, the use of thermoelectric devices to condition the fuel, specifically in the fuel filter, during cold weather operation. The second proposed application is the use of thermoelectric modules to generate power using the hot exhaust gas stream produced by the engine. The final suggested application is the use of thermoelectric devices to control the passenger compartment temperature in lieu of a more traditional heating and cooling system. Morelli [14] presents a similar paper, which notes an additional possible use of thermoelectric devices in the cooling of automotive microelectronic systems, which could allow greater concentrations of electronics. The author also goes into greater detail regarding the conditioning of the passenger cabin noting that thermoelectric refrigeration systems can achieve higher coefficients of performance than a traditional vapor compression refrigeration system. In addition, the author brings up the concept of seat cooling utilizing thermoelectric devices, and mentions that applicability to vehicles can be improved when hybrid vehicles are being considered due to the availability of a more robust electronics system. Also the paper thoroughly covers some of the drawbacks to the use of new technology, including thermoelectric devices, noting that novel systems

must make up for the increased weight gain and possible exhaust blockages loss of engine efficiency in automobile applications. The automaker must trade off the reduction in fuel efficiency and performance that is associated with a higher weight that extra systems entail with whatever the potential gains the system proposes. The above papers provide the initial foray into the specific area that this research is contained within.

The remainder of the literature review on thermoelectric technology can be roughly broken down in to two separate areas. The first area described in Section 1.4.1.1 deals with thermoelectric devices utilized for heat transfer. The second area described in Section 1.4.1.2 describes the use of thermoelectric devices in power generation applications.

1.4.1.1. Heat Transfer

As two phases of the proposed system utilize a thermoelectric device to transfer heat, it is prudent to examine past research utilizing thermoelectric devices for heat transfer applications. Luo et al examine the use of a thermoelectric heat pump to create a type of residential water heater specifically for instantaneously heating bath water. This paper represents important work relative to the current research since thermoelectric heat transfer is typically for cooling purposes. The authors demonstrate that through proper system design, a thermoelectric heat pump can outperform typical electrical resistance type heaters, while identifying three operational parameters associated with improving thermoelectric heat pump performance. The thermoelectric element's figure of merit is proportional to the heat pump's efficiency. Next, decreased temperature difference between the thermoelectric junctions will improve performance. This is especially important to the thesis research as it partially leads to the desire for a eutectic compound

latent heat storage device as opposed to a more traditional heat storage device. Finally, increasing the temperature the system operates at overall will improve the heat pump coefficient of performance.

Vasquez et al. [16] present a version of a thermoelectric fuel conditioning system, which was read to provide a basis for this research. The authors examine several aspects of designing a thermoelectric fuel conditioning system including element layout, filter redesign, optimum heat power supplied, and element selection. The authors also utilize a eutectic compound latent heat storage device. Utilizing a flat thermoelectric module, placed on the bottom of the fuel filter, the authors determine that a thermoelectric fuel conditioning system is viable with sufficient filter changes. These changes include heat pipes and fins in the filter. These changes increased the weight of the fuel filter, which as mentioned above can prove detrimental to the vehicle. However, it should be noted that fins are common even in currently adopted resistive heating type fuel conditioning systems. Vasquez and Bobi [17] continued this research with a finite element analysis. The models revealed the electrical power required for a thermoelectric system is less than that of a traditional system. The authors also raise an important point about the design of fuel conditioning system, noting that if the system is driven too hard, the fuel could be caused to flash, or combust, in the filter. The authors also note that the addition of a simple low power resistive heater wire in the center of the filter can improve performance significantly. These two papers lead to the conclusion that it was worthwile to conduct further research into thermoelectric fuel conditioning systems to see if the addition of control laws and further refinements in geometry could improve the performance futher.

To gain additional insight into thermoelectric heat transfer applications, further research was conducted on the topic in related areas. Thermoelectric chip cooling is a more common application of thermoelectric refrigeration, which is pertinent as the heat transfer is in the same direction as desired for the thesis research. Chein and Huang [18] examine the use of thermoelectric devices for the cooling of electronic chips. The paper provides various formulations for the calculation of the heat transfer, and also show that the chip cooling is improved as the junction temperature difference is decreased as mentioned above by Vasquez [18].

Another area in which thermoelectric heat transfer devices are being considered is in the biomedical field. Wijngaards et al, [19] discuss the use of thermoelectric devices for active heating and cooling in microscale applications especially in the biomedical field. The authors show the effect that differing types of temperature measurement have on the control schemes being utilized, and that thermoelectric devices are ideal for cooling within biomedical applications. However, while the authors recommend using the same thermoelectric element for heating due to benefits, such as a more simplified part and cost compared to having two different elements one each for heating and cooling, other than efficiency, they show that in this particular application of microscale biomedical devices the thermoelectric element is outperformed by a simple resistive heating element. This is important because it shows that in this application a thermoelectric device for heat transfer applications is not superior to the simpler resistive heating element.

1.4.1.2. Power Generation

The third phase of proposed operation for the thermoelectric device in this research is power generation and therefore past research for thermoelectric devices used for power generation is detailed below. In the paper Palacios and Li delve into some of the specifics of commercial thermoelectric modules used for power generation. In addition, the paper provides an overview of thermoelectric generation noting two important aspects to consider when designing a thermoelectric generator. First, the temperature on the face of the module is immaterial for performance, only the heat flow through the module matters. Also, the fall-off in voltage associated with drawing high currents will quickly lead to the generation of less power, thus leading to the conclusion that high voltage and low currents are more desirable. This means that for the current research during Phase 3, the power generation phase, operation the temperature for the hot and cold reservoirs are less important than the heat flux obtained through the thermoelectric elements.

A more in depth analysis of thermometric power generation is provided by Bell [21]. Bell describes various equations governing thermoelectric thermodynamic power generation cycles. The author breaks down the various types of power generation into four basic categories. The first, where both the hot and cold sides are isothermal, is the most common boundary assumption. The next two categories involve one isothermal side and the other side as a convective media. The final category involves both the hot and cold sides represented as convective media. Bell segments the categories into twelve different configurations, and then compares each with the standard system (with two isothermal boundary conditions) to obtain their possible efficiencies as a function of the

standard system's efficiency. Each of the twelve configurations has its relevant equations explored. The use of more accurate boundary conditions allow for a more accurate analysis of a generator's efficiency. This provides a way to further refine the current research.

A higher level approach is provided by Crane and Jackson [22]. Crane and Jackson present research, which covers a system's level approach to improving the performance of a thermoelectric waste heat recovery system. The two main factors which influence the performance of a thermoelectric system are the thermoelectric conversion efficiency and the effective heat exchange design. As the first is essentially a materials problem, the paper focuses upon the second objective. The authors create a set of equations and models that estimate the power generated per ten thousand dollars. The model is optimized to achieve the best power for the least amount of money. The parametric study performed shows tube spacing, tube diameter, and thermoelectric element length all exhibit strong maxima when varied from the optimum design. This paper helps lead to the conclusion that an improved geomentry could significantly improve the performance of the proposed thermoelectric system.

A specific application of thermoelectric generation research is provided by Furue et al. [23]. Furue et al. explore the use of thermoelectric generators in the recovery of the waste heat contained in the exhaust gas stream of a power plant. Exhaust gas flow rate is found to have an effect on the power generation. Next, the effect of introducing fins into the hot exhaust stream to augment the generation process was examined. Finally, the length of the thermoelectric elements was varied and an increased thermoelectric element length improves the efficiency of the system. The author's calculations were based upon

a complex thermal network and an iterative algorithm which matched the results to a set exhaust temperature. This mainly leads to the conclusion that more thermoelectric elements improve power generation.

A similar waste heat recovery application of thermoelectric elements is provided by Ikoma et al. [24]. Ikoma et al. examine the use of a thermoelectric generator utilizing the exhaust gas stream of an automobile. The authors state that a standard gasoline engine rejects about thirty percent of its energy in the form of wasted heat in the exhaust stream. If six percent of that energy could be converted back into electrical energy, there would be a ten percent reduction in fuel consumption. The silicon germanium (Si-Ge) thermoelectric module used in the research, which involves constructing a test bed for the module, is introduced. The module achieves a small amount of power generation; however the authors recommended improvements in the thermoelectric material and the heat transfer across the module. This paper provides some of the motivation for the current research as it shows that any waste heat recovery can lead to a significant impact on the fuel economy of the vehicle.

The research by Tsuyoshi et al [25] presents another thermoelectric generation as a power plant application, and investigates the use of a thermoelectric generator using a thermal accumulator as a heat source, which is then compared back to the use of a thermoelectric generator with no accumulator. The thermal accumulator stores the heat from the combustion and releases it over time. The paper describes how thermoelectric generators can be used to harness the heat generated by refuse incinerators. The temperatures obtained by these incinerators are often not sufficient for a practical steam generation cycle, however are suitable for thermoelectric generation. Since the

incinerators are currently operated non-continuously, it is economically advantageous to reduce the number of thermoelectric generators and allow the system to generate power continuously using a thermal accumulator to release the stored heat from the day's combustion over a twenty-four hour period. The efficiency of a generator run off of the accumulator is examined as are the benefits of slowing down the thermal cycle to maintain larger temperature differences longer. The research reveals a reduction in efficiency due to the reduction in heat flux if the accumulator is used and a further reduction if there is not control on the generation rate, than if the heat stored in the thermal accumulators were allowed to be released at a natural rate. While the efficiency declines, the cost effectiveness increases due to the significantly lower number of thermoelectric elements required. The research presents a case for the cost effectiveness of using heat storage devices in conjunction with thermoelectric technology. This research shows that control of the rate at which the thermoelectric generator is allowed to run can have a significant impact on the amount of energy generated.

Research which further shows the tradeoffs required in regards to thermoelectric devices is presented by Vázquez et al. [26]. Vázquez et. al. investigate the current state of thermoelectric technology in regards to electricity generation from the exhaust gas stream in an automobile. The paper includes an overview of a thermoelectric generator and issues with the mounting required to take advantage of the car's exhaust stream. The first issue raised is generator location with possabilites of just after the manifold, between the manifold and the catalytic converter, and after the catalytic converter. Several other factors are involved in the design of the mounting system for the generator, but since location of the generator mount accounts for the vast majority of the generator weight, it

would appear that location is the main factor that determines weight. The selection of a location affect the thermoelectric module type since it will need to be tailored to the temperature at that point. The authors also raise some other important points such as the means by which the modules will be maintained in contact with the heat source.

Yang [27] provides more research in the area of engine waste heat generation, and examines various ways to utilize waste heat in an automobile. As mentioned previously, much of the energy from the gasoline in a car is wasted and any amount that can be recovered could result in a significant boost in fuel efficiency. Specifically with the ever increasing electrical requirements and the inherent inefficiencies in converting mechanical power to electrical power, a thermoelectric waste heat generator system is advantageous in offsetting the increasing electrical energy needs of the vehicle. Additionally, if the thermoelectric generator recovers enough of the waste heat it could reduce the load on the engine by reducing the size of the alternator the vehicle requires. The author examines the status of the thermoelectric generation in regards to the variety of new thermoelectric materials becoming available specifically, Bi_2Te_3 and Sb_2Te_3 superlattices and PbSeTe and PbTe quantum dots, which show ZT values as high as 3.6. The ZT value is a measure of how well the thermoelectric element will perform as a generator. This examination of materials is done by determining what ZT value is necessary for a ten percent fuel savings. The research concludes with an economic analysis that shows how much money a ten percent fuel savings represents. The author stresses that the current trend in increasing vehicle electrical consumption continually makes waste heat recovery more attractive, which provides further motivation for the current research.

1.4.2. Eutectic Compounds

A brief literature review of past research on eutectic compounds is provided. The review focuses mainly on work related to the tuning of the melting point of the eutectic compound. Also, some research in the area of thermal cycling of eutectic compounds is detailed.

Tuncbilek et al. [28] explores the use of a lauric acid and palmitic acid mixture to achieve a unique eutectic fluid. As discussed above in Section 1.3.3 there are three major ways to store thermal energy. Latent heat storage which stores heat by utilizing the latent heat of fusion for a material is an especially attractive method due to the energy per unit volume ratio and the consistency of the temperature output when energy is removed from storage. A large portion of the research in this area has focused on salt hydrates because of the desirable melting point, however there are other problems associated with them such as corrosiveness. The authors show that a lauric acid and palmitic acid mixture can achieve a melting point which is lower than either of the acids on its own, while retaining a high latent heat of fusion. This research is relevant as it helps to solidify the choice of a fatty acid blend type of eutectic compound. Additionally, the authors show that the melting point can be depressed through a proper blending scheme.

Another paper "Phase diagram of the ternary system lauric acid–capric acid–naphthalene" [29] focuses in the area of melting point tuning, and investigates the use of naphthalene to improve the melting point of a lauric acid – capric acid eutectic fluid latent heat storage device. Naphthalene is an inexpensive additive that if suitable would allow for the production of a eutectic fluid with a very low melting point. Varying mixtures of lauric acid, capric acid, and naphthalene were tested and the varying results

of solidification were found. This allowed for the creation of graphs from which it can be seen that it is possible to lower the melting point when using a lauric acid, capric acid, and naphthalene compound, which is desirable since the proposed application can require a eutectic compound with a relatively low melting point.

Since the proposed application is for use in the automotive industry the ability of a latent heat storage device to withstand the cycling necessary for practical use is important. Sari et al. [30] explore the use of various fatty acid mixtures for use as thermal energy storage including: lauric acid, stearic acid, palmitic acid, and myristic acid. By mixing the acids in varying ratios a wide range of melting points for the substance can be tailored for the application. In addition, the properties of several of these mixtures were subjected to thermal cycling. For each of the mixtures the heat of fusion was also determined. The heat of fusion has a direct effect on how much energy can be stored in the phase change. The endurance testing of the eutectic mixtures showed that while some variation in the heat of fusion and the melting point occurred, it was not significant. Therefore, all are viable for use as part of a eutectic compound to be subjected to melting and freezing processes as would be required of a thermal energy storage system, especially in an application such as the one in the current research.

1.4.3. Biodiesel

A literature review of biodiesel research is presented beginning with a basic text on biodiesel. The remainder of the research reviewed deals with the cold weather properties of biodiesel, which is important as explained previously in Section 1.1

Tickell [6] provides a guide to the benefits of using vegetable oil, in its various forms, as a fuel. He presents problems with basing an economy heavily on fossil fuels, and proposes an economy that relies on renewable fuels as its basis. With a case for a renewable fuel source given and the technology for its implementation explained, biodiesel is suggested as the solution. Especially notable is a graph which presents the reduction in emissions that are associated with switching to biodiesel. Also several interesting legislative statistics are provided, and the means of biodiesel integration in the United States can be achieved. This book presents a good case for biodiesel being the best fuel for the future as mentioned above, which provides impetus for the current research.

As mentioned by Tickell the cold weather properties of biodiesel can be problematic. Knothe [31] explores the effects that the fatty esters have on the various important properties of biodiesel in regards to its use as a fuel. As mentioned above in Section 1.3.2, the process of making biodiesel is the transesterification of oil with an alcohol. This process will yield the fatty ester which is biodiesel. The most common alcohol due to its relative low cost is methanol, which in turns yields biodiesel comprised of fatty acid methyl esters (FAME). In diesel fuels, the cetane number (CN) is an indicator of the basic quality of the fuel, just as the octane number is indicative of the quality of gasoline. The cetane number is directly responsible for the amount of nitrogen oxide (NO_x) emissions that the diesel engine will produce. The relationship between CN and NO_x tends to be less pronounced as the pressure of the cylinder increases. The cold temperature properties of a biodiesel are directly related to the type of fatty ester present in the fuel. The cloud point, when wax crystals begin to form in the fuel, is of particular

importance as it is the point at which the fuel filters and lines will begin to experience clogging problems. The cloud point can be improved by removing the saturated fatty esters through a straining process leaving the unsaturated fatty esters, which will begin to cloud the fuel at a lower temperature. Also, the cold properties of the biodiesel can be improved by switching to a branched ester, basically an ester produced by increasing the complexity of the alcohol. The only economically viable ester is one of the isopropyl variety, which would be obtained by transesterification using an alcohol like iso-propanol. Other properties such as viscosity, lubricity, and oxidative stability are also directly linked to the fatty ester chains. This is important because it shows that a wide variety of biodiesel cold weather properties based on the specifics of the way it is manufactured.

Since the cold weather properties of biodiesel vary greatly, research has been conducted into ways to improve the cold weather properties of biodiesel. "Impact of cold flow improvers on soybean biodiesel blend" [32] covers the various means by which the cold weather viability of biodiesel may be improved. There are three main ways to combat the problem of low temperatures of biodiesel: fuel system heaters, fuel additives, and blending the fuel. The authors state that while the cloud point and the pour point are commonly recognized properties given for fuel, neither one will predict the viability of a fuel at a given temperature with complete accuracy. Therefore, the low temperature filterability (LTFT) is also examined. Tests were conducted using soybean biodiesel with zero, ten, and twenty percent kerosene blended into the biodiesel. The results show that the higher the kerosene percentage and the stronger the additive, the more cold temperature properties improved. It should be noted that kerosene blending has its own

limit on the viability of the fuel as a whole as at some point it begins affecting the combustion characteristics of the fuel, while the additives main limiting factor becomes the cost of the additive. This is important because it shows that while the cold weather problem can be alleviated by other means the problem will still remain if only blending and additives are used.

Another means of improving the cold weather properties of biodiesel that has been proposed is the use of ozonized vegetable oil. Soriano et al. [33] cover the use of the addition of ozonized vegetable oil as an additive to biodiesel to improve its cold weather properties. The authors show the results of mixing various amounts of ozonized vegetable oil with sunflower, soybean, palm and rapeseed (canola) oil. It is shown that with the exception of palm oil, the addition of the ozonized vegetable oil lowers the pour point of the biodiesel, while leaving the cloud point relatively unaffected. This means that the low temperature filterability (LTFT) will be reduced somewhat leading to some amount of improved cold weather properties. This result is true of all biodiesels with the exception of palm biodiesel regardless of the ozonized vegetable oil added. The most effective oil to be ozonized depends on the type of biodiesel the ozonized oil is being mixed with. This again shows that while other methods exist for improving the cold weather properties of biodiesel, the problem will not be completely ameliorated through blending and additives alone.

1.5. Research Objectives

The current research is being undertaken with the goal of examining the economic viability of the proposed E-TE system. The ever increasing numbers of vehicles utilizing biodiesel and thus requiring fuel conditioning combined with rising fuel costs and falling

thermoelectric costs makes this an ideal time to examine the E-TE system as a potential replacement for electrical resistance heaters for the next generation of vehicles. The research has one main goal, which is to create models to investigate the performance of the E-TE system. The secondary goal is to design an experimental setup that can later be constructed to perform testing on the system if the system proves to be viable in the modeling portion of the work.

2. Model Development:

Model development proceeded in two phases. The initial model development focused on the solution of the three dimensional heat transfer equation using separation of variables. A solution to the equation was obtained, however it proved to be too complex for implementation into a control law. Next, a lumped parameter approach was applied to the solution. The lumped parameter approach yielded a solution that was implementable into a control law, but the lumped parameter assumption proved invalid due to the poor thermal conductivity of the fuel and the high amount of effective heat flux through the filter wall. This model development is termed the *alpha* model.

Due to the inadequacies of the initial approach a second approach was merited. The second approach involves treating the model as a thermodynamic system. The second approach, termed the *beta* model, yielded a controllable solution and was thus implemented into Simulink© for feasibility assessment.

To aid in understanding, a simple concept drawing of a E-TE system is shown in Figure 2, and a basic overall schematic of relevant automotive systems is shown in Figure 3.

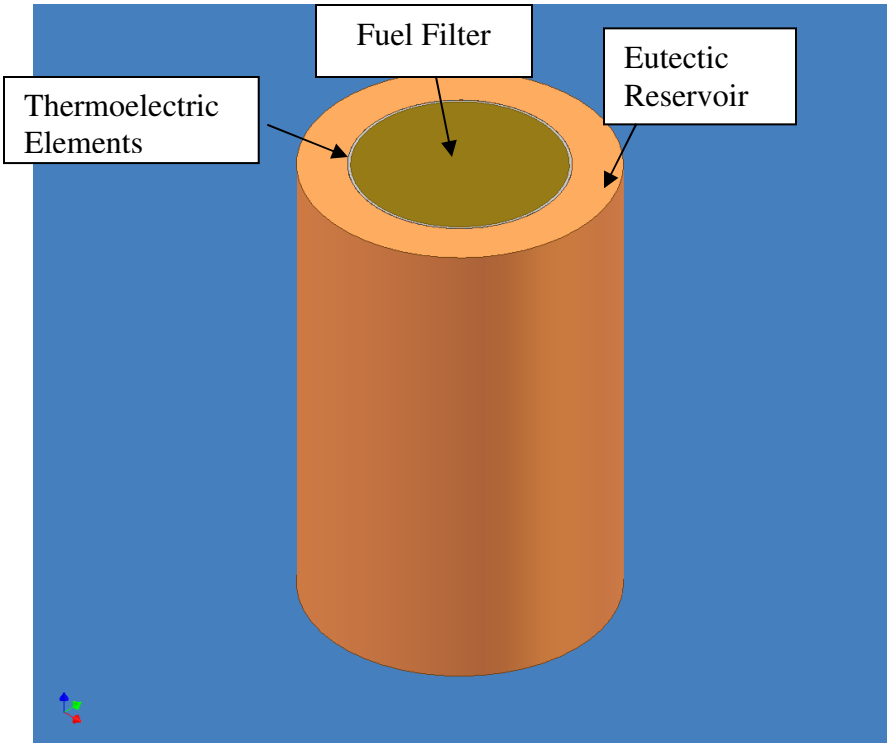

Figure 2: Simplified E-TE System Drawing

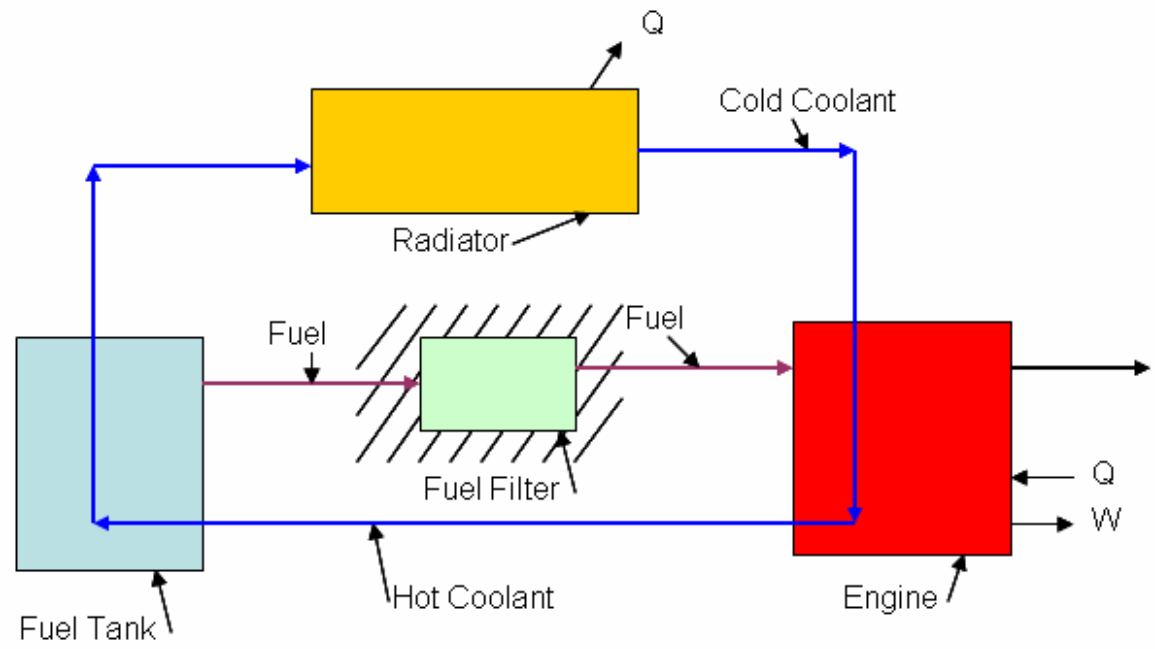

Figure 3: Basic Schematic of Relevant Engine Systems

The basic E-TE schematic (Figure 2) shows the fuel filter surrounded by an annulus of thermoelectric elements, which are in turn surrounded by an annulus of eutectic compound. The basic engine schematic (Figure 3) shows the engine as a red block, the fuel filter as a green block, the fuel tank as a blue block, and the radiator as an orange block. The fuel line is shown as a set of brown lines, delivering fuel from the tank to the filter and then from the filter to the engine. The blue coolant line shows the coolant being moved through the engine while cooling it, moving through the fuel tank while heating the fuel, and then returning to the radiator to be cooled itself. Note, the coolant is not warming the fuel in the tank during initial startup as the engine and thus the coolant pump is off.

To assist in the understanding of the heat transfer for Phase 1, the startup phase, a portion of the cross section of the system is shown in Figure 4.

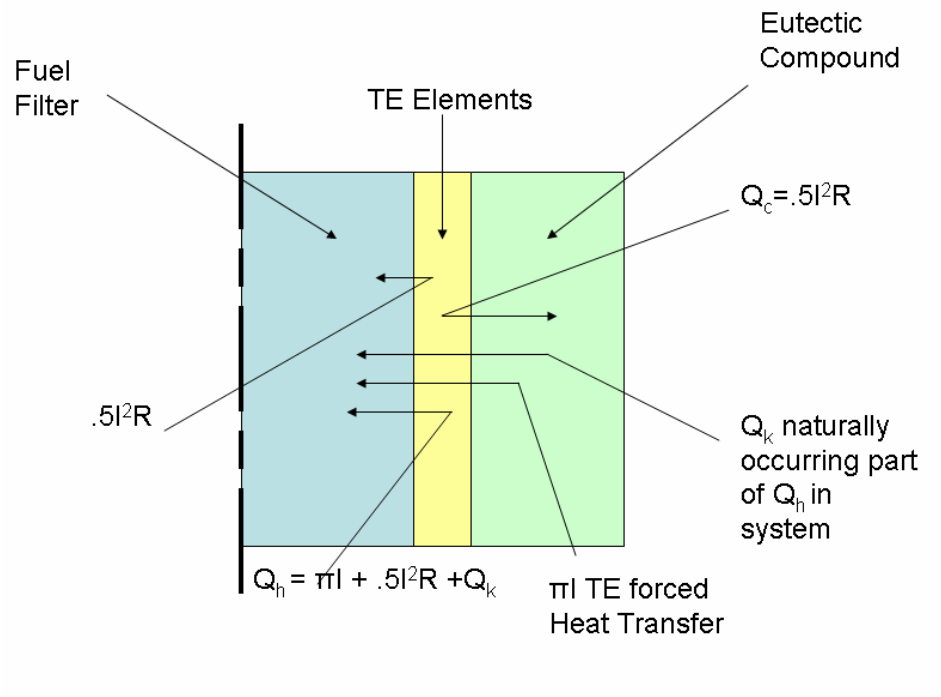

Figure 4: Radial Section of System Model

Figure 4 shows the heat transfer occurring during Phase 1. The blue section represents the fuel, the green section the thermoelectric elements, and the yellow section the thermoelectric elements. Q_h and Q_C show the total heat being supplied to each of the sides of the thermoelectric elements. The other terms all show the individual portions of the total Q terms. These include the electric heating, the conductive heating, and the thermoelectric heating.

With a basic understanding of the heat transfers under investigation a mathematical model was developed.

2.1. System Concept

The proposed E-TE system will have four distinct portions. As the system will operate in three phases a model is required for each phase. In addition, a supervisory control law is required to record data and switch between the models for each of the other phases.

Phase 1 is the initial phase of operation. During Phase 1, or the Startup Phase, the system will send a current to the thermoelectric elements from the battery to force a heat transfer from the eutectic reservoir into the fuel filter. This heat is required to melt the fuel and begin vehicle operation.

The Phase 1 model is adapted to for a Transitional Phase model to allow the system to transition smoothly from transferring heat into the fuel to transferring heat into the eutectic reservoir to recharge it. The Transitional Phase is treated as part of Phase 1 and utilizes the essentially the same model as Phase 1. During the Transitional, or Initial Vehicle Operation, Phase the engine starts and cold fuel begins flowing into the fuel filter from the fuel tank. The Phase ends when the incoming fuel has reached its final

operational temperature. The current supplied in during this portion of operation is small and can be both positive and negative.

The model when completed with Phase 1 and the Transitional Phase begins operation in Phase 2. During Phase 2, or the Recharge Phase, excess heat is removed from the fuel and transferred back into the eutectic reservoir. This is done by supplying a current to the thermoelectric elements that is in the reverse of the current supplied during Phase 1. Phase 2 ends when the eutectic reservoir has replaced all of the heat removed from it during the previous phases, changing the eutectic reservoir from a mixed liquid solid phase back to a fully liquid phase.

As soon as Phase 2 ends Phase 3 may begin. Phase 3, or the Power Generation Phase, allows the thermoelectric elements to act as a electrical generator. Natural heat conduction across the elements from the hot fuel to the relatively cold eutectic reservoir generates a current in the thermoelectric elements. Phase 3 ends when the vehicle ceases operation.

A second option is to delay Phase 2 till after the vehicle has shut down, and begin Phase 3 operation immediately after the Transition Phase. This should minimize the electrical energy that needs to be supplied to the thermoelectric elements, because some of the heat that would need to be stored will have been stored during the Phase 3 operation.

To aid in the understanding of the Phase methodology two timing diagrams are shown below, one for each Phase change strategy. The black line is the temperature of the fuel in the fuel filter, $\underline{T_o}$. The blue line is the temperature of the incoming fuel ending at the final incoming fuel temperature, T_i. The green line is the temperature of the

eutectic reservoir, T_e. The engine's status is represented at the bottom of each diagram. As can be seen the only real difference between the two strategies is in which order Phases 2 and 3 occur. Note, the temperatures are shown only approximately and are not to scale. In both diagrams it can be seen that the engine is turned on at the end of Phase 1 which occurs when the temperature of the fuel, T_0, is equal to 95% of the goal temperature, T_g. The Transition Phase then begins and runs for five minutes to allow the engine to reach operating temperature. Next, either Phase 2 or Phase 3 is used depending on the strategy being utilized. In strategy 1 Phase 2 occurs and runs until the eutectic reservoir is recharged. In strategy 2 Phase 3 occurs and runs until the engine is turned off. The final Phase differs depending on the strategy chosen. In strategy 1 the final Phase is Phase 3 which, runs until there is no excess energy in the fuel. In strategy 2 Phase 2 is the final Phase and runs until the reservoir is recharged.

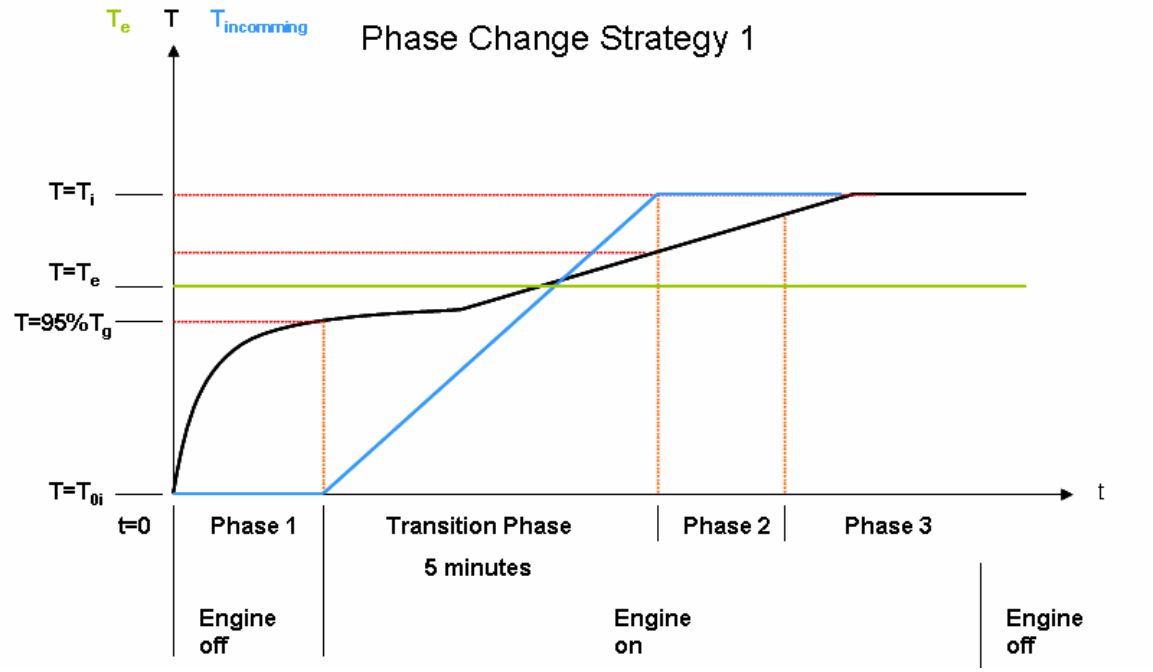

Figure 5: Phase Change Strategy 1 Timing Diagram

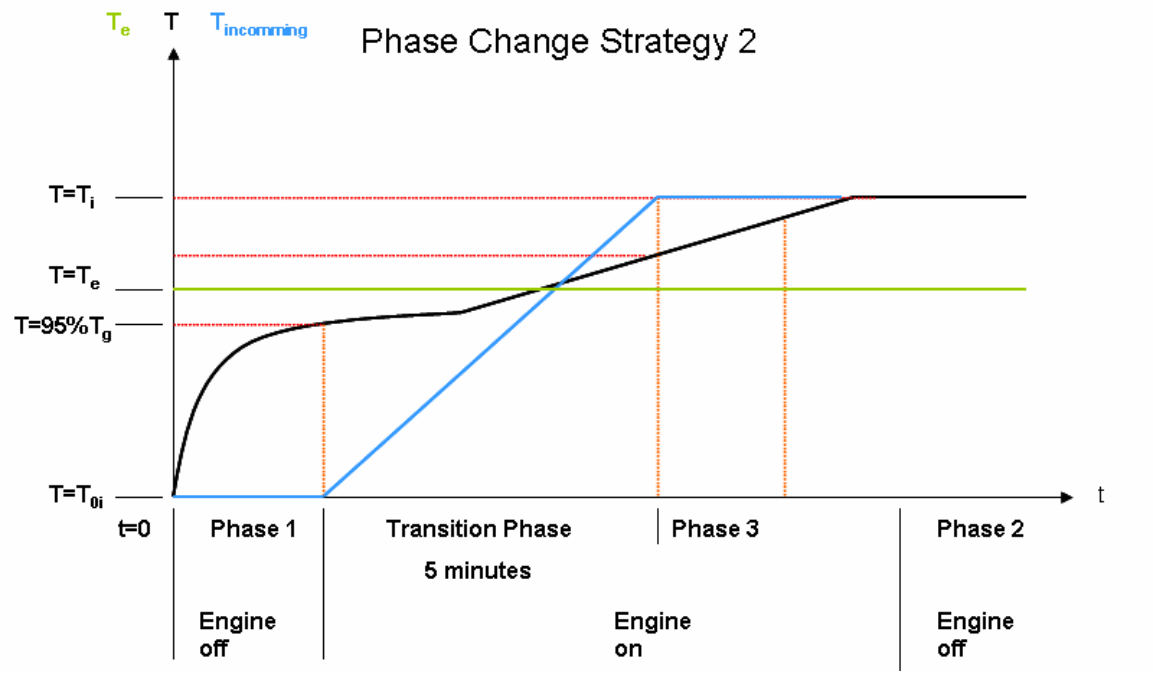

Figure 6: Phase Change Strategy 2 Timing Diagram

The fourth distinct portion of the system is the supervisory control law. The supervisory control law is responsible for switching between the different Phases and making the logical decisions necessary in order to switch. The supervisory control law also records the data that is required to make the decisions and to evaluate the system's performance. In addition, the supervisory control law graphs the data collected.

To proceed with model development, the *alpha* mathematical model governing the heat transfer for the system must be developed.

2.2. Alpha Plant Mathematical Model

Model development began with solving approximate versions of the three dimensional heat conduction equations. By assuming that all heat supplied by the

eutectic compound is supplied by the latent heat of fusion, the eutectic compound can be assumed to be at a constant temperature. Furthermore, by assuming that there is no angular (θ) dependence or height (z) dependence, the problem now is a one dimensional transient problem in cylindrical coordinates. Finally, by assuming the thermal conductivity of the filter paper when soaked in fuel does not significantly differ from the thermal conductivity of the fuel itself, the domain is simplified to be a simple circular region. The simplified differential equation, with the corresponding boundary conditions is given by Equation 1.

$$\begin{aligned} &\frac{\partial T_0}{\partial t} = \frac{\alpha}{r}\frac{\partial}{\partial r}\left(r\frac{\partial T_0}{\partial r}\right) \\ &@\ r = 0, Bounded \\ &@\ r = R, k_{fuel}\left(\frac{\partial T}{\partial r}\right) = h\left(T_E - T_0\right) + \frac{\dot{Q}_{TE}}{A} \\ &@\ t = 0, T = T_{0i} \end{aligned} \tag{1}$$

Note: h is not representing true convection but rather the natural conduction of heat from the eutectic reservoir to the fuel filter. As the temperature distribution across the thermoelectric elements is not desired information this approach. h is simply the thermal conductivity of the thermoelectric elements divided by the thickness of the thermoelectric elements. Due to this simplification it appears as a convection term.

Next, the problem will be non-dimensionalized to ease the mathematical manipulations. This is done by setting up a number of scales for the problem. The obvious scale for the radius is the outer radius of the filter, R. The temperature scale is chosen to be T_M, the melting point of the fuel. This nondimensionalization will yield a time scale of τ which is equal to R^2/α. Non dimensionalizing the boundary conditions will also yield the dimensionless quantity:

$$\gamma = \frac{hR}{k_f} \tag{2}$$

And the dimensionless heat

$$Q_{ND} = \frac{Q_{TE}}{2k_f T_M \pi H} \tag{3}$$

These manipulations will yield the equation and boundary conditions shown in Equation 4.

$$\begin{aligned}
&\frac{\partial \overline{T}}{\partial \bar{t}} = \frac{1}{\bar{r}} \frac{\partial}{\partial \bar{r}} \left(\bar{r} \frac{\partial \overline{T}}{\partial \bar{r}} \right) \\
&@\, \bar{r} = 0, Bounded \\
&@\, \bar{r} = 1, \left(\frac{\partial \overline{T}}{\partial \bar{r}} \right) = \gamma \left(\overline{T}_E - \overline{T} \right) + Q_{ND} \\
&@\, \bar{t} = 0, \overline{T} = \overline{T}_{0i} \\
&where \\
&\overline{T}_0 = \frac{T_0}{T_M}, \overline{T}_{0i} = \frac{T_{0i}}{T_M}, \overline{T}_E = \frac{T_E}{T_M}, \bar{r} = \frac{r}{R}, \\
&\bar{t} = \frac{t\alpha}{R^2}, \gamma = \frac{hR}{k_f}, Q_{ND} = \frac{Q_{TE}}{2\pi k_f T_M H}
\end{aligned} \tag{4}$$

The next step is to homogenize the boundary condition at the outer radius by assuming a form:

$$\overline{T}_0 = G + B \tag{5}$$

A suitable form is given by

$$\overline{T}_0 = G + \overline{T}_E + \frac{Q_{ND}}{\gamma}, \tag{6}$$

This will now yield the equations and boundary conditions in Equation 7.

$$\begin{aligned}
&\frac{\partial G}{\partial \bar{t}} = \frac{1}{\bar{r}}\frac{\partial}{\partial \bar{r}}\left(\bar{r}\frac{\partial G}{\partial \bar{r}}\right) \\
&@\ \bar{r} = 0, Bounded \\
&@\ \bar{r} = 1, \left(\frac{\partial G}{\partial \bar{r}}\right) + \gamma \bar{T}_0 = 0 \\
&@\ \bar{t} = 0, G = \bar{T}_{0_i} - \bar{T}_E - \frac{Q_{ND}}{\gamma}
\end{aligned} \tag{7}$$

Assuming a separable solution of the form in Equation 8

$$G = \sum_n A_n(\bar{t}) B_n(\bar{r}) \tag{8}$$

Substituting the assumed solution form will yield the form in Equation 9.

$$\begin{aligned}
&\frac{1}{\bar{r}}\frac{\partial}{\partial \bar{r}}\left(\bar{r}\frac{\partial B_n(\bar{r})}{\partial \bar{r}}\right) = -\delta_n^2 B_n(\bar{r}) \\
&@\ \bar{r} = 0, Bounded \\
&@\ \bar{r} = 1, \frac{\partial B_n(\bar{r})}{\partial \bar{r}} + \gamma B_n(\bar{r}) = 0
\end{aligned} \tag{9}$$

Where δ_n are the eigenvalues of the problem. This is a Sturm Liouville Problem, which means that the orthogonality of the eigenvalues is guaranteed with respect to the following inner product of Equation 10.

$$\langle f, g \rangle = \int_0^1 (rfg)dr \tag{10}$$

Furthermore, by observing the equation, it can be seen that the solution will be given by Equation 11 in which J_0 and Y_0 are zero order Bessel functions of the first and second kind.

$$B_n(\bar{r}) = C_{1n} J_0(\delta_n \bar{r}) + C_{2n} Y_0(\delta_n \bar{r}) \tag{11}$$

It can be quickly seen from the boundary condition at the center that all C_{2n} must be equal to zero for the solution to be bounded, and thus the solution simplifies to:

$$B_n(\bar{r}) = C_n J_0(\delta_n \bar{r}) \tag{12}$$

Substituting this back into the equation for G yields:

$$G = \sum_n A_n(\bar{t}) J_0(\delta_n \bar{r}) \tag{13}$$

By taking the inner product with respect to $J_0(\delta_n)$ for both sides of Equation 13 will yield Equation 14 and its eigenvalue relationship, which can be readily solved using an integrating factor.

$$\begin{aligned} &\frac{dA_n(\bar{t})}{d\bar{t}} + \delta_n^2 A_n(\bar{t}) = -\frac{1}{\gamma}\frac{dQ_{ND}}{d\bar{t}}\frac{\langle 1, J_0(\delta_n \bar{r})\rangle}{\langle J_0(\delta_n \bar{r}), J_0(\delta_n \bar{r})\rangle} \\ &@\ \bar{t} = 0, G = \overline{T}_{0i} - \overline{T}_E - \frac{Q_{ND}}{\gamma} \\ &-\delta_n J_1(\delta_n) + \gamma J_0(\delta_n) = 0 \end{aligned} \tag{14}$$

However, it can be seen that since the system control is based on changing the current supplied to the thermoelectric elements which will change the ODE that needs to be solved for time component of the separation of variables. This would require numerical methods to deal with the infinite series nature of the solution. However, in the limiting case where the problem is dominated by k_f, a direct analytical solution can be obtained, which is essentially a lumped capacitance approach. To begin the lumped parameter approach, Equation 4 will be integrated over the total volume as shown in Equation 15.

$$\int_0^1\int_0^{2\pi}\int_0^h \bar{r}\frac{\partial \overline{T}_0}{\partial \bar{t}}\partial\bar{r}\partial\theta\partial z = \int_0^1\int_0^{2\pi}\int_0^h \frac{\partial}{\partial \bar{r}}\left(\bar{r}\frac{\partial \overline{T}_0}{\partial \bar{r}}\right)\partial r\partial\theta\partial z \tag{15}$$

Simplifying Equation 15 and integrating will yield Equation 16.

$$\frac{\partial \overline{T}_0}{\partial \overline{t}} \frac{\overline{r}^2}{2}\Bigg|_0^1 = \left(\overline{r} \frac{\partial \overline{T}_0}{\partial \overline{r}} \right)\Bigg|_0^1 \tag{16}$$

By substituting in the boundary conditions from Equation 4, the lumped parameter equation shown as Equation 17 will be found.

$$\frac{1}{2} \frac{\partial \overline{T}_0}{\partial \overline{t}} = \gamma\left(\overline{T}_E - \overline{T}_0\right) + Q_{ND} \tag{17}$$

Q_{TE} is given by Equation 18 and shown graphically in Figure 4.

$$Q_{TE} = \pi_p I + \tfrac{1}{2} I^2 R_{TE} \tag{18}$$

Substituting Equation 18 into Equation 3 and then substituting Q_{ND} into Equation 17 will yield the plant to be controlled, which is shown in Equation 19.

$$\frac{1}{2} \frac{\partial \overline{T}_0}{\partial \overline{t}} = \gamma\left(\overline{T}_E - \overline{T}_0\right) + \frac{\pi_P I + \tfrac{1}{2} I^2 R_{TE}}{2\pi k_{fuel} T_M H} \tag{19}$$

Distributing Equation 19 and rearranging terms will yield Equation 20.

$$\frac{\partial \overline{T}_0}{\partial \overline{t}} + 2\gamma \overline{T}_0 = 2\gamma \overline{T}_E + \frac{\pi_P I + \tfrac{1}{2} I^2 R_{TE}}{\pi k_{fuel} T_M H} \tag{20}$$

Before proceeding any further with model development the lumped parameter assumption made for the model must be checked. Unfortunately, due to the nature of the thermoelectric elements moving heat and the relative thinness of the surface through which heat is conducted by the γT terms in Equation 20, the effective convection coefficient for the Biot number, $h_{eff}L_{eff}/k_f$, calculation is many orders on magnitude larger than the thermal conductivity of the fuel. This leads to a Biot number well over one, which in turn leads to the invalidation of the lumped parameter assumption. Ergo a new

approach to the model must be made. The new model will be referred to as the *beta* model.

2.3. Beta Plant Mathematical Model

Given that the *alpha* heat transfer model is unacceptable, a new *beta* plant thermodynamic based model was developed. Consider the cross-section of the thermoelectric element fuel filter system illustrated in Figure 7, and the end view of the system shown in Figure 8.

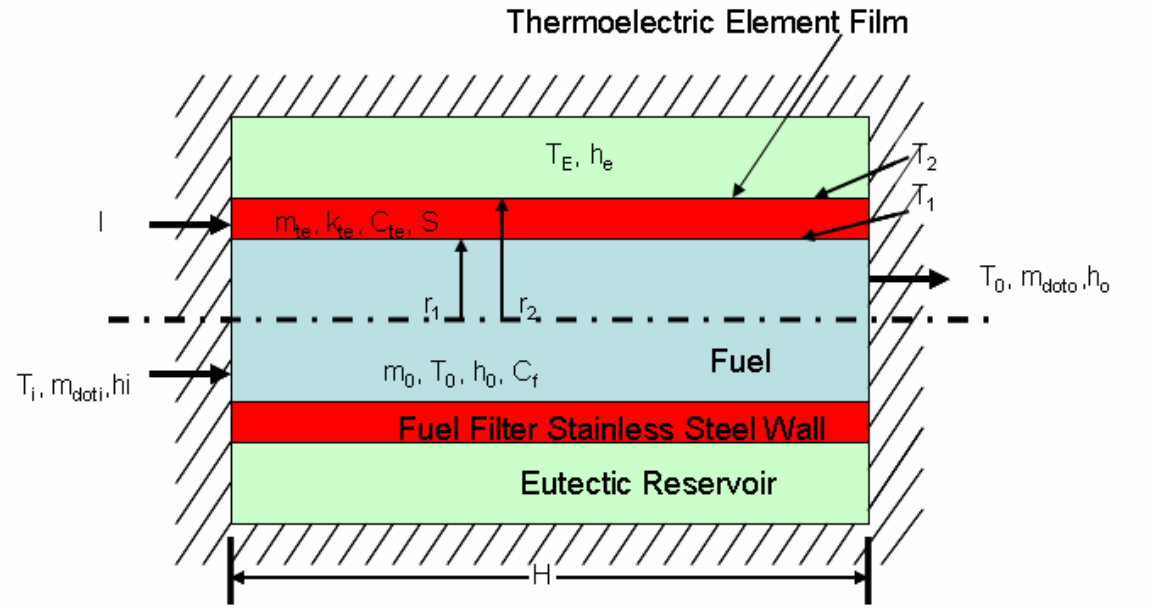

Figure 7: Fuel Conditioning System Cross Section

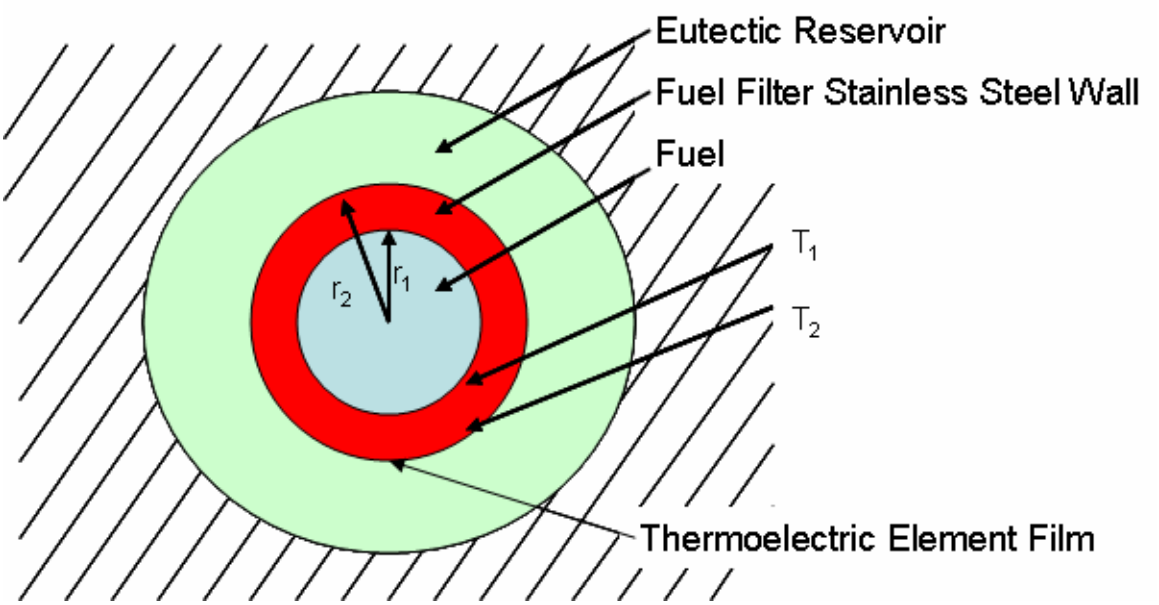

Figure 8: Fuel Conditioning System End View

Model development began with the construction of a simple diagram to aid in the understanding of the equations. Radius r_1 is the distance from the center of the fuel slug within the blue shaded fuel filter to the wall of the filter. The temperature at the wall is T_1. Radius r_2 is the distance to the outside of the red shaded thermoelectric elements which includes the stainless steel wall thickness of the fuel filter. The overall length of the fuel filter assembly is H. The temperature at the outer wall of the thermoelectric elements is T_2. The temperature of the green shaded eutectic reservoir and the bulk temperature of the fuel in the filter are T_E and T_0 respectively. The fuel flow rate is $\dot{m}_i$ and $\dot{m}_o$. The temperature of the incoming fuel is T_i, whereas the temperature of the fuel leaving the filter is taken to be the bulk fuel temperature of T_0. The mass of the fuel in the filter is m_o, and has a specific heat of C_f. The convection coefficient for the heat transfer from the wall of the thermoelectric device to the filter matrix is h_o. The thermoelectric elements have a mass of m_{te}, an effective thermal conductivity of k_{te}, a Seebeck coefficient of S, and an effective specific heat of C_{te}. The thermoelectric

element is considered to be composed of the thermoelectric modules and the structural stainless steel wall of the filter. The current supplied to the thermoelectric elements is *I*. The temperature of the fuel slug is assumed to be uniform and that the fuel soaked filter paper does not differ significantly, in its physical properties, from the rest of the fuel in the filter. Also, the temperature of the fuel exiting the filter is assumed to equal to the bulk temperature of the fuel filter. In all following model development the standard heat in positive work in negative sign convention is used.

To begin the derivation of the model equations the conservation of mass will be examined. It is assumed that the change of the mass of fuel in the fuel filter, m_o is equal to zero, which leads to the fact that $\dot{m}_i$ is equal to $\dot{m}_o$.

$$\frac{dm_0}{dt} = \sum \dot{m}_i - \sum \dot{m}_e = 0 \qquad \dot{m}_i = \dot{m}_o = \dot{m} \tag{21}$$

Next, the conservation of energy for the fuel slug will be examined. The basic energy equation is given by:

$$\frac{dE_0}{dt} = \dot{Q}_0 - \dot{W}_0 + \dot{m}\left(h_{0i} + \frac{V_{0i}^2}{2} + gz_{0i} \right) - \dot{m}\left(h_{0e} + \frac{V_{0e}^2}{2} + gz_{0e} \right) \tag{22}$$

Several simplifying assumptions will now be made. The first assumption is that the height difference between the inlet and outlet is negligible that is that $z_i = z_e$. Also the velocities at the inlet and outlet are assumed to be equal, $V_i = V_e$, as the fuel flow velocity into the filter is approximately the same as the fuel flow velocity flowing out of the filter to be burned in the engine. As there is no shaft or boundary work and therefore $\dot{W}_0$ is assumed to be zero. Finally as there is no change in kinetic or potential energy within the fuel slug, dE_0/dt is assumed to be entirely due to the change in the internal energy U_0 with

respect to time. Applying these assumptions to Equation 22 will yield the simplified equation:

$$\frac{dU_0}{dt} = \dot{Q}_0 + \dot{m}\left(h_{0i} - h_{0e}\right) \tag{23}$$

It will now be assumed that the fuel is incompressible. Equation 23 can be simplified, using the specific heat of the fuel, to:

$$m_0 C_f \frac{dT_0}{dt} = \dot{Q}_0 + \dot{m} C_f \left(T_i - T_0\right) \tag{24}$$

Now the heat term $\dot{Q}$ will be expanded. The heat input to the system consists of two parts. The first is the heat forced in by the thermoelectric elements and is equal to the Peltier coefficient, π_p, multiplied by the current supplied, *I*, to the thermoelectric elements, this heat is taken to be part of this equation as heat is absorbed and desorbed at the junction. It is possible that it would be more correct to treat it as temperature term in the thermoelectric model, but the forcing nature of this term was desirable. The second is the heat convected from the surface at r_1. The Peltier coefficient, π_p, is assumed to vary linearly with the temperature of the thermoelectric elements with a constant Seebeck coefficient assumed. The temperature of the thermoelectric elements is taken to be the average of T_1 and T_2. These manipulations will yield the final fuel slug model shown in Equation 25. It should be noted that slug flow is still a type of lumped parameter approach, however the Biot number is not a concern for this type of model.

$$m_0 C_f \frac{dT_0}{dt} = h_0 \left(2\pi r_1 H\right)\left(T_1 - T_0\right) + \frac{S}{2}\left(T_1 + T_2\right)I + \dot{m} C_f \left(T_i - T_0\right) \tag{25}$$

With a mathematical model for the fuel slug obtained, a model for the combined thermoelectric elements and fuel filter wall must be obtained. The conservation of mass is trivial as this is a solid. The conservation of energy is given by:

$$\frac{dE_{te}}{dt} = \dot{Q}_{te} - \dot{W}_{te} + \dot{m}_{te}\left(h_{tei} + \frac{V_{tei}^2}{2} + gz_{tei}\right) - \dot{m}\left(h_{tee} + \frac{V_{tee}^2}{2} + gz_{tee}\right) \tag{26}$$

Several assumptions will now be made. As mentioned above there is no mass flow associated with the thermoelectric elements and there is no associated work. As with the fuel slug, it is assumed that there is no change in the kinetic or potential energy of the system. Thus:

$$\frac{dU_{te}}{dt} = \dot{Q}_{te} \tag{27}$$

The thermoelectric model is a solid so there is no pressure or volume change. The internal energy is assumed to be related to the average of the two wall temperatures T_1 and T_2. This yields the following equation:

$$\frac{m_{te}C_{te}}{2}\frac{d(T_1 + T_2)}{dt} = \dot{Q}_{te} \tag{28}$$

The thermoelectric elements are moving heat into and out of the eutectic reservoir during system operation. Due to the unique melting point of the eutectic reservoir, the heat will be removed and added during the eutectic compound's phase change. This means that it can be assumed that the eutectic reservoir temperature T_E is constant. A further assumption will be made that the outer wall temperature T_2 is constant and remains at the temperature T_E throughout operation. This simplifies the thermoelectric model to:

$$\frac{m_{te}C_{te}}{2}\frac{dT_1}{dt} = \dot{Q}_{te} \tag{29}$$

The next step is to expand the heat term for the thermoelectric elements. The elements lose heat that is convected away into the fuel slug. Additionally heat conducts from the surface at r_2 to the surface r_1. This term is necessary for the system to behave correctly with no supplied heat. For this conduction, for simplicity, it is assumed that the wall thickness given by the difference between r_2 and r_1 is small enough that radial effects are minimal. This term also assumes that the temperature profile within the thermoelectric elements is linear in nature. The surface area for the conduction is taken to be at the middle of the wall thickness, $(r_1+r_2)/2$. Finally the operation of the thermoelectric elements produces joule heating, which is equal to the electrical resistance of the thermoelectric elements, R_{te}, multiplied by the square of the current supplied, I, to the elements. Thus the final thermoelectric model is given by:

$$\frac{m_{te}C_{te}}{2}\frac{dT_1}{dt} = I^2 R_{te} - h_0\left(2\pi r_1 H\right)\left(T_1 - T_0\right) + k_{te}\frac{(\pi)(r_1 + r_2)H\left(T_2 - T_1\right)}{\left(r_2 - r_1\right)} \qquad (30)$$

2.4. Beta Plant Simulink© Model

The two models, based on Equations 25 and 30, are now ready to be implemented into a single Simulink© model. To begin, Simulink© will be used to implement the *beta* plant model in a manner that will allow the *beta* plant to be validated. The *beta* plant validation model is shown in Figure 9.

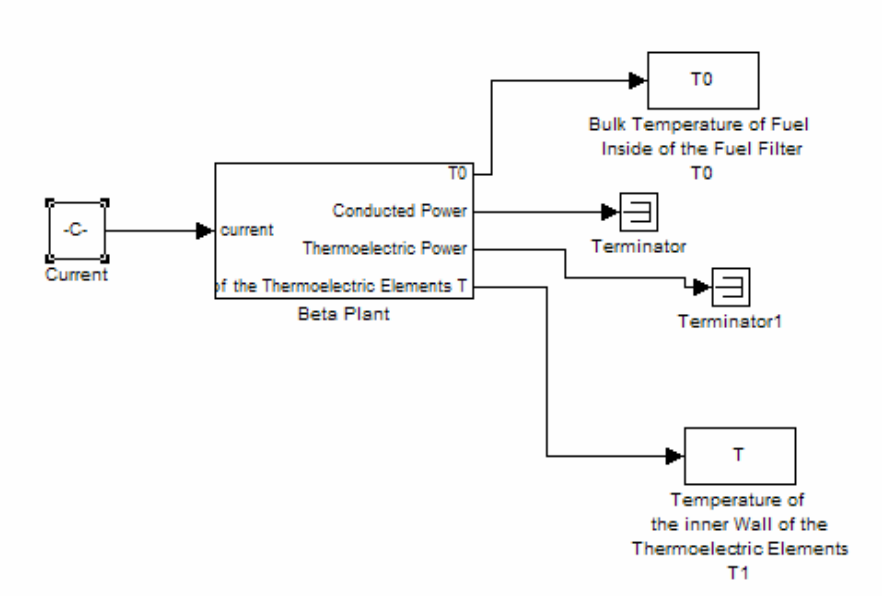

Figure 9: *Beta* Plant Simulink© Model

As can be seen the *beta* plant model takes a single input, which is the current and has four outputs. The outputs are the temperatures T_0, and T_1, and two parameters for supervisory control law purposes which are the conducted power and the thermoelectric power. The *beta* plant model itself is contained within the *beta* plant subsystem block is. The *beta* plant subsystem is shown in Figure 10. To remain within Simulink© nomenclature and to clarify, the Simulink© model containing the *beta* plant subsystem Simulink© block will be referred to as simply the *beta* plant model. The subsystem block is referred to as the *beta* plant subsystem.

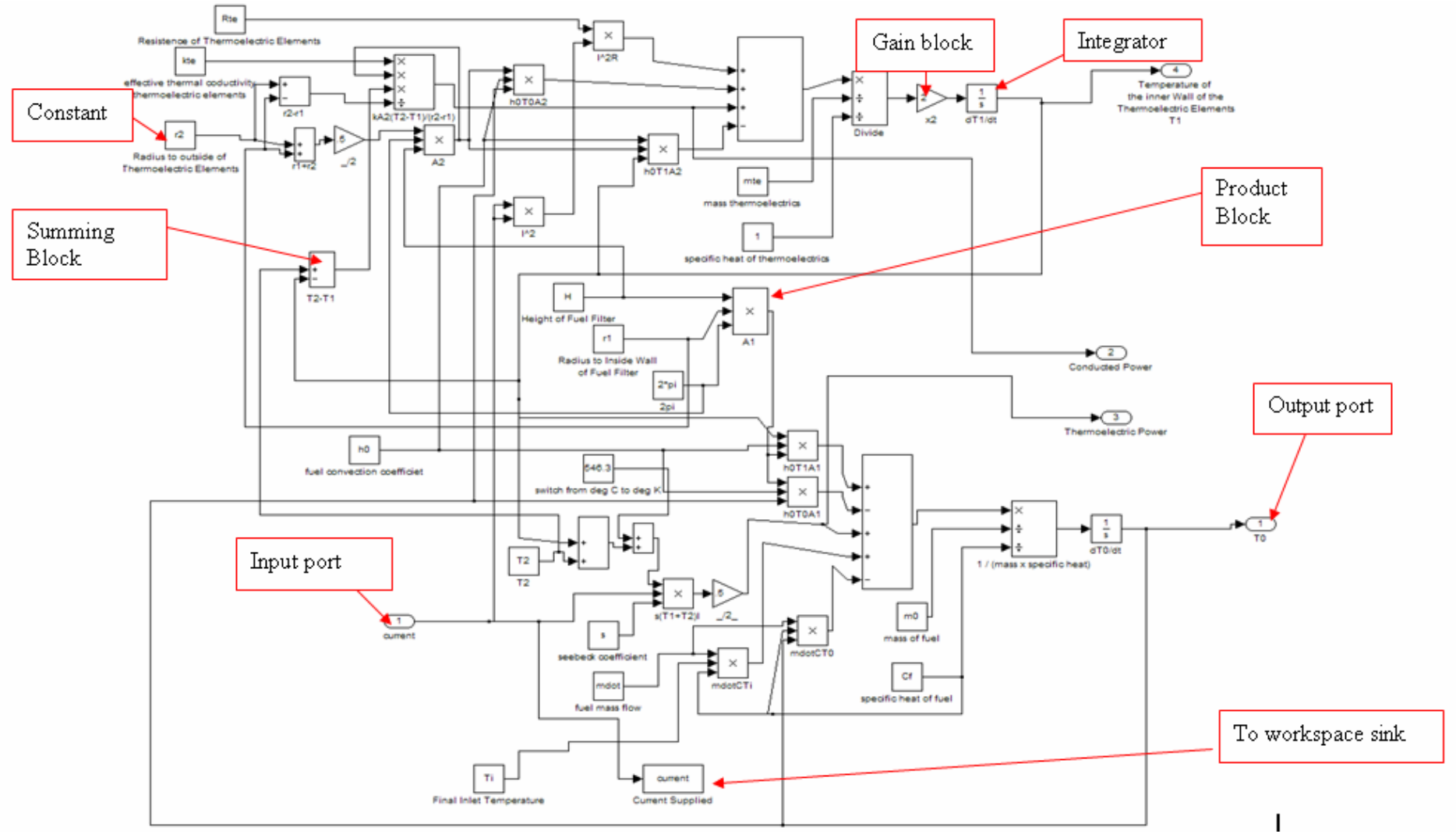
Gain block
Integrator
Constant
Product Block
Summing Block
Output port
Input port
To workspace sink
Rte
Resistance of Thermoelectric Elements
kte
effective thermal coductivity thermoelectric elements
r2
Radius to outside of Thermoelectric Elements
I^2R
h0T0A2
A2
h0T1A2
I^2
mte
mass thermoelectrics
specific heat of thermoelectrics
Divide
x2
dT1/dt
Temperature of the inner Wall of the Thermoelectric Elements T1
T2-T1
H
Height of Fuel Filter
r1
Radius to Inside Wall of Fuel Filter
2*pi
2pi
A1
Conducted Power
Thermoelectric Power
h0
fuel convection coefficiet
546.3
switch from deg C to deg K
h0T1A1
h0T0A1
T2
current
seebeck coefficient
mdot
fuel mass flow
mdotCTi
mdotCT0
m0
mass of fuel
Cf
specific heat of fuel
1 / (mass x specific heat)
dT0/dt
T0
Ti
Final Inlet Temperature
current
Current Supplied

Figure 10: *Beta* Plant Subsystem Simulink© Model

To begin the detailed discussion of the *beta* plant model a brief overview of block types will be useful in understanding the model. The various block types are labeled in Figure 10. The input port passes data from the overall system to the subsystem, in the *beta* plant subsystem model there is one input port, which passes the current supplied to the thermoelectric modules to the *beta* plant subsystem from the *beta* plant overall system model. The output ports pass data from the subsystem to the overall system. The *beta* plant subsystem has four output ports corresponding to the values of T_0, T_1, conducted power, and thermoelectric power. The input ports and the output ports, within the *beta* plant subsytem match up one to one with the input and the outputs on the *beta* plant subsystem block in the *beta* plant model, Figure 9. There are several constant blocks in the *beta* plant subsystem, Figure 10. Their purpose is to supply a constant value to the model. In most cases, this constant relates to one of the physical parameters of the model. The exceptions are the `2pi` block and the `switch to degree K` constant blocks. Those blocks supply a constant value of 2π for circumference calculations, and the value of *2*273.15* to switch the temperatures for the actual Peltier coefficient, π_p, calculation to degrees Kelvin from degrees Centigrade. There are two integrator blocks in the *beta* plant subsystem. Each one integrates its input to produce the appropriate temperature either T_0 or T_1. There are several product blocks in the model which simply multiply their inputs together. Additionally, there are several summing blocks in the model, which sum their inputs and output the sum. The gain blocks simply multiply the input by a constant value. Finally, there is a single to workspace sink block, which records the value and reports it to the Matlab© workspace for recording.

To begin the construction of the *beta* plant subsystem the fuel slug model, Equation 25, and the effective thermoelectric model, Equation 30, are both manipulated such that the temperature derivative terms are alone on the left hand side of the equation and they have no coefficient. The manipulated equations are shown as Equations 31 and 32, respectively.

$$\frac{dT_0}{dt} = \frac{1}{m_0 C_f}\left[h_0 (2\pi r_1 H)(T_1 - T_0) + \frac{S}{2}(T_1 + T_2) I + \dot{m} C_f (T_i - T_0) \right] \tag{31}$$

$$\frac{dT_1}{dt} = \frac{2}{m_{te} C_{te}}\left[I^2 R_{te} - h_0 (2\pi r_1 H)(T_1 - T_0) + k_{te} \frac{(\pi)(r_1 + r_2) H (T_2 - T_1)}{(r_2 - r_1)} \right] \tag{32}$$

Then two integrator blocks are placed in the subsystem model. Each one corresponds to either the dT_0/dt fuel slug equation or the dT_1/dt effective thermoelectric equation. In this model, the fuel slug integrator is on the bottom right and the effective thermoelectric integrator is on the top right of Figure 10. The integrator blocks input is dT_0/dt or dT_1/dt and thus corresponds to the left hand sides of the previously manipulated equations. The output of the integrators as mentioned above is a temperature. Next, two product blocks are placed which allow for the common multiplying factor on the right to be multiplied by some input. This input is constructed through the use of the two large summing blocks. Finally the constant blocks are placed allowing for the inputs to the large summing blocks to be wired to various constants, summing, and product blocks to produce the terms on the two right hand sides of Equations 31 and 32.

Now that the *beta* plant model has been obtained, it is useful to discuss how the parameters used in the model were obtained. A list of the model parameters along with the reference from where they were obtained is shown in Table 1.

Table 1: Model Parameters

Variable	Value	Units	Source
h_0	5	W/m^2K	Assumed
T_i	60	℃	[16]
H	0.1524	m	Physical Filter Measurements
r_1	0.0508	m	Physical Filter Measurements
r_2	0.0524	m	Physical Filter + assumed 1/8 inch wall thickness
R_{te}	1953	ohms	[34]
T_2	40	℃	Assumed equal to T_e which is specifiable
k_{teeff}	15.06	w/mk	Equation 35
$m0$	1.131	kg	[35]
$\dot{m}$	0.0024	kg/s	[36]
mte	0.6374	kg	[37]
S_{eff}	0.5074	V/K	Equation 34
C_f	2890	J/kgK	[37]
Cte	489.4	J/kgK	Equation 33
$thickness$	9.80E-06	m	[34]
$N_{klegpairs}$	1170	-	[38]
S_p	2.54E-04	V/K	[38]
S_n	-1.79E-04	V/K	[38]
k_{te}	0.80	W/mK	[39]
k_{ss}	15.1	W/mK	[37]
T_g	35	℃	Specified parameter
$powerfacto$	26.74E-4	W/mK^2	[38]

The physical dimensions of the system were based on a typical fuel filter, the FF749 fuel filter for a Ford Diesel engine. The wall thickness was assumed to be one eighth of an inch. The fuel's mass, m_0, was calculated by taking the volume of the fuel slug and multiplying it by the density of the fuel [37]. C_f, the specific heat of the fuel, was obtained by assuming that the fuel has a specific heat nearly equal to that of paraffin. The fuel convection coefficient, h_0, was assumed to be approximately $5\ W/mK$. This value is based off of the IIT paper [16] where they determine the convection coefficient within the filter to be $5\ W/m^2K$. The mass flow rate, $\dot{m}$, was obtained by using the

average required miles per gallon for a light diesel truck, an assumed average speed of 55 miles per hour, and the density of the fuel. The final inlet fuel temperature is based upon the IIT paper [16], which states that the operating fuel temperature is *60 °C*. The temperature, T_2, is a specifiable temperature and should be marginally higher than the goal temperature of the fuel, and as mentioned in the above assumption is equal to T_e. The goal temperature was taken as *35 °C*. The *35 °C* goal was chosen to give a factor of safety to the previously stated *16 °C* as the high point for biodiesel flow problems [6]. The effective mass of the thermoelectric elements was determined by adding the mass of the stainless steel and the mass of the thermoelectric elements. To determine the effective specific heat of the thermoelectric elements and the filter wall the following equation was used.

$$C_{te} = \frac{(CV\rho)_{bismuth} + (CV\rho)_{stainless}}{(V\rho)_{bismuth} + (V\rho)_{stainless}} \tag{33}$$

Equation 33, is simply a weighted average where the contribution to the effective specific heat, C_{te}, is based on the mass weighted values of the various constituents. It is assumed that the bismuth telluride thermoelectric elements are mostly bismuth. This does not greatly affect the calculation since the higher mass of stainless steel dominates this term. To determine the rest of the bulk thermoelectric properties the number of thermoelectric leg pairs must be determined. This was done by taking the outside surface area of the fuel filter and multiplying it by an amount of leg pairs known to fit in a given area [38]. This operation yields *1170* leg pairs covering the filter wall surface at r_2. With the total number of leg pairs determined, the effective Seebeck coefficient can be determined by the following formula, wherein S_p and S_n are taken from the literature [38]

$$S_{eff} = \left(S_p - S_n\right) * N_{pairs} \tag{34}$$

The effective thermal conductivity coefficient of the thermoelectric element filter wall combination was determined by taking the resistance of a given density of thermoelectric elements and multiplying it by the area of the outside of the fuel filter wall, r_2. The effective thermal conductivity of the thermoelectric elements and filter wall was determined using the following equation:

$$k_{teeff} = \frac{k_{te} thickness + k_{ss}\left(r_2 - r_1\right)}{\left(r_2 - r_1\right) + thickness} \tag{35}$$

2.5. Beta Plant Simulink© Model Validation

Now that the model parameters have been determined, several limiting cases can be run to begin the model validation and to determine the impact certain parameters have on the model response. In all cases the initial fuel temperature is taken to be *0°C*, additionally in all cases the response is shown for *200 seconds,* additionally in all cases the *beta* plant Simulink© model is used.. The first case is where the model has no mass flow and no current supplied to it. T_0 and T_1 for Case 1 are shown below in Figure 11 and Figure 12.

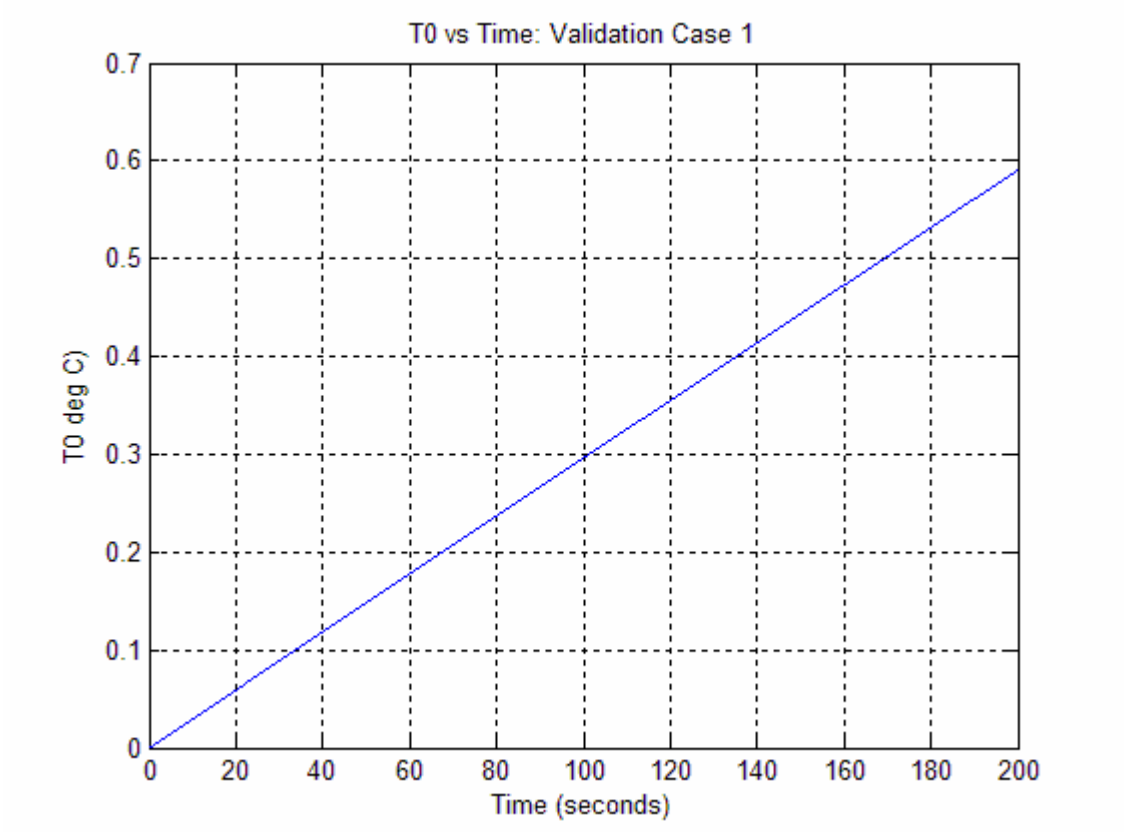

Figure 11: T_0 versus Time: Validation Case 1

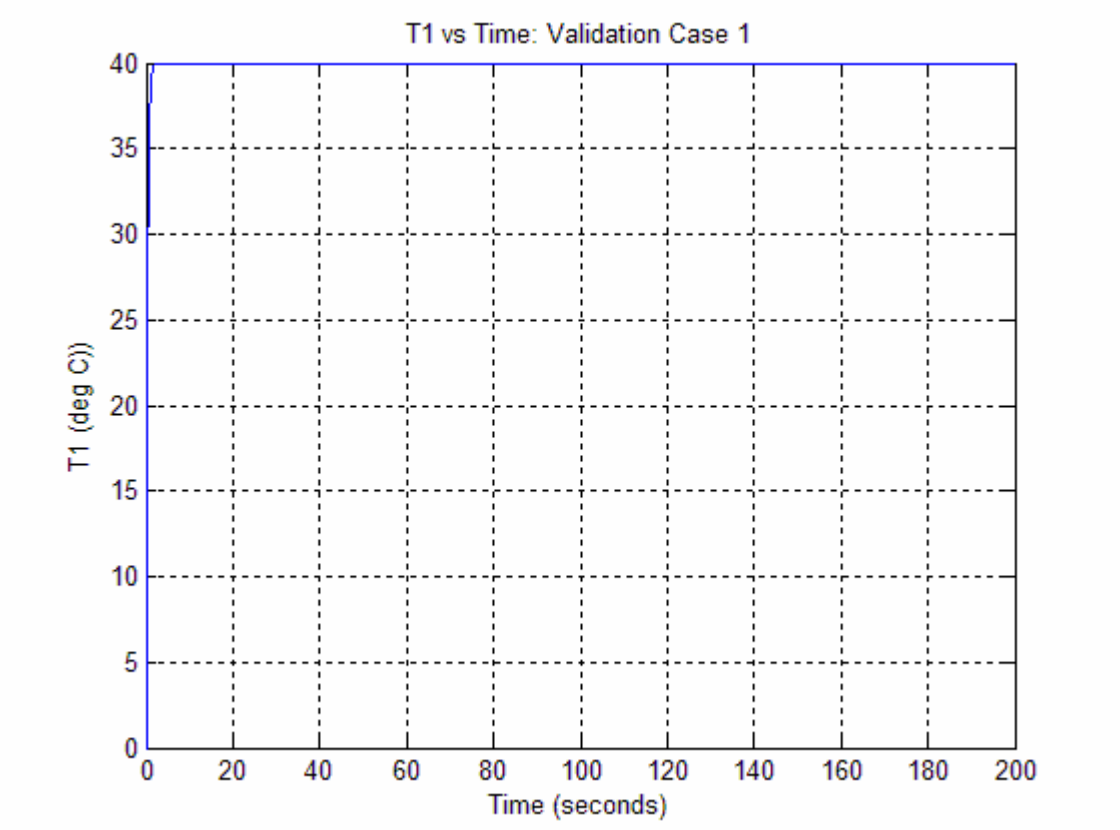

Figure 12: T_1 versus Time: Validation Case 1

As can be seen from Figure 11 the value of T_0 appears to increases linearly from the initial value of *0 °C*. However, it can be seen that this rate of increase is very slow, which shows the necessity of the thermoelectric elements for an adequate response. The value of T_1 increases almost instantly to its steady state temperature of *40 °C*. The linear response of T_0 is anticipated as the heat being transferred into the filter is essentially constant as soon as T_1 reaches steady state since the temperature change in T_0 is so small compared to the difference between T_0 and T_1. This suggests that the conduction term in the thermoelectric model is more dominant in the approach to steady state, than the convection term. To further investigate this phenomenon it is prudent to see what occurs when the conduction term is varied.

Case 1.1 changes the value of k_{te} in an attempt to better illustrate the relationship between the conductivity term and the convection term. Case 1.1 utilizes the same parameters as Case 1 except the effective thermoelectric conductivity, k_{te}, is reduced by a factor of 10 from a value of *15.06 W/mK* to a value of *1.506 W/mK*. Figure 13 shows the time response of T_0 and Figure 14 shows the response of T_1.

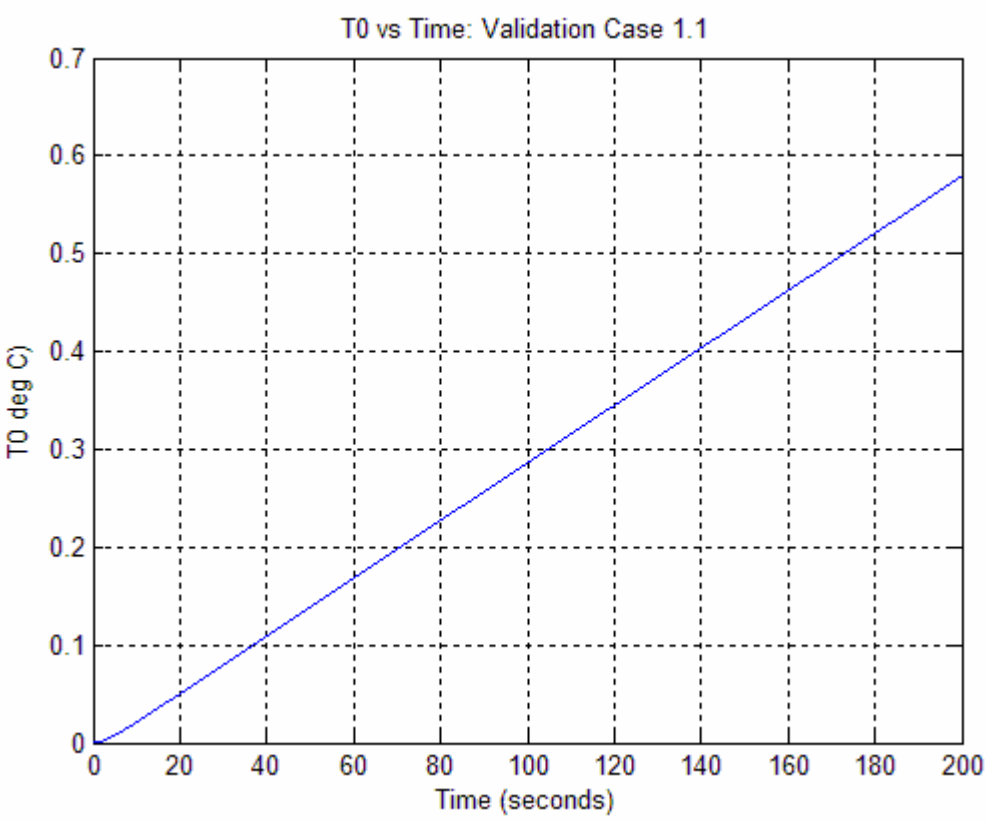

Figure 13: T_0 versus Time: Validation Case 1.1

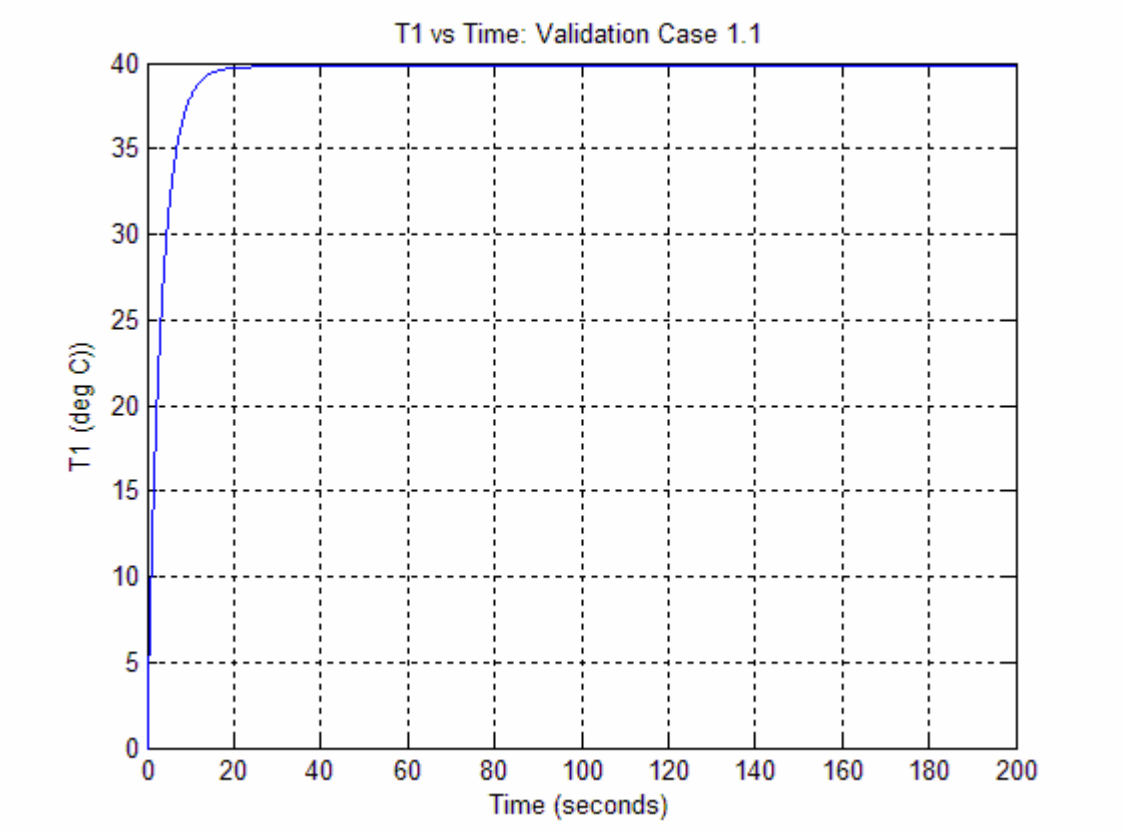

Figure 14: T_1 versus Time: Validation Case 1.1

It can be seen from Figure 14 that this reduction in the thermal conductivity indeed slows down the response T_1 which means that it is likely that the thermoelectric model is largely dominated by the conduction term. It also should be noted that there is a nonlinear portion to the T_0 response while T_1 is approaching steady state that can now be more easily seen in Figure 13.

In Case 1.2 the effective thermoelectric conductivity, k_{te}, is reduced by a further factor of 10 to a value of *0.1506 W/mK*. This changes the response curves of T_0 and T_1 to Figure 15 and Figure 16, respectively.

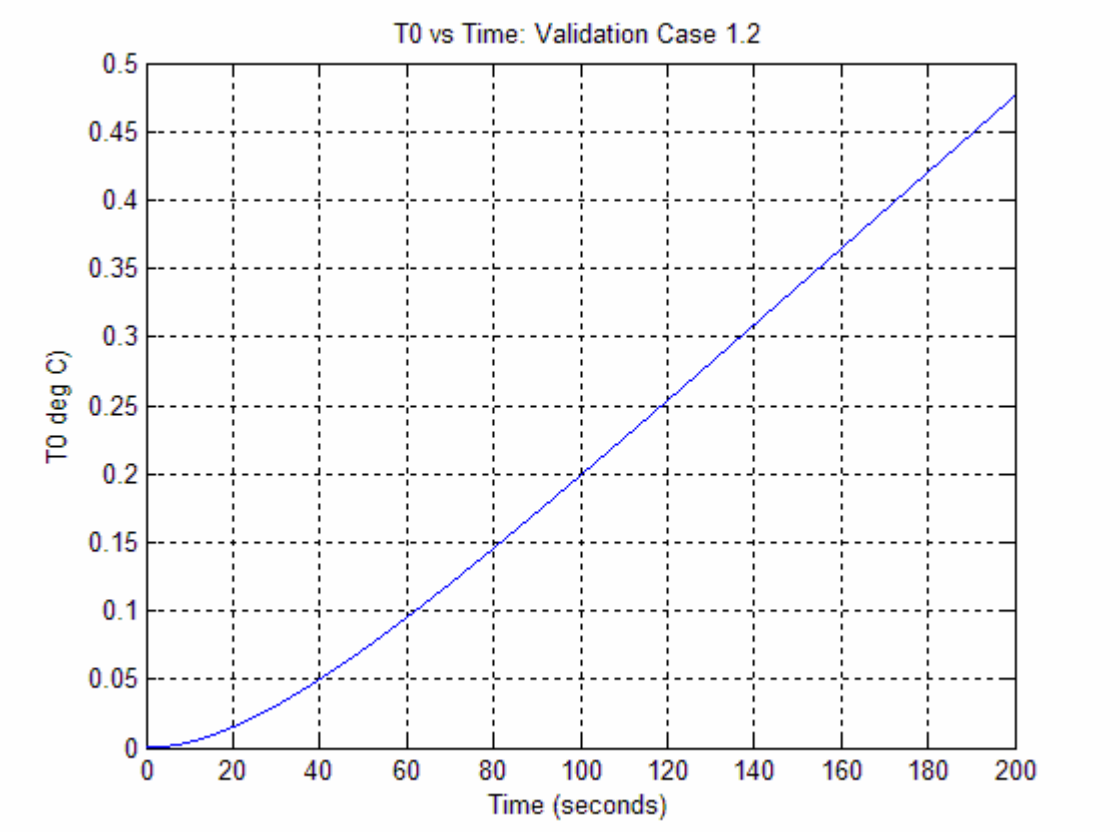

Figure 15: T_0 versus Time: Validation Case 1.2

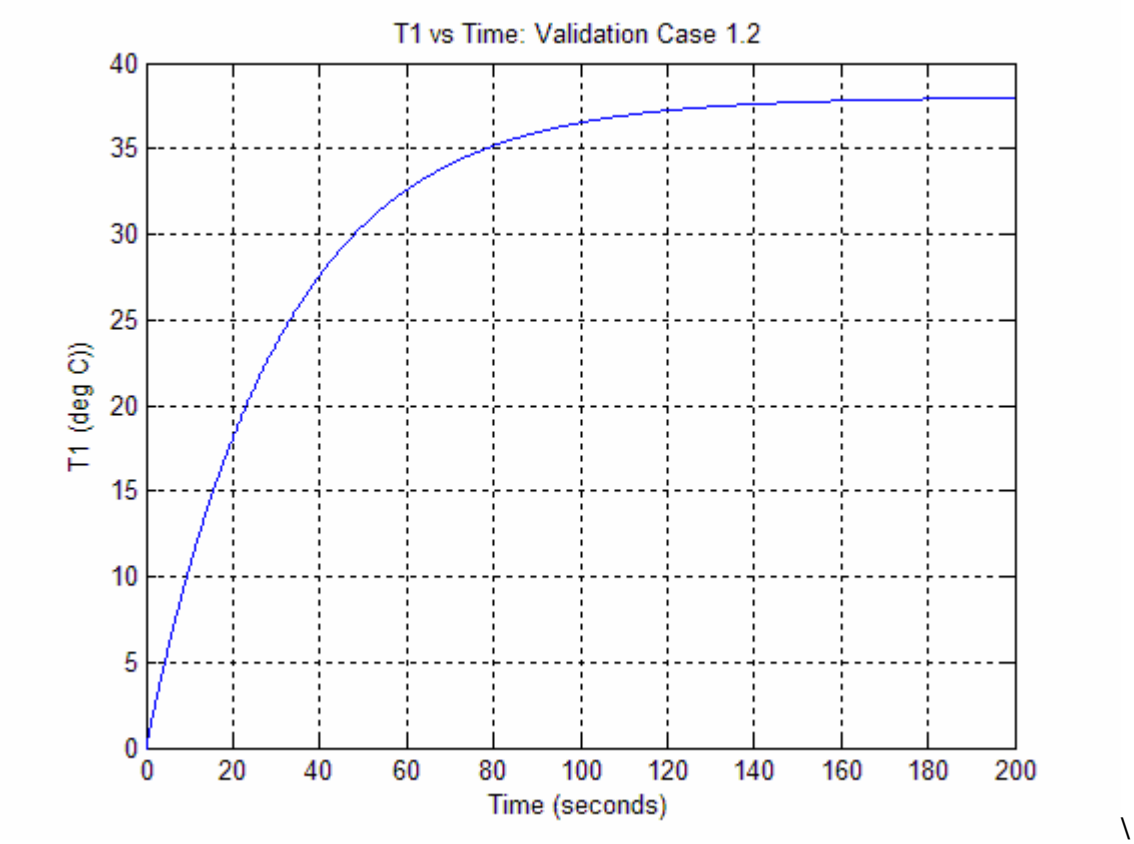

\

Figure 16: T_1 versus Time: Validation Case 1.2

As expected the T_1 response time is now significantly longer and in fact T_1 never completely reaches steady state. The T_0 response curve should also show a larger nonlinear portion at the beginning of the response, which it does.

Finally, to be sure that the conduction term is indeed dominating the model as believed, Case 1.3 increases the effective thermoelectric conductivity,. k_{te} is increased from its original value by a factor of 10 to *150.6 W/mK*. The T_0 and T_1 response curves are shown in Figure 17 and Figure 18, respectively.

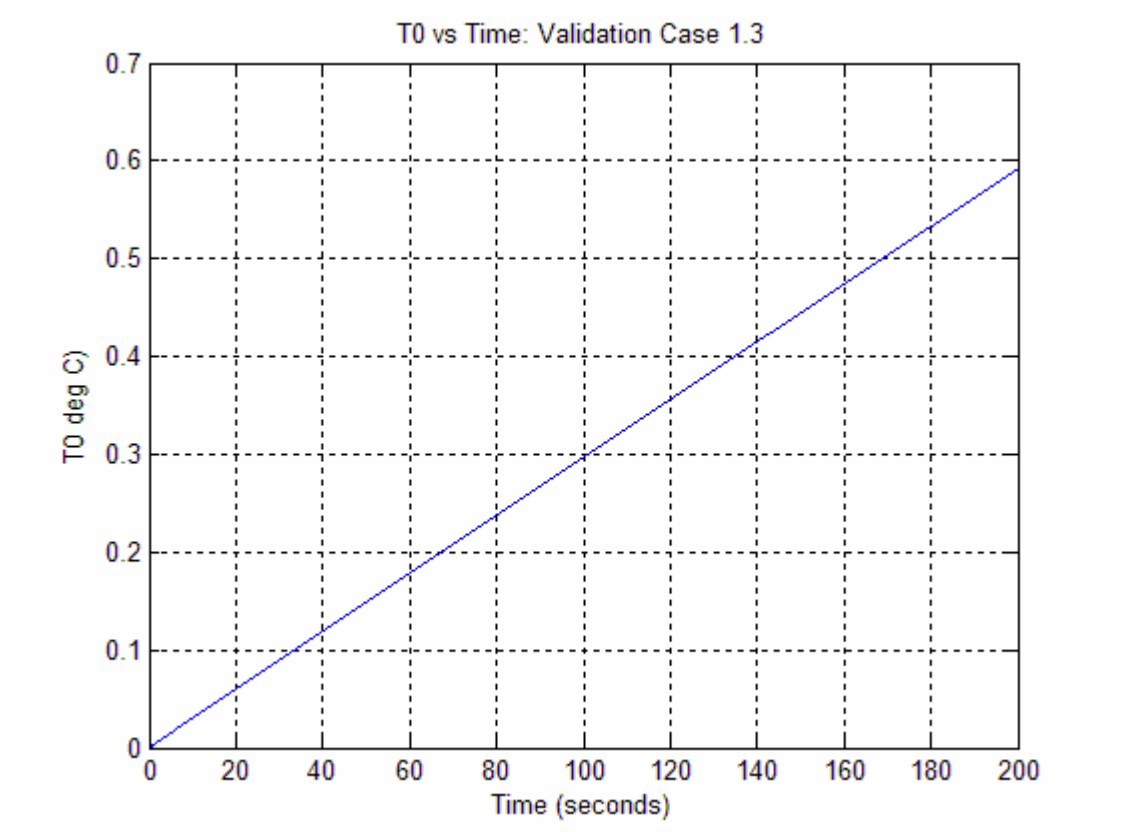

Figure 17: T_0 versus Time: Validation Case 1.3

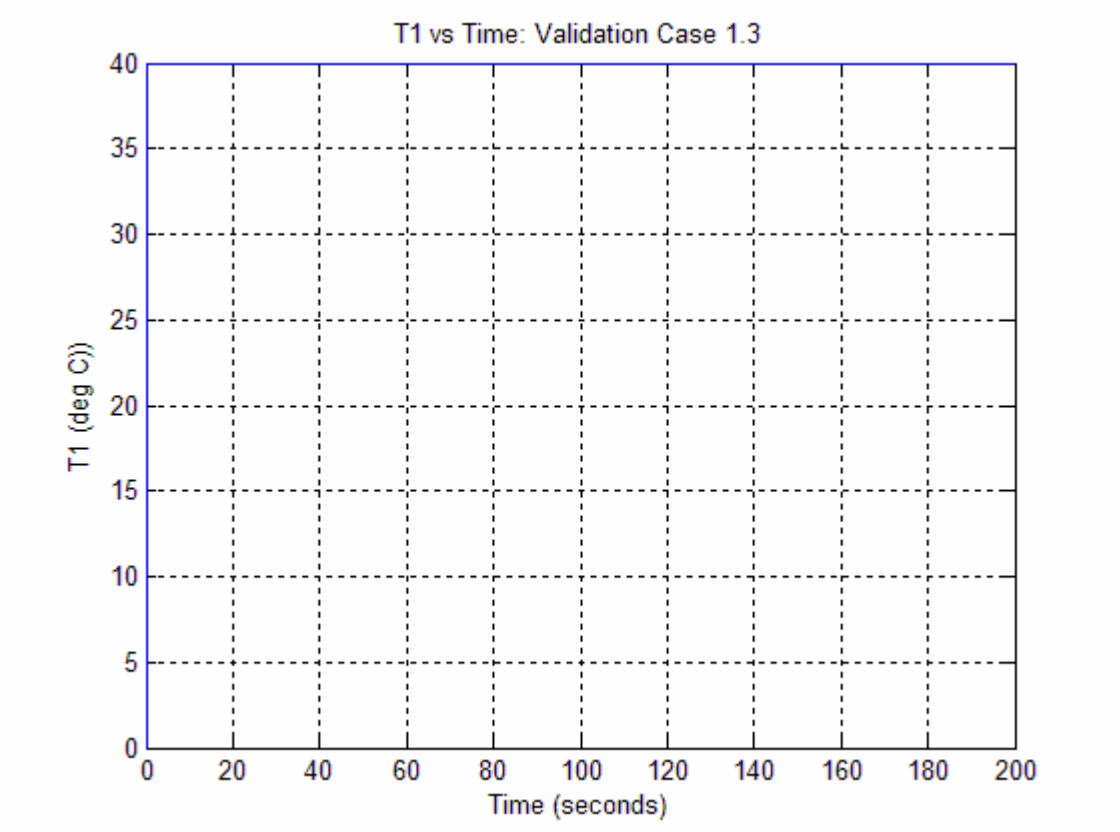

Figure 18: T_1 versus Time: Validation Case 1.3

As expected the T_0 curve now appears to be linear again and the T_1 response appear to reach steady state almost immediately. This means that the effective thermoelectric conductivity, k_{te}, term is large enough that the model reaches steady state very quickly during its operation.

In Case 2 the model still has no mass flow, but the current is increased to one ampere. T_0 and T_1 are shown in Figure 19 and Figure 20, respectively.

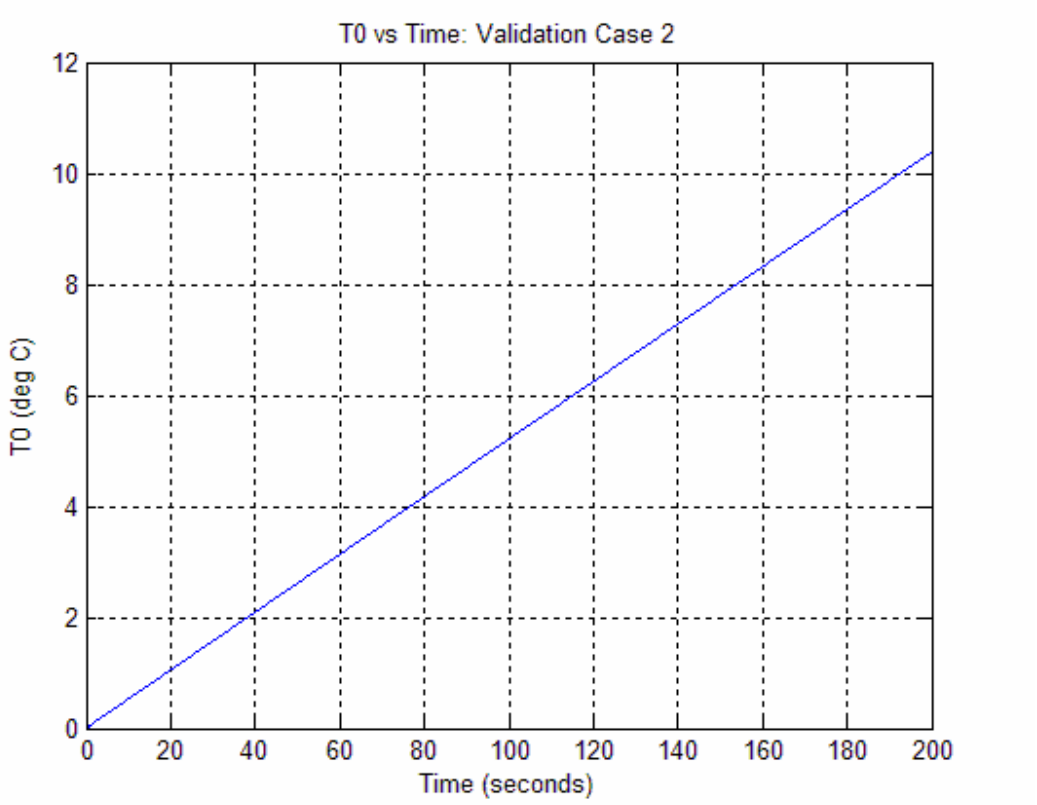

Figure 19: T_0 versus Time: Validation Case 2

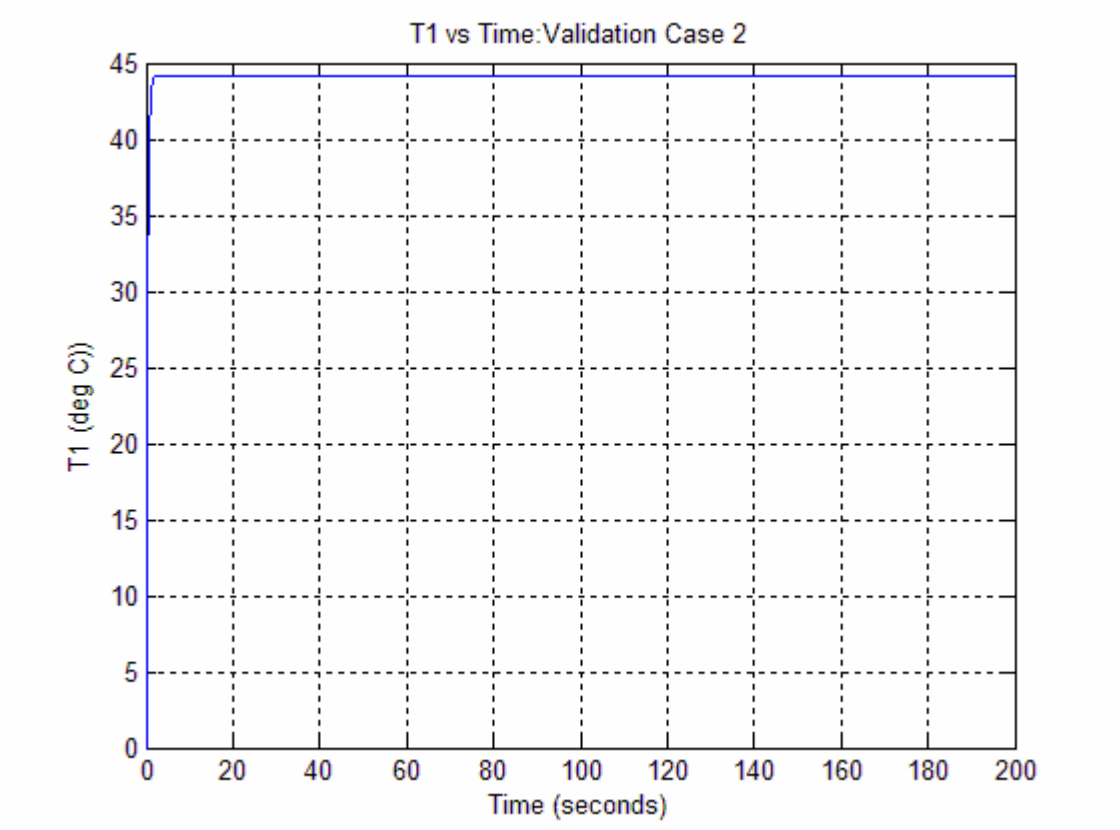

Figure 20: T_1 versus Time: Validation Case 2

The Case 2 T_0 response curve again appears to be linear. This is also expected. As can be seen in Case 1, the heat transfer due only to convection is very small. Therefore, this larger change in temperature is due almost entirely to the heat transfer due to the current supplied to the thermoelectric elements. The T_1 response again shows that the effective thermoelectric element model reaches steady state very quickly. The higher steady state temperature is due to the heat being generated in the thermoelectric elements due to Joule heating. It is expected therefore that if the current were increased, the value of T_0 at the end of *200* seconds should be higher but the response should still be linear. The steady state temperature of T_1 should also be significantly higher.

Case 3 increases the current supplied to the maximum value of six amperes, while maintaining a mass flow rate of *0 kg/s*. T_0 and T_1 are shown below in Figure 21 and Figure 22.

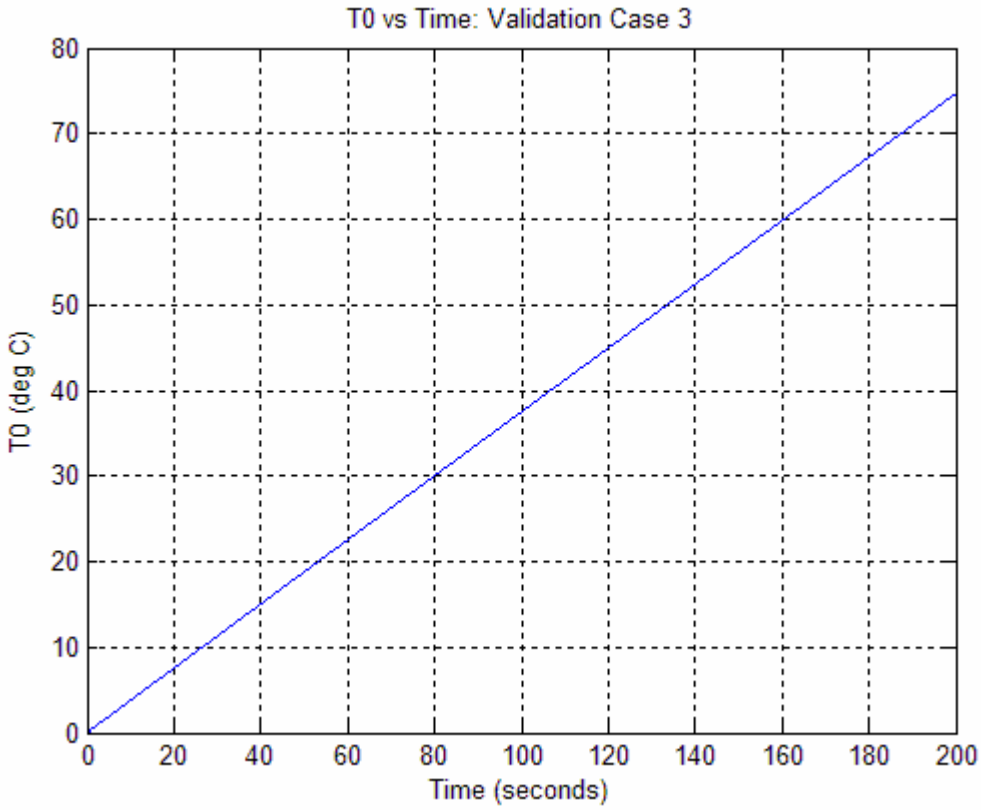

Figure 21: T_0 versus Time: Validation Case 3

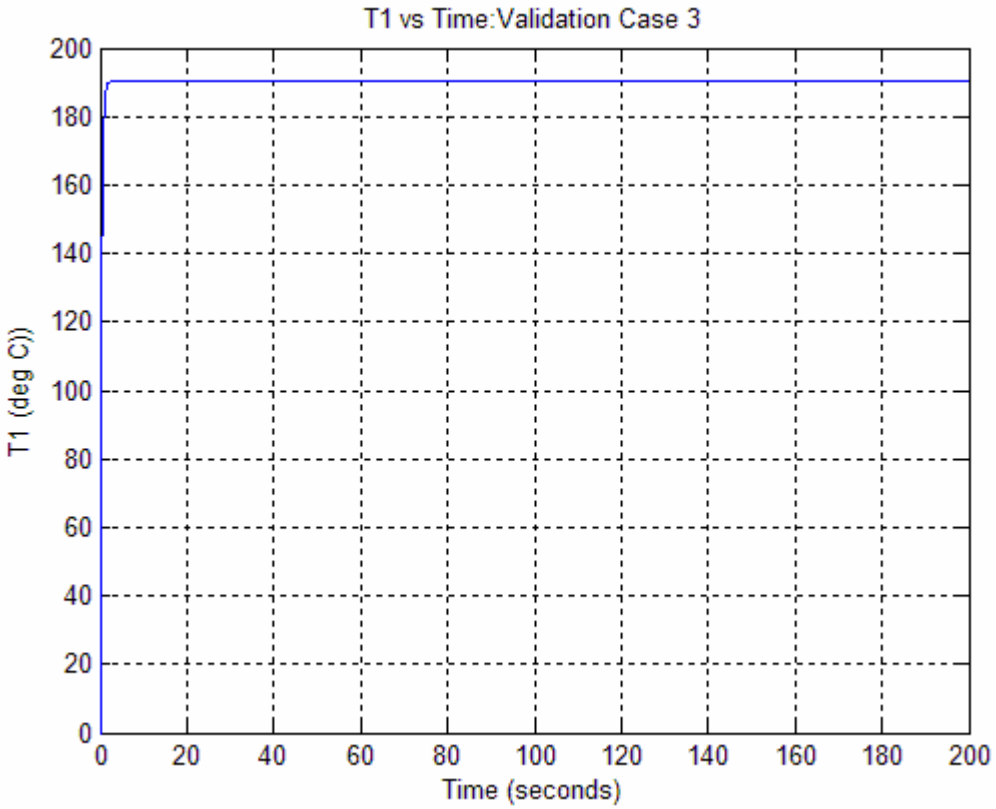

Figure 22: T_1 versus Time: Validation Case 3

The response curve for T_0 as expected shows a much higher increase in temperature with a higher current supplied to the thermoelectric elements model. As expected the steady state temperature of the effective thermoelectric model, T_1, is significantly higher than before. The increase is very large, but this should be expected since the Joule heating increases as the square of the current. The next step is to investigate how the model responds due to heating from the mass flow.

In Case 4 there is no current but the mass flow is increased to the typical engine value when the engine is running of *0.0024 kg/s*. The T_0 and the T_1 response curves are shown below.

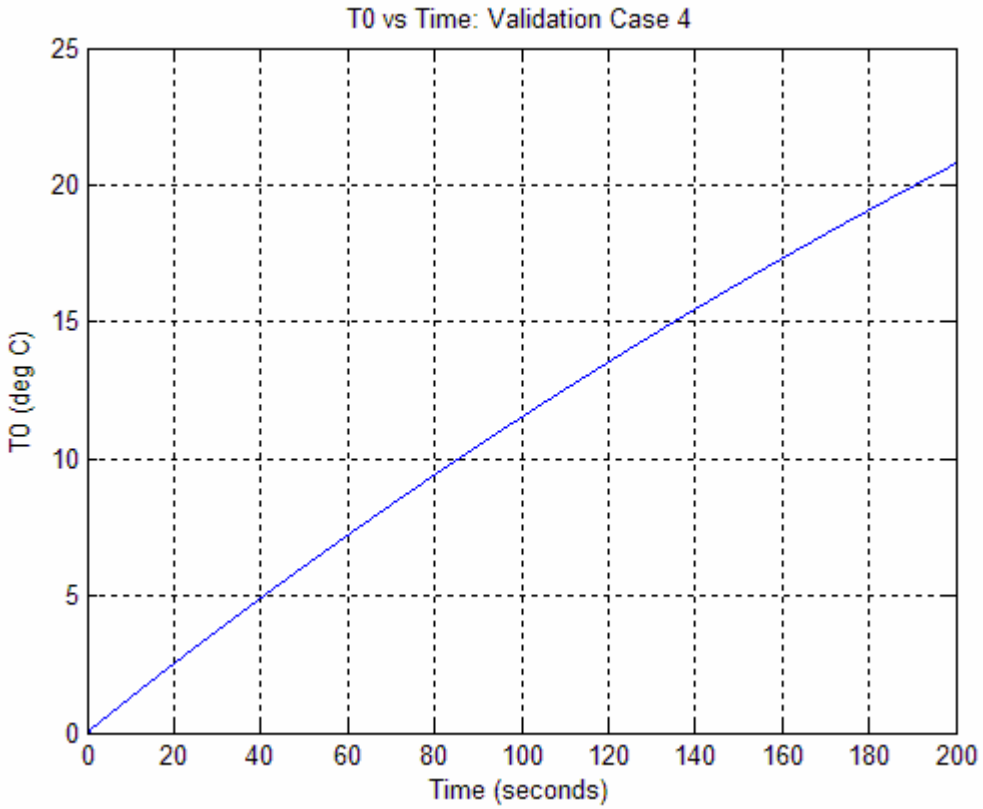

Figure 23: T_0 versus Time: Validation Case 4

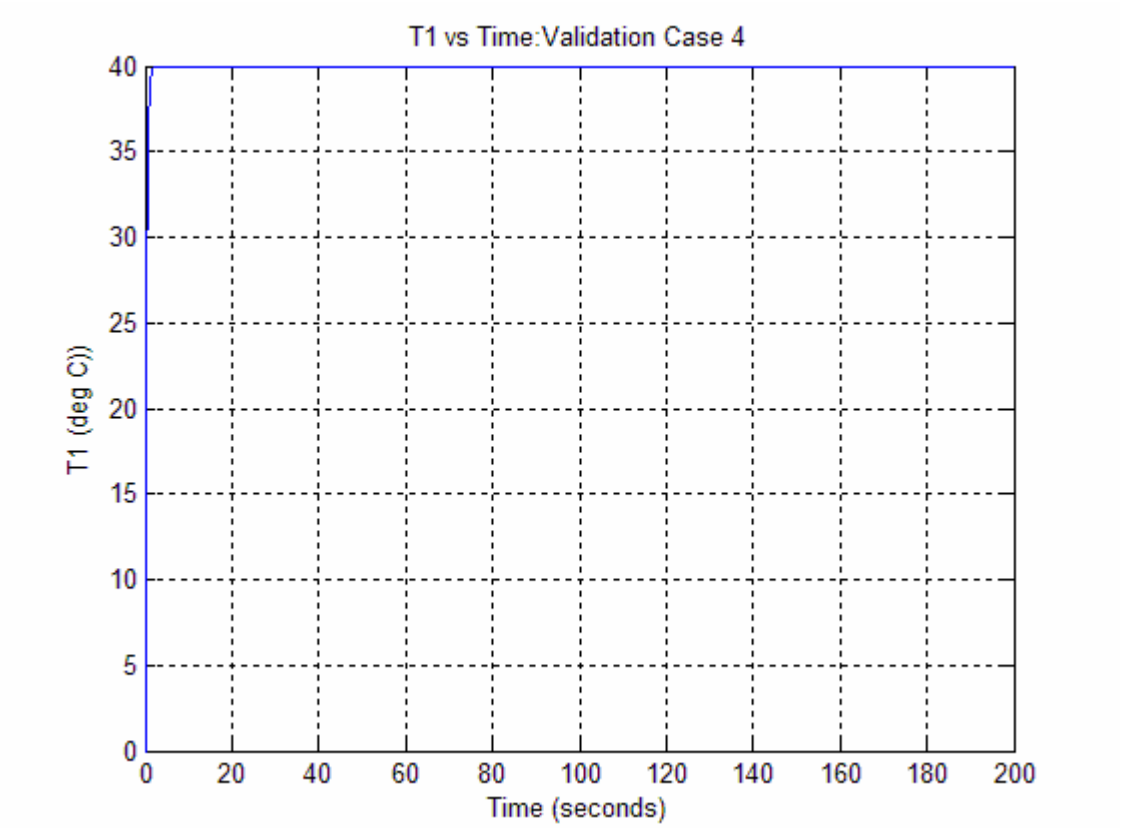

Figure 24: T_1 versus Time: Validation Case 4

The T_0 response appears to be nearly linear again. It is not completely linear, but this is anticipated since as the bulk temperature of the fuel, T_0, increases the heat leaving the filter with the mass flow increases with it. This means that the temperature curve should increase exponentially approaching the inlet temperature of the fuel. It can be seen that the mass flow is bringing significant amounts of heat into the system as the temperature change is greater than that due to heat being convected into the system. To make sure that the fuel temperature T_0 is indeed converging toward the final fuel inlet temperature an additional subcase must be run.

Case 4.1 utilizes the same parameters as Case 4, but the model is run for *1500* seconds. The temperature response curves are shown in Figure 25 and Figure 26, respectively.

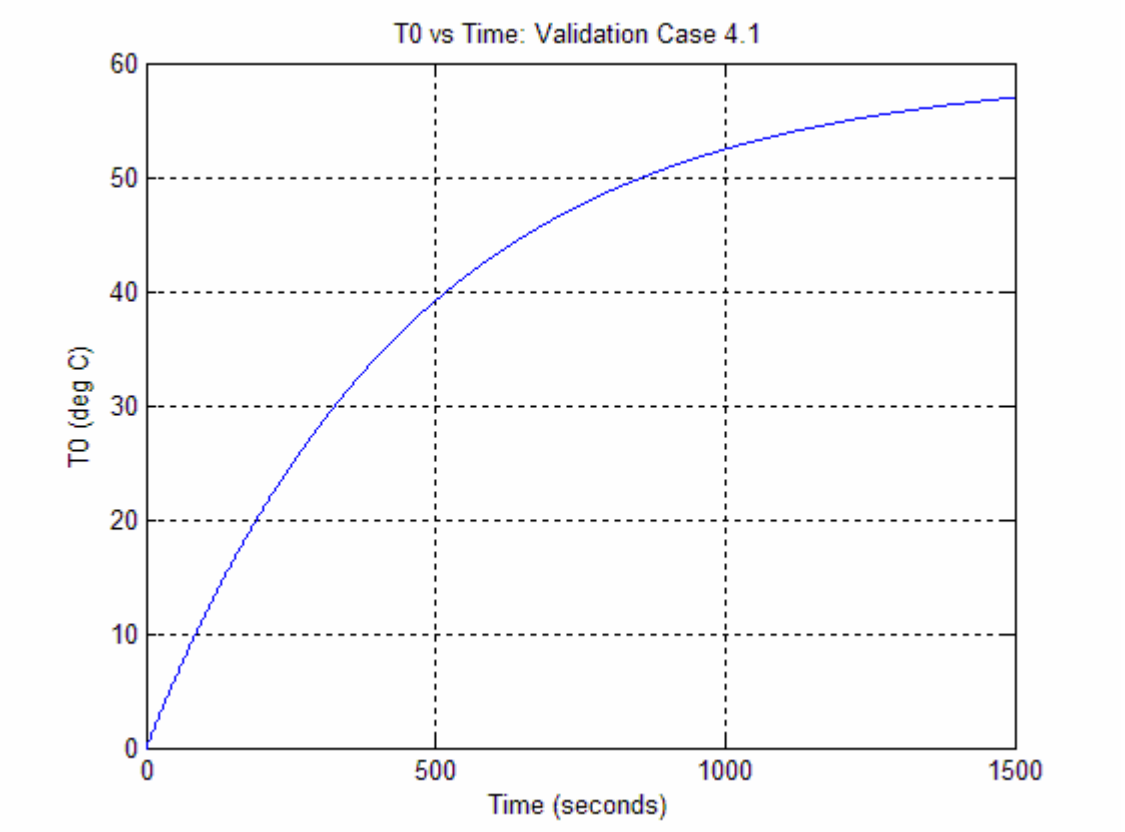

Figure 25: T_0 versus Time: Validation Case 4.1

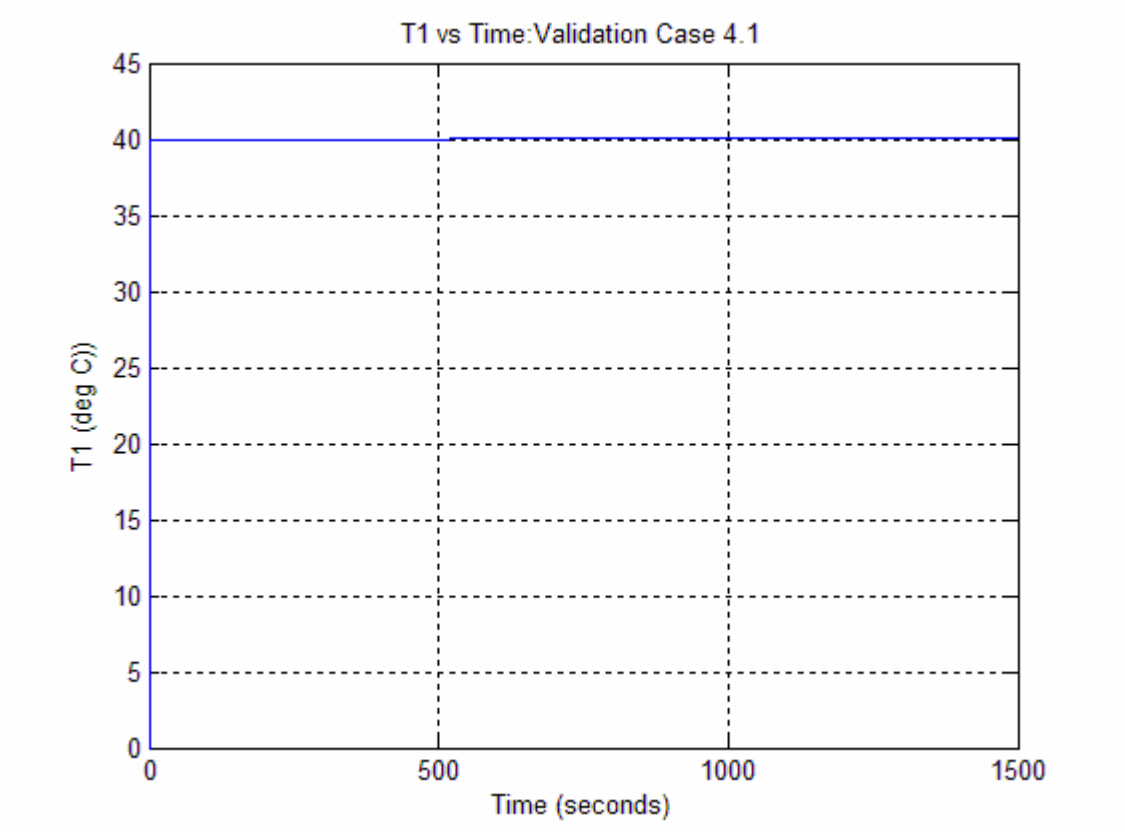

Figure 26: T_1 versus Time: Validation Case 4.1

As expected the T_0 response curve is indeed approaching a temperature of *60 °C*, which is the final inlet temperature of the fuel. It is worth noting here that during true Phase 1 and transition operation the fuel inlet temperature will increase linearly from an initial value equal to the ambient temperature to a value of T_i, which is the final operating temperature of the fuel. The T_1 curve as expected is maintaining its steady state temperature of *40 °C*.

Next, to further validate the *beta* plant model, Case 1 will be solved analytically. To do so, an additional assumption is required. From Figure 12 it can be seen that in Case 1 the temperature, T_1, should be constant once the system reaches steady state which occurs very quickly. Therefore, it will be assumed for the purposes of obtaining an

analytical solution that T_1 is at a constant value, where $T_1 = T_2$, which in turn means that dT_1/dt is equal to *0*. This is essentially assuming there is negligible thermal resistance across the filter wall and thermoelectric elements. This assumption and the Case 1 specification simplify Equation 25 to:

$$m_0 C_f \frac{dT_0}{dt} = h_0 (2\pi r_1 H)(T_2 - T_0) \tag{35}$$

Now the terms will be rearranged to move all T_0 terms to the left hand side of the equation, also the equation will be divided by $m_0 C_f$ to make the coefficient of the dT_0/dt term *1*. These manipulations yield:

$$\frac{dT_0}{dt} + \frac{h_0 (2\pi r_1 H)}{m_0 C_f} T_0 = \frac{h_0 (2\pi r_1 H)}{m_0 C_f} T_2 \tag{36}$$

This is a non separable first order ordinary differential equation. Of the form:

$$\frac{dy}{dx} + p(x)y = q(x) \tag{37}$$

Where:

$$\frac{dy}{dx} = \frac{dT_0}{dt}$$

$$p(x) = \frac{h_0 (2\pi r_1 H)}{m_0 C_f}$$

$$y = T_0$$

$$q(x) = \frac{h_0 (2\pi r_1 H)}{m_0 C_f} T_1$$

and

$$u = e^{\int p(x)dx}$$

The solution is then:

$$y = \frac{\int uq(x)dx + C}{u} \tag{38}$$

Substituting and integrating yields the analytical solution to Case 1:

$$
\begin{aligned}
u &= e^{\frac{h_0(2\pi r_1 H)}{m_0 C_f}t} \\
T_0 &= T_1 + \frac{C}{e^{\frac{h_0(2\pi r_1 H)}{m_0 C_f}t}} \\
@\, t = 0, T_0 &= 0 \\
0 &= T_1 + C \\
\therefore C &= -T_1 \\
T_0 &= T_1 - T_1 e^{-\frac{h_0(2\pi r_1 H)}{m_0 C_f}t}
\end{aligned}
\tag{39}
$$

A preliminary check for the model is checking the following condition: as t $\rightarrow\infty$ T_0 should approach T_1, which it does by inspection. The analytical solution was implemented in Excel©, and a graph was produced showing the analytical value of T_0 versus time and is shown in Figure 27.

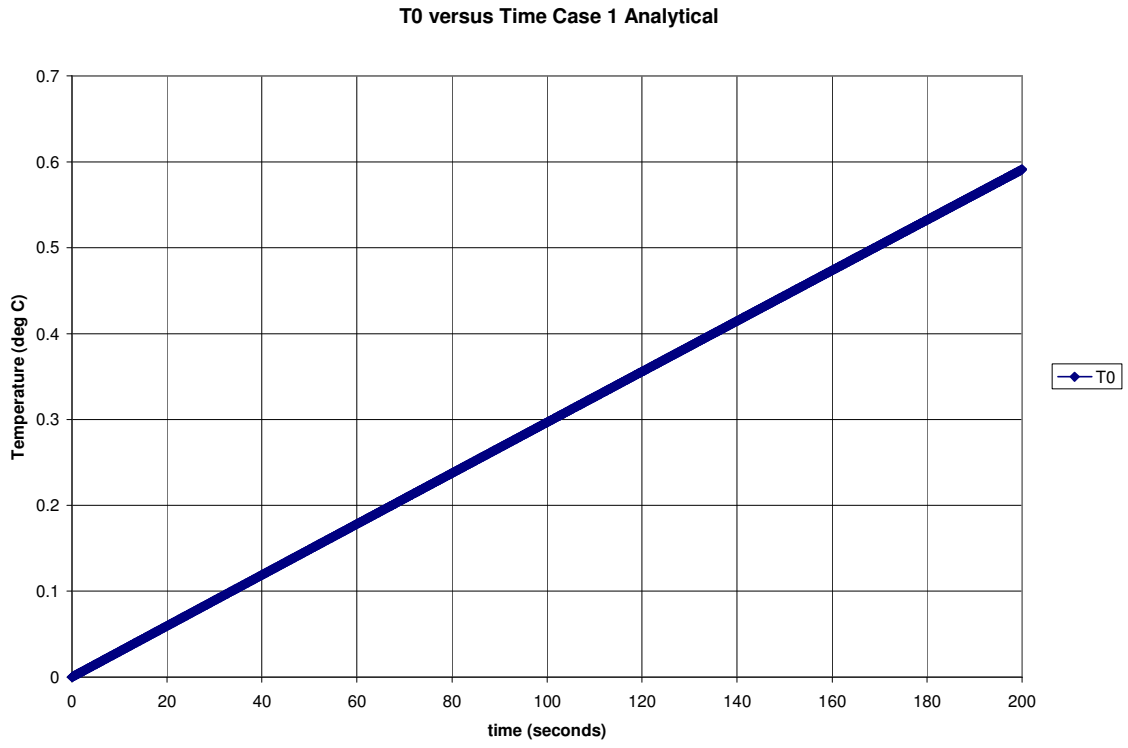

Figure 27: T_0 versus Time: Validation Case 1 Analytical

The analytical solution appears to match the Case 1 model very closely showing the linear approach to a temperature, T_0, of approximately *0.6 °C*. The actual computed values of the value of T_0 at $t = 200$ are *0.5899 °C* and *0.5911 °C* for the Case 1 and Case 1 analytical models respectively. This is a 0.2% difference over 200 seconds. This suggests that the Simulink© model is accurately depicting the system behavior. It should be noted that the analytical model should be slightly higher since it takes a few seconds for T_1 to actually reach steady state.

2.6. Beta Plant Simulink© Model Sensitivity

Next, the sensitivity of the *beta* plant model to various parameters will be examined. The parameters to be examined are h_0, R_{te}, T_E (and by extension T_2), and S_{eff}. The temperature of the eutectic reservoir, and therefore T_2, the resistance of the thermoelectric elements, and the effective Seebeck coefficient will be examined as they are directly changeable model parameters. The parameter, h_0, will be examined as it is the most uncertain of the physical parameters as it is based on a related fuel filter's measured convection coefficient. Each will be examined using the validation case that most appropriately represents that particular mode having the most impact. Therefore h_0 and T_E will be examined using Case 1, where the only method of heat transfer is based on conduction through the effective thermoelectric model and then convection into the fuel slug model. R_{te} will be examined using Case 3, where the joule heating occurring is maximized due to the squared nature of the joule heating term versus the linearity of the

thermoelectric heating term.. S_{eff} will be examined using Case 2, which is the case where joule heating is minimized, but current is still supplied.

The first parameter to be examined is h_0. The nominal model value of h_0 is *5 W/mK*. To examine the performance first Case 1 was run with h_0 reduced to a value of *2.5 W/mK*. The temperature graphs for T_0 and T_1 for the parameter sensitivity are shown in Figure 28 and Figure 29.

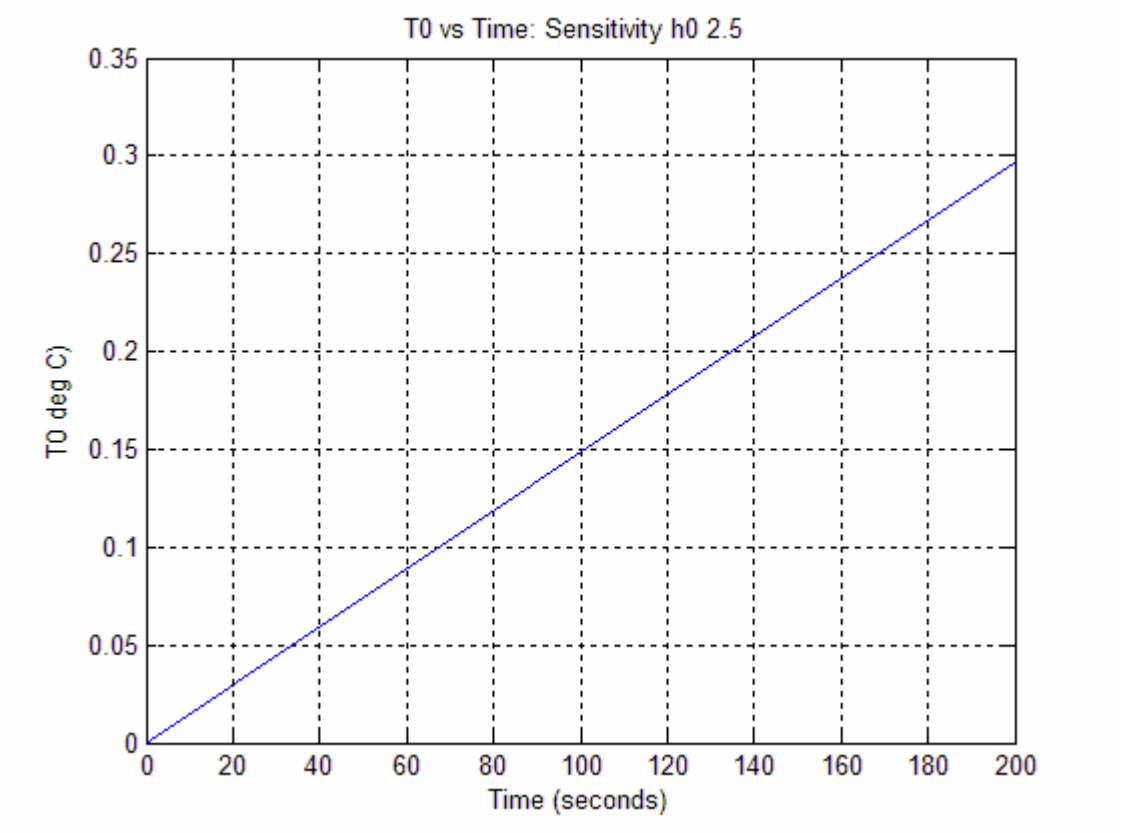

Figure 28: T_0 versus Time: Sensitivity h_0 2.5

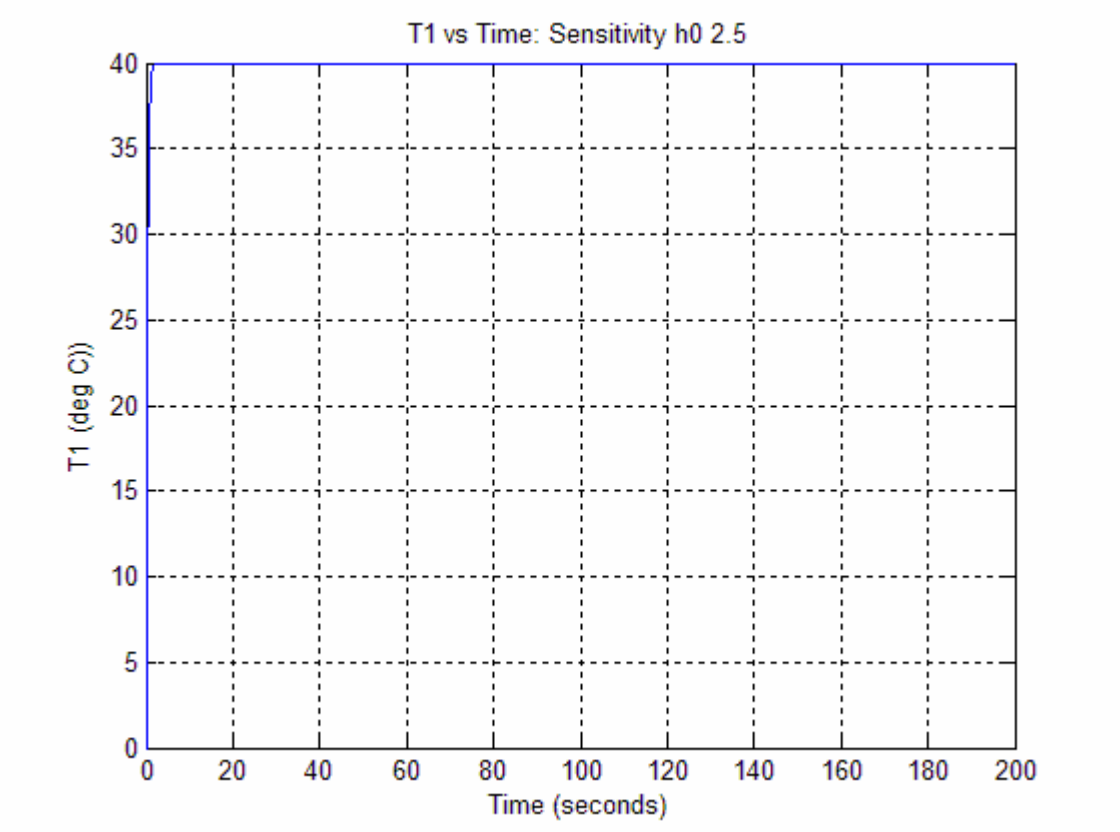

Figure 29: T_1 versus Time: Sensitivity h_0 2.5

As can be seen the T_1 graph shows no change which is as expected since the conduction term is already great enough to maintain the temperature of T_1 even with the larger original value of h_0. The T_0 graph shows a reduction of the slope to half of what occurred originally in Case 1. This is also expected since in Case 1 the convection term is the only way heat gets into the fuel with these parameters supplied to the model and it has been reduced in half.

Next the value of h_0 is changed to *10 W/mK*. The temperature graphs are shown below.

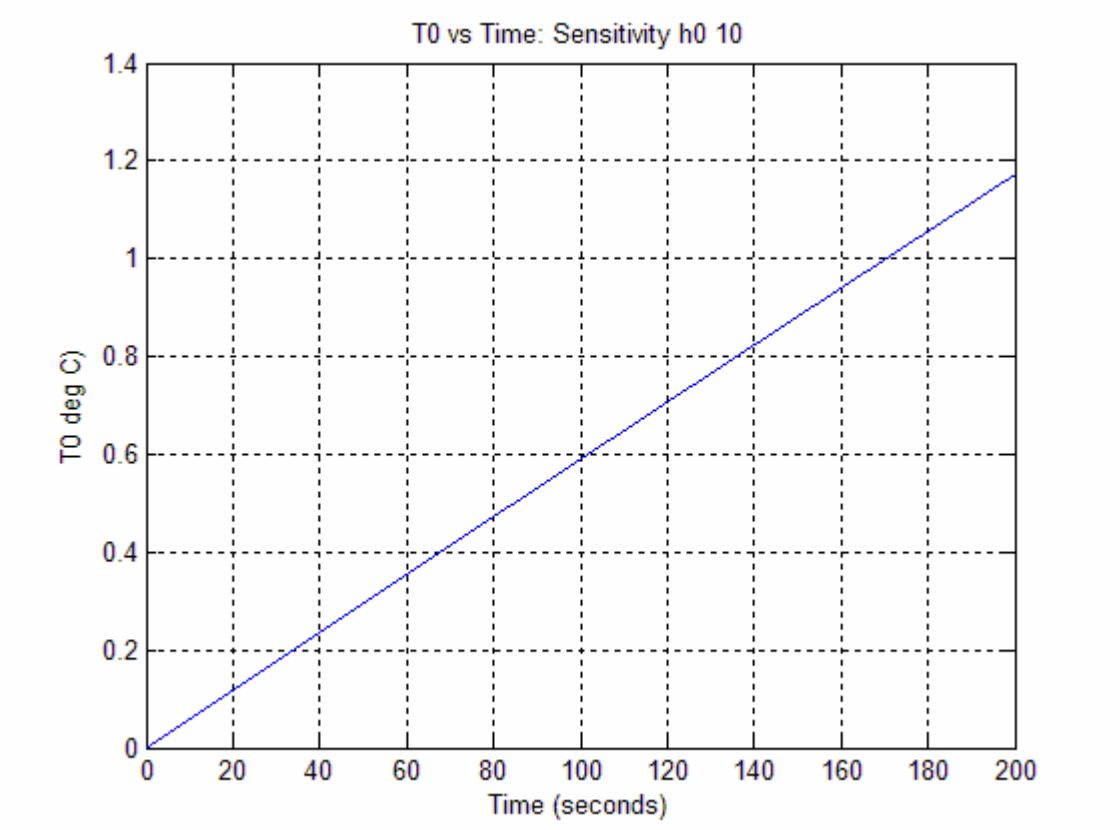

Figure 30: T_0 versus Time: Sensitivity h_0 10

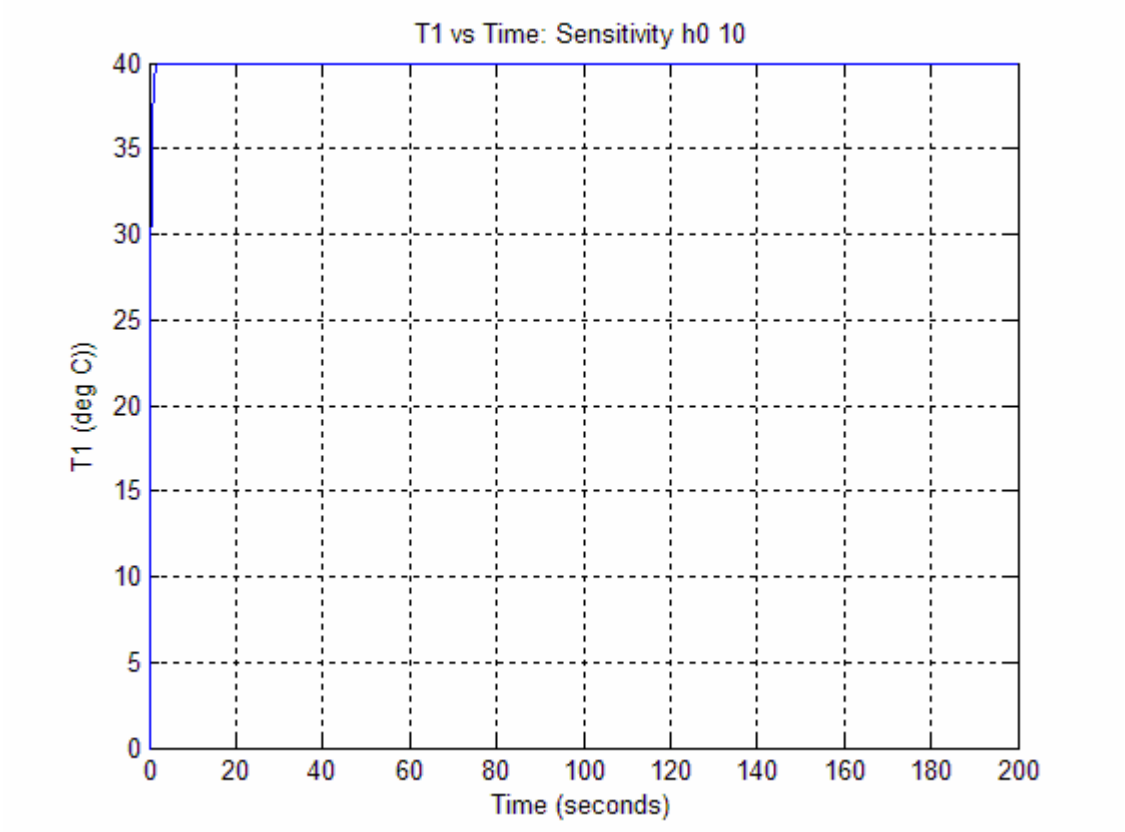

Figure 31: T_1 versus Time: Sensitivity h_0 10

As expected the T_0 graph doubles its slope with the doubling of the convection coefficient. The T_1 graph remains at a constant *40 °C*, which is also expected as the conduction term is still much larger in magnitude than the convection term.

The sensitivity of the *beta* plant model to the temperature of the eutectic compound and by extension the temperature of T_2 will be examined. The temperature T_2 will be reduced to *20 °C* for a Case 1 validation model run. The graphs for the temperatures T_0 and T_1 are shown in Figure 33 and Figure 34.

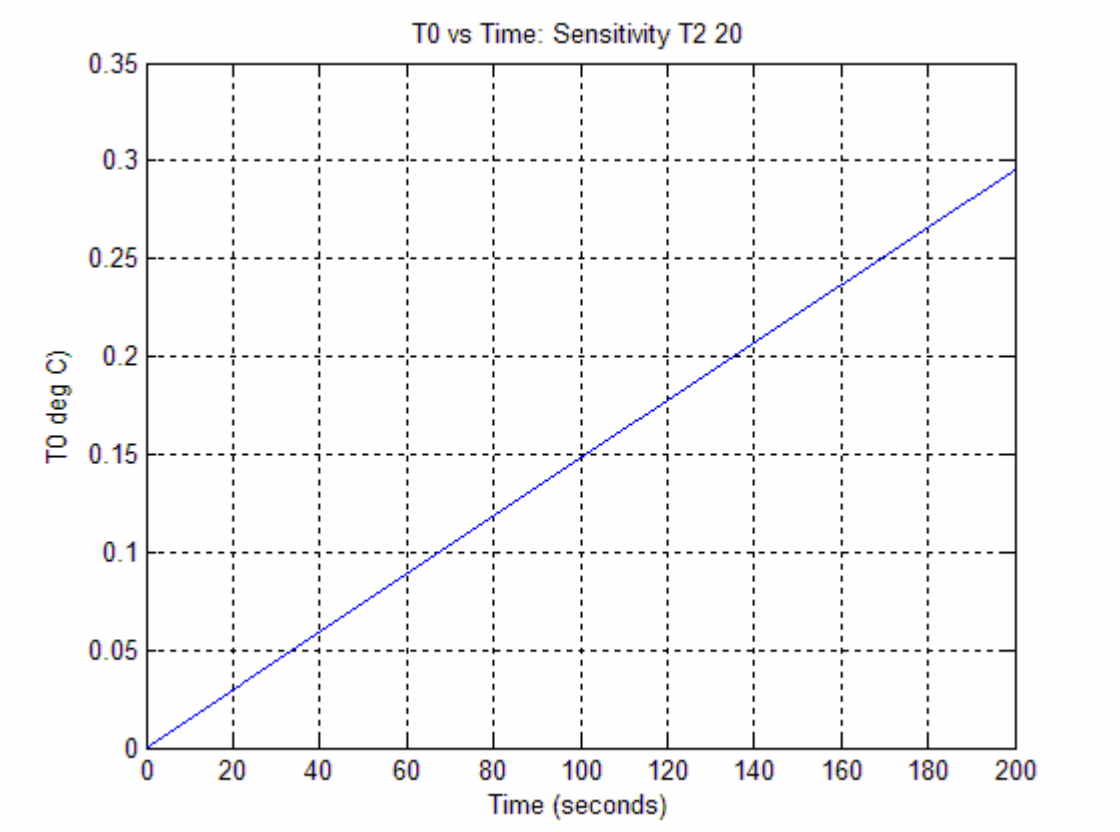

Figure 32: T_0 versus Time: Sensitivity T_2 20 °C

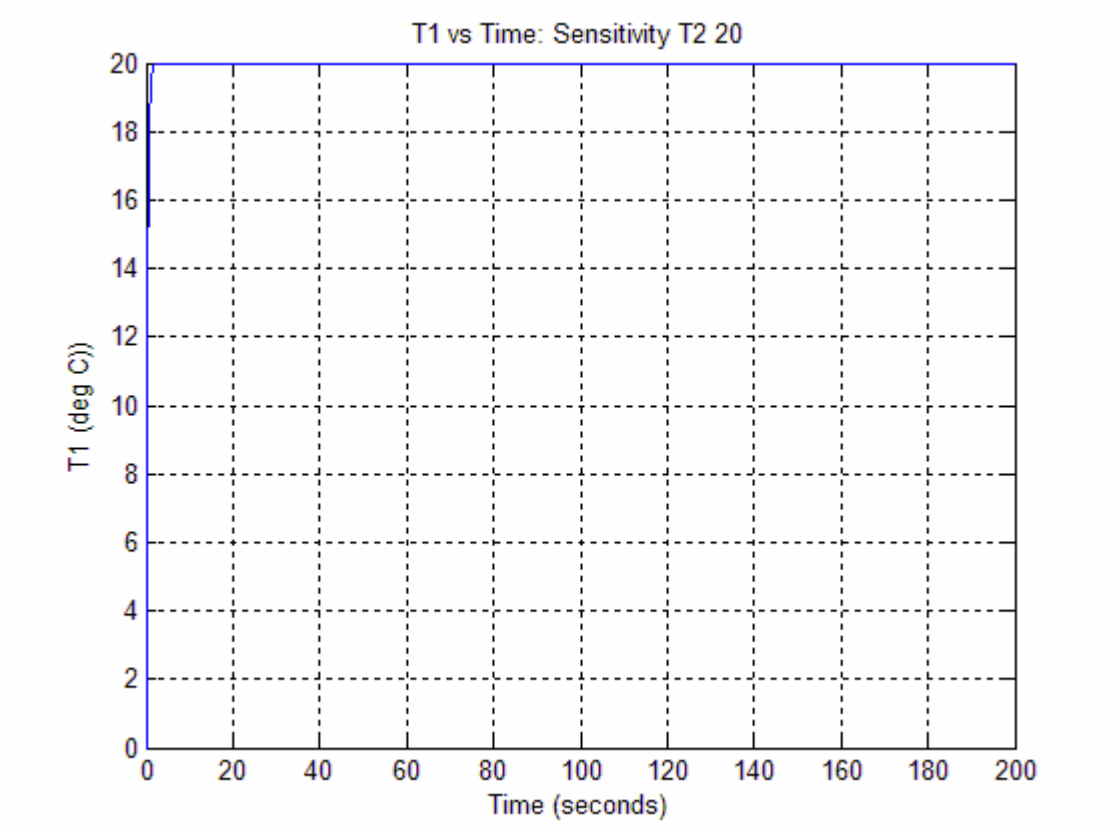

Figure 33: T_0 versus Time: Sensitivity T_2 20 °C

The temperature graph for T_0 again shows a reduction in slope by half. This is as anticipated. At first it may not be readily apparent, why the slope shouldn't change more, but when one considers the scale of T_0 over the 200 seconds it is essentially constant, when compared to the temperature of T_1 in the convection term. The temperature graph for T_1 has the same shape as in the Case 1 validation, but the steady state temperature of T_1 is shifted down to equal the new temperature of T_2.

Now the T_2 temperature will be changed to be double its original value and be equal to *80 °C*. The new temperature graphs are shown below.

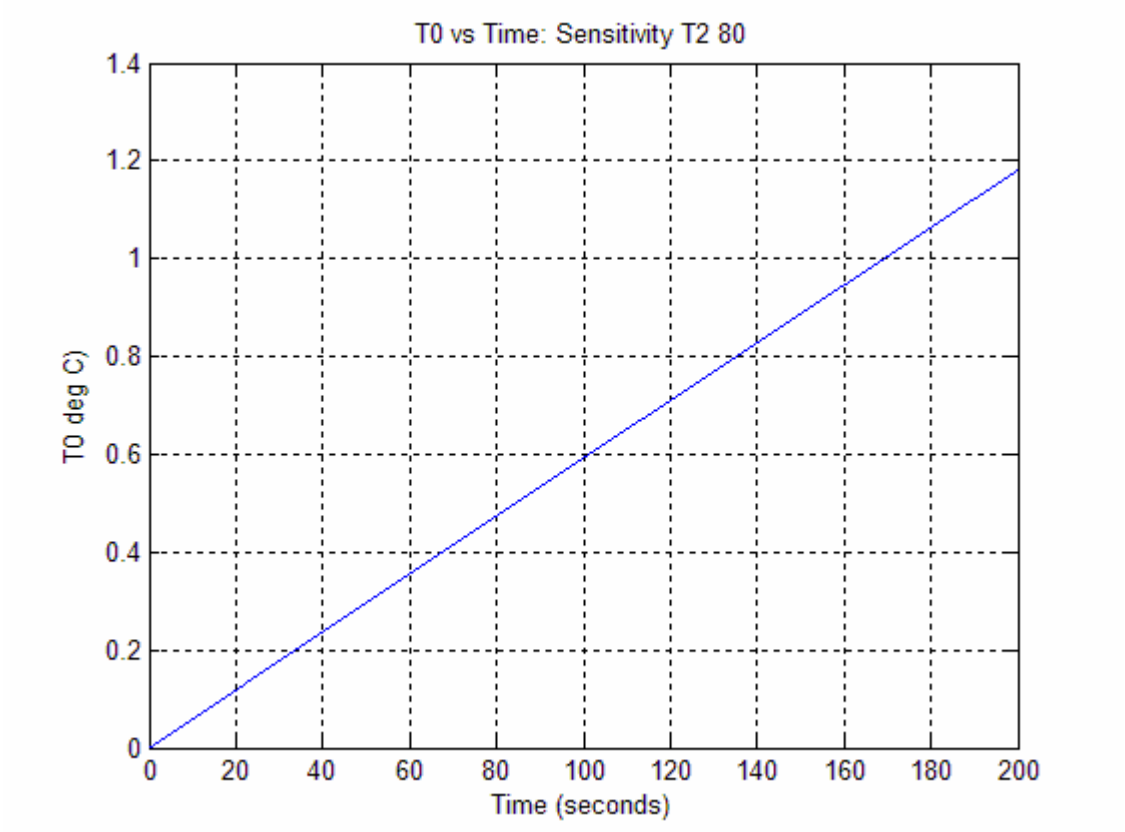

Figure 34: T_0 versus Time: Sensitivity T_2 80 °C

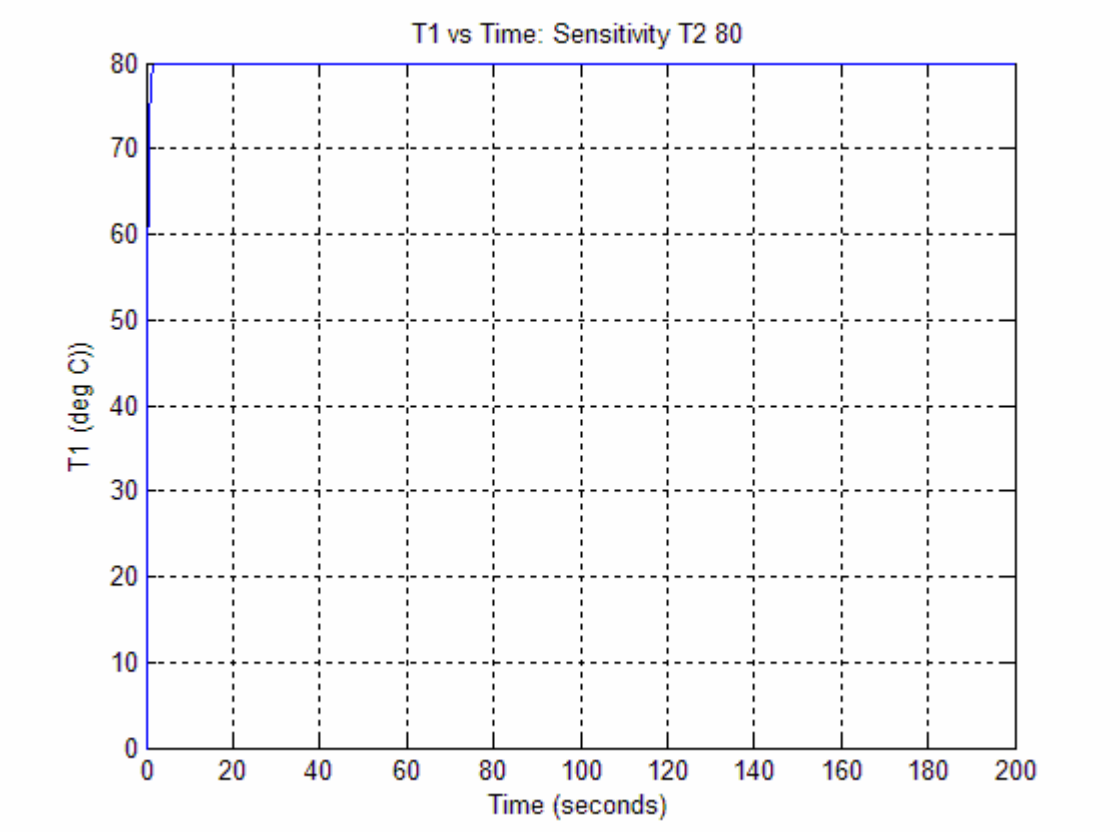

Figure 35: T_1 versus Time: Sensitivity T_2 80 °C

As expected the slope of the T_0 graph has doubled with the doubling of the T_2 value. Likewise as expected the steady state temperature of the T_1 graph has doubled to match the new value of T_2.

Next, the sensitivity of the *beta* plant model to the electrical resistance of the thermoelectric elements, R_{te}, will be examined. This is done using the Case 3 validation run parameters, because as mentioned above the dependence of joule heating on the square of the current should maximize the changes due to the electrical resistance. First, the electrical resistance is halved to a value of *976 ohms*. The new T_0 and T_1 temperature graphs are shown below.

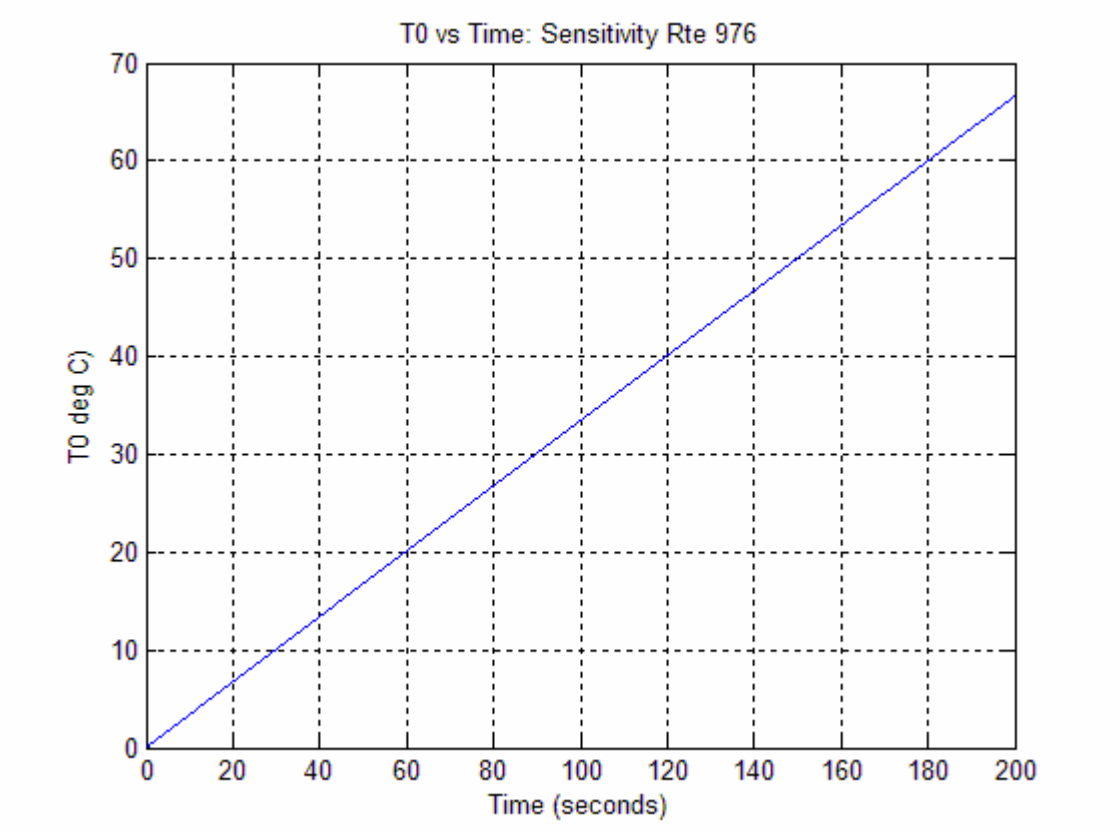

Figure 36: T_0 versus Time: Sensitivity R_{te} 976 Ω

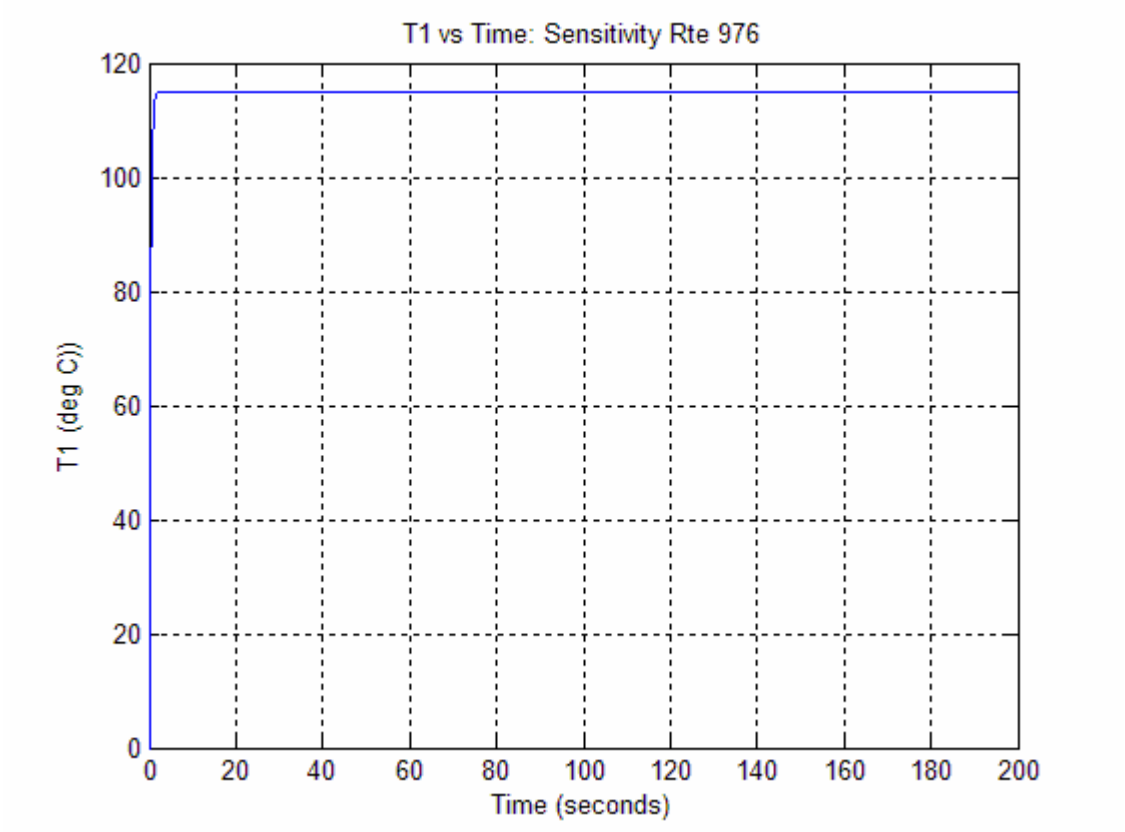

Figure 37: T_1 versus Time: Sensitivity R_{te} 976 Ω

As expected the change in resistance has reduced the steady state temperature of T_1 to approximately *115 °C*. One would also expect the final temperature of the fuel slug, T_0, to be reduced, which it is. However, it should not be halved as the current supplied has not changed; only the joule heating has changed due to the change in electrical resistance. A 50% value for the electrical resistance has induced approximately a 15% reduction in the final value of T_0. This means that the majority of the heating in the fuel is due to the Peltier heat transfer.

The electrical resistance is now doubled such that $R_{te} = 3906\ ohms$. The corresponding new temperature graphs are shown in Figure 38 and Figure 39.

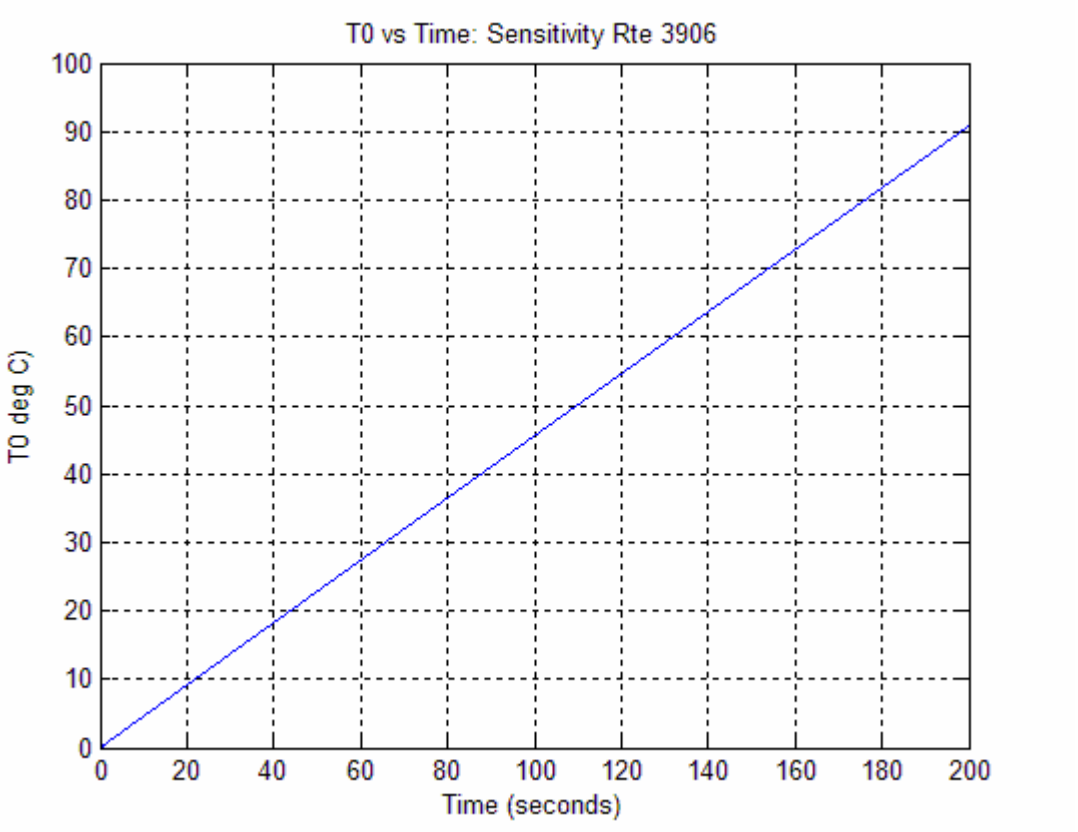

Figure 38: T_0 versus Time: Sensitivity R_{te} 3906 Ω

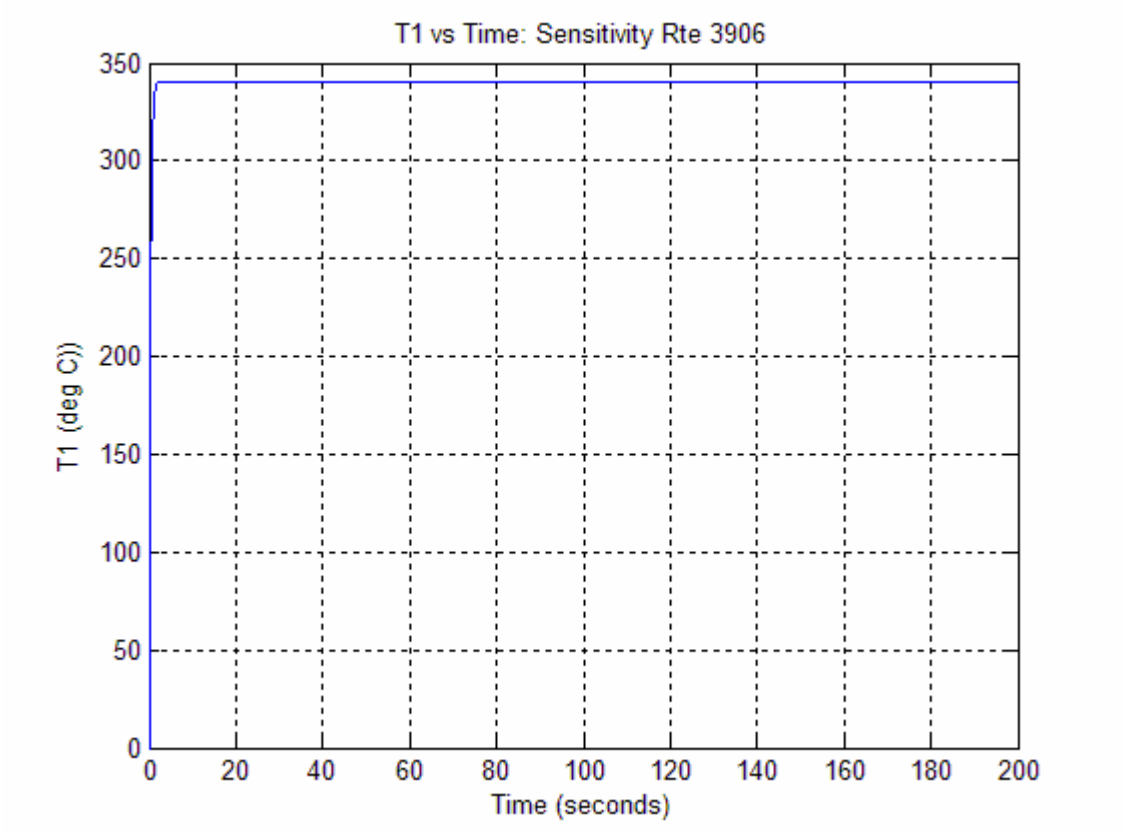

Figure 39: T_1 versus Time: Sensitivity R_{te} 3906 Ω

The steady state temperature has greatly increased to a value of *340 °C*. The final value of T_0 has also increased as expected. Though again it is not a doubling due to the thermoelectric heat transfer being the majority of the heat transfer.

The *beta* plant system will now be examined for sensitivity due to changes in the effective Seebeck coefficient, S_{eff}. The Case 2 run type will be used as the low current supplied to the system should maximize changes in the thermoelectric based part of the equation as the joule heating term is minimized due the square of the current being equal to the current itself. To begin with S_{eff} being changed to a value of *0.254 V/K* half of its original value. The temperature graph for the fuel slug temperature, T_0, is shown in

Figure 40, and the effective thermoelectric element temperature, T_1, is shown in Figure 41.

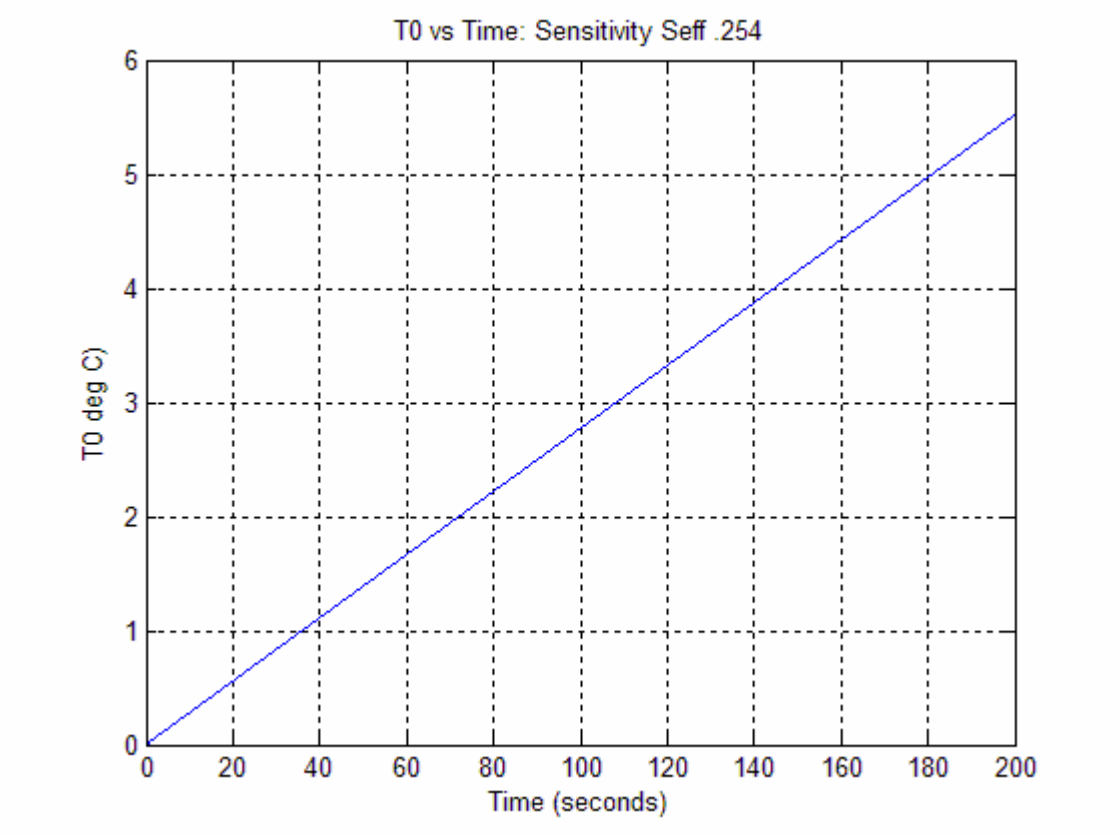

Figure 40: T_0 versus Time: Sensitivity S_{eff} 0.254 V/K

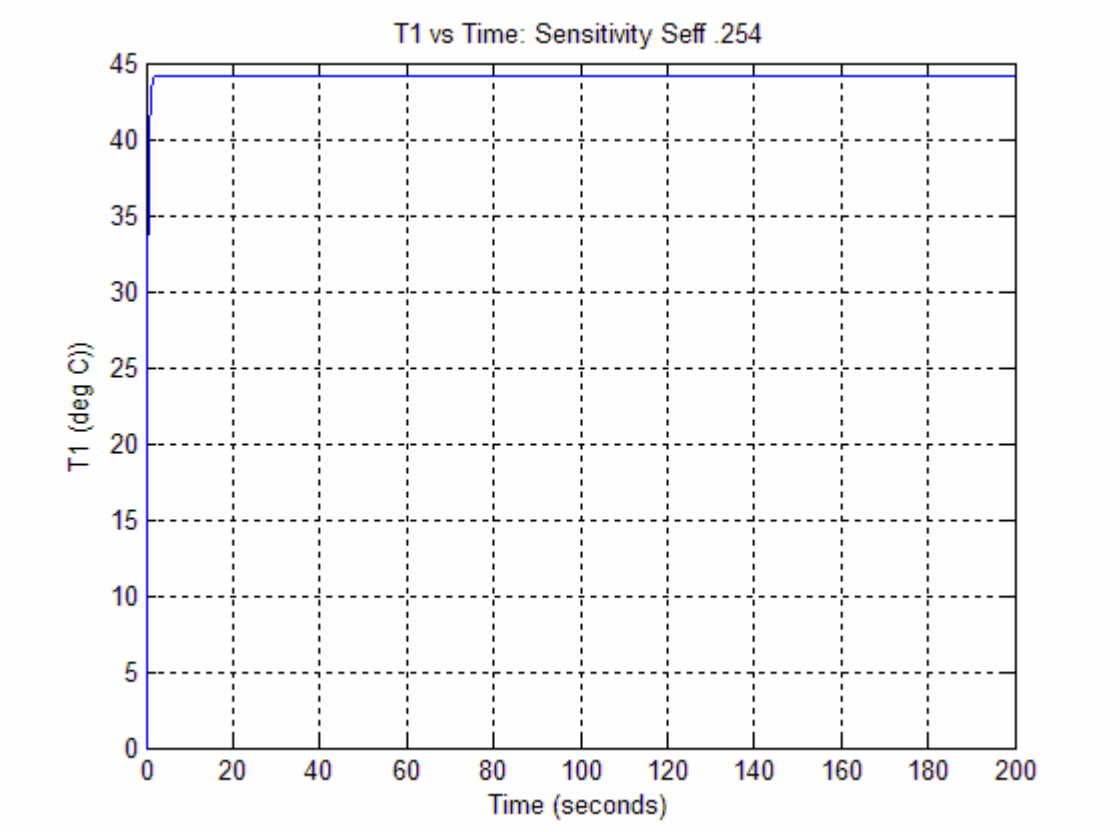

Figure 41: T_1 versus Time: Sensitivity S_{eff} 0.254 V/K

As can be seen the change in S_{eff} caused a reduction in the final value of T_0. This reduction is not quite equal to half of the original final value of T_0 in the Case 2 validation, but it is a percentage reduction than when the value of R_{te} was reduced. This means that as stated above the temperature of the fuel slug, T_0 is more dependent on the thermoelectric heat supplied as opposed to the joule heating. The steady state value of T_1 does not change due to the effective Seebeck coefficient being changed, which is as expected since the Seebeck coefficient does not directly affect the temperature of the effective thermoelectric element model.

Now the value of the effective Seebeck coefficient, S_{eff}, will be changed to double its original value to a value of *1.014*. The temperature graphs for T_0 and T_1 are shown below.

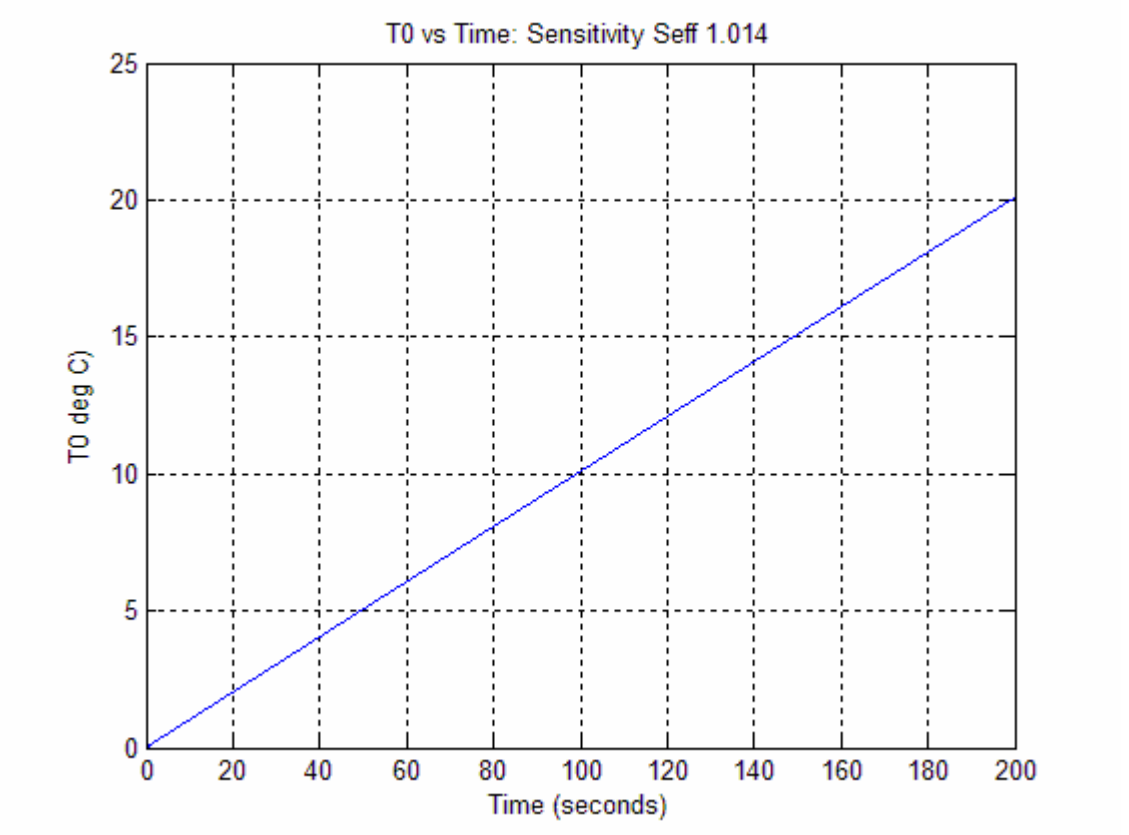

Figure 42: T_0 versus Time: Sensitivity S_{eff} 1.014 V/K

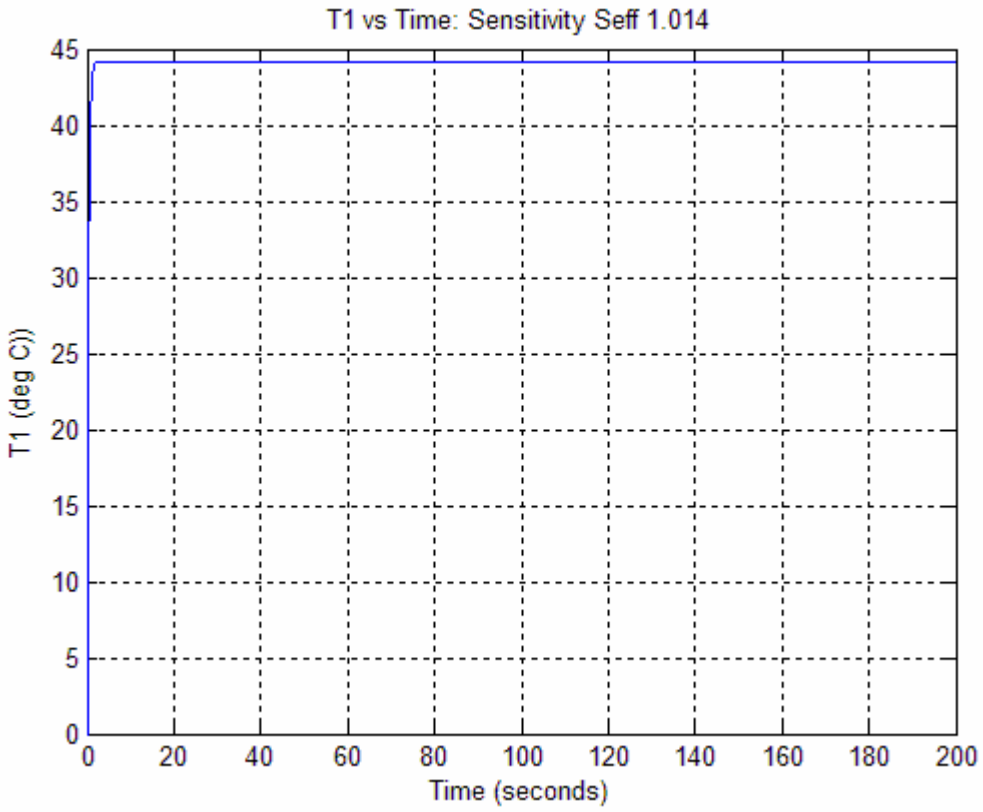

Figure 43: T_1 versus Time: Sensitivity S_{eff} 1.014 V/K

As expected the value of T_0 has increased, though as predicted not by a factor of two. The steady state temperature value of T_1 is still the same as it was in the Case 2 validation.

2.7. Beta Plant Control Law Development

With the sensitivity study completed the models are ready to have their control laws implemented. The first model to deal with is the Phase 1 and Transition model. This model is the first model to run and has portions. The first part is the Phase 1 portion, wherein the temperature of the fuel slug is raised from its initial value to a final

value that is within 95% of the goal temperature. This temperature is sufficient to allow the engine to start. Once the engine starts the Transition portion of the Phase 1 and Transition model is run. The Transition portion is almost identical to the Phase 1 portion, which is why they are lumped together. The changes are that the ending condition is different, in that the Transition portion runs for a specified warm up time of 5 minutes. And secondly that the Transition portion of the model has mass flow in it. Since the engine is off during the Phase 1 portion, the $\dot{m}$ term in the model is zero. The inlet temperature is assumed to linearly ramp up from the initial fuel filter temperature, which should be the ambient air temperature, to a final value of $T_i = 60\ °C$. See the parameter section below Table 1 to see a discussion on how the value was chosen.

The Phase 1 and Transition model will use the *beta* plant subsystem as its main building block. The main final differences are that the current will be controlled by a control law and that the ending conditions will be modified from a basic runtime of 200 second. The next step in building the model is to close the loop such that the current supplied to the *beta* plant subsystem is based on the error signal. The error signal is simply the difference between some goal temperature and the value of T_0 at that instant. Therefore the control law will drive the system harder as the system is further from the goal temperature. The most basic control law is proportional gain control law, called P control. In P control the error signal is multiplied by some gain constant called k_p, or the proportional gain. The basic P control law for the *beta* plant subsystem is shown below.

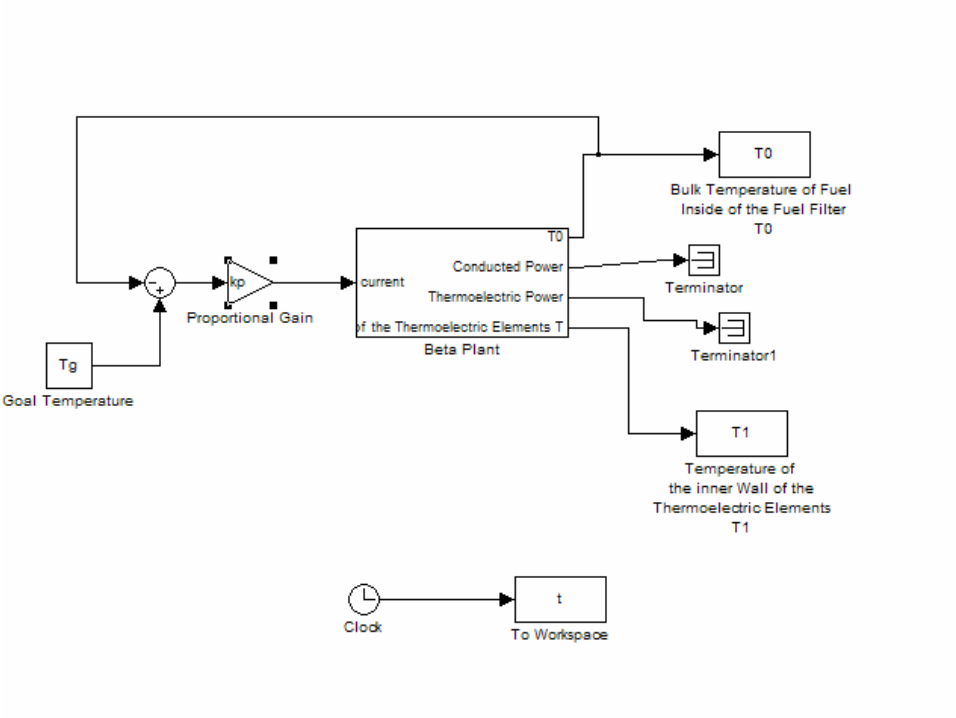

Figure 44: *Beta* Plant Phase 1 Proportional Control Law

As can be seen this model is very similar to the *beta* plant model. As mentioned all that has changed in this model in regards to the pure *beta* plant model is that the current is now driven by a control law. As a test the model was run to show how the response time has improved. The value of k_p for this trial run was left as 1. The goal temperature was chosen to be *35 °C*. The other parameters were identical to a Case 2 run. The temperature graphs for T_1 and T_2 are shown in Figure 45 and Figure 46.

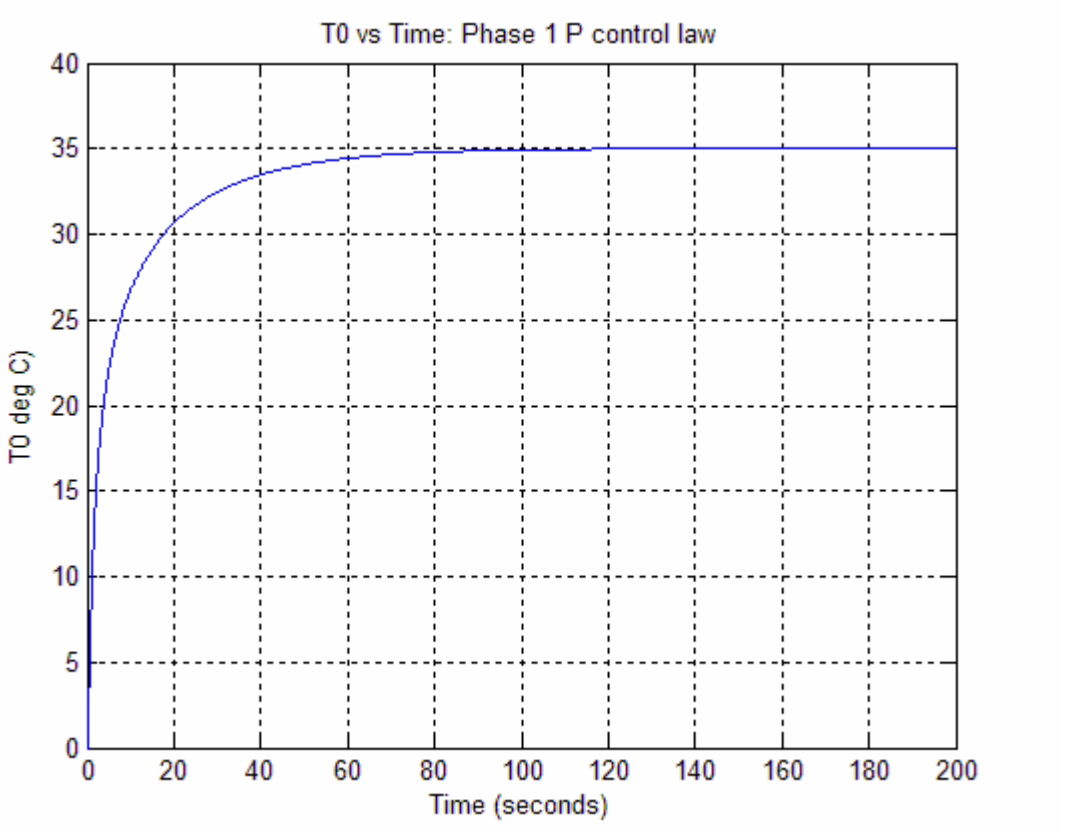

Figure 45: T_0 versus Time: Phase 1 Proportional Control Law

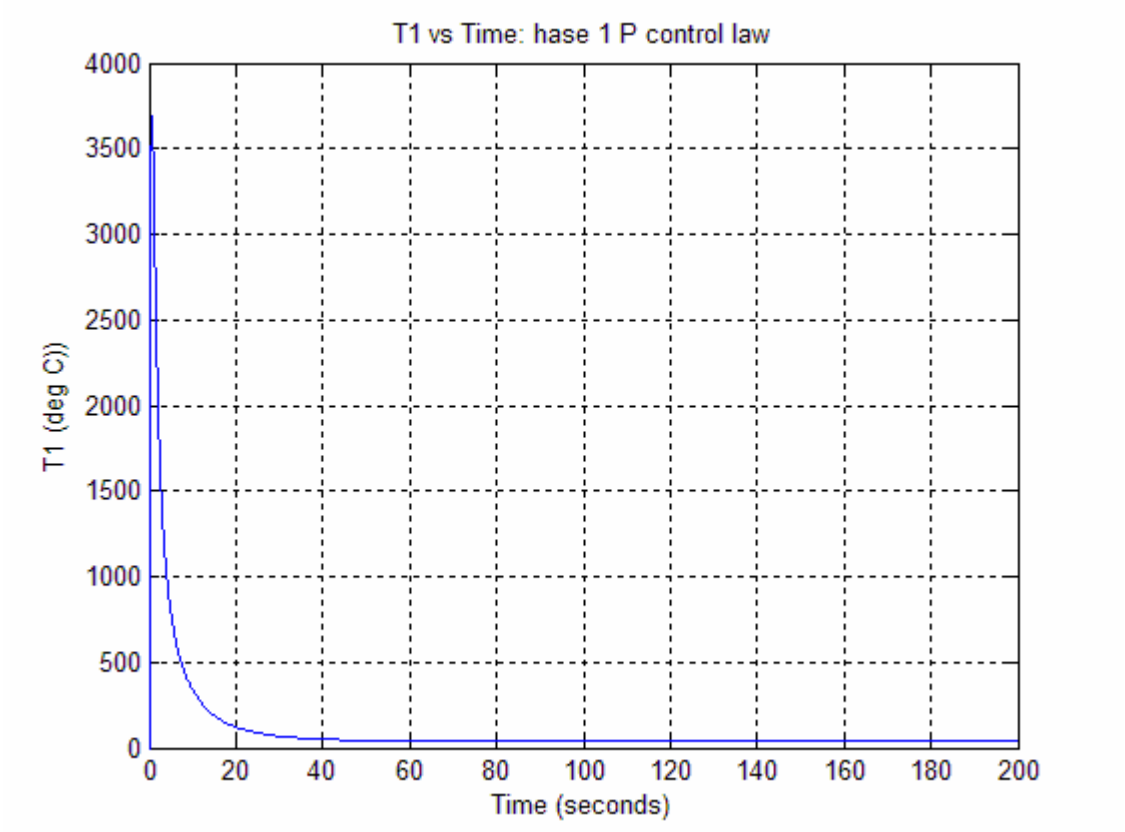

Figure 46: T_1 versus Time: Phase 1 Proportional Control Law

As can be seen T_0 quickly reaches the goal temperature of *35 °C*. However, T_1 is very high nearly instantly increasing to more than *3500 °C*. Obviously this is much higher than the materials will allow. To get a better idea of why the temperature, T_1, is so high the current supplied to the model is shown in Figure 47.

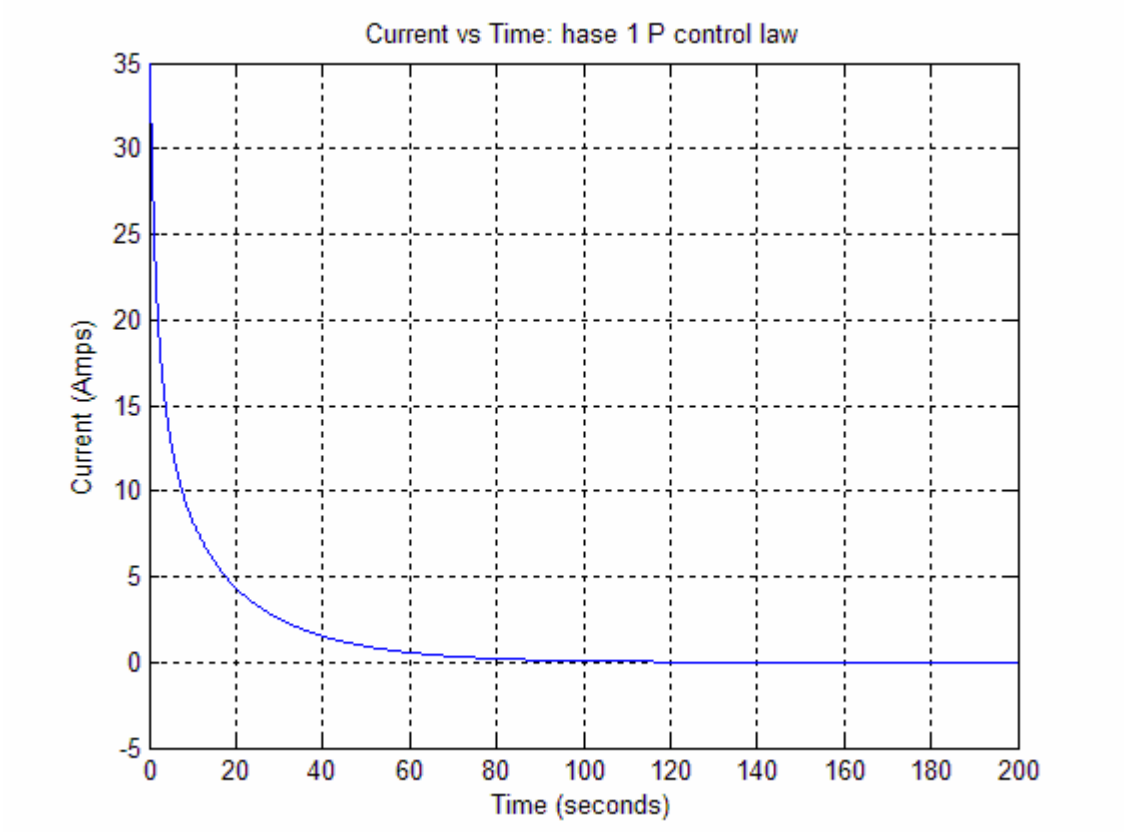

Figure 47: Current versus Time: Phase 1 Proportional Control Law

The current for the basic proportional control law begins at more than *30 A*, which is far more than the thermoelectric elements can handle. This explains the extremely high T_1 value. However, it can be seen that the current swiftly is under *5 amps*, which is more than acceptable. The idea is that you spend a greater current initially to minimize power usage in the long run, and speed up response time.

The next step is to tune the proportional gain. Ideally, this is accomplished through the use of optimization code. However, since this is only a temporary model the gain shall be chosen. A good first choice is to tune the gain such that the maximum current of the thermoelectrics is not exceeded. A good choice for maximum current based on current thermoelectric elements is *6 amperes*. This is based on commercially

available modules, however it does yield a very high power generation namely greater than *70 kW*, which may end up being more than the thermoelectric modules can handle. Since the maximum temperature difference is 35°C, it is trivial to discover that a value for k_p of *0.17* will yield an initial current of *6 amperes*. This is done by multiplying the initially desired current by the initial temperature difference. The temperature graphs for this new gain are shown below.

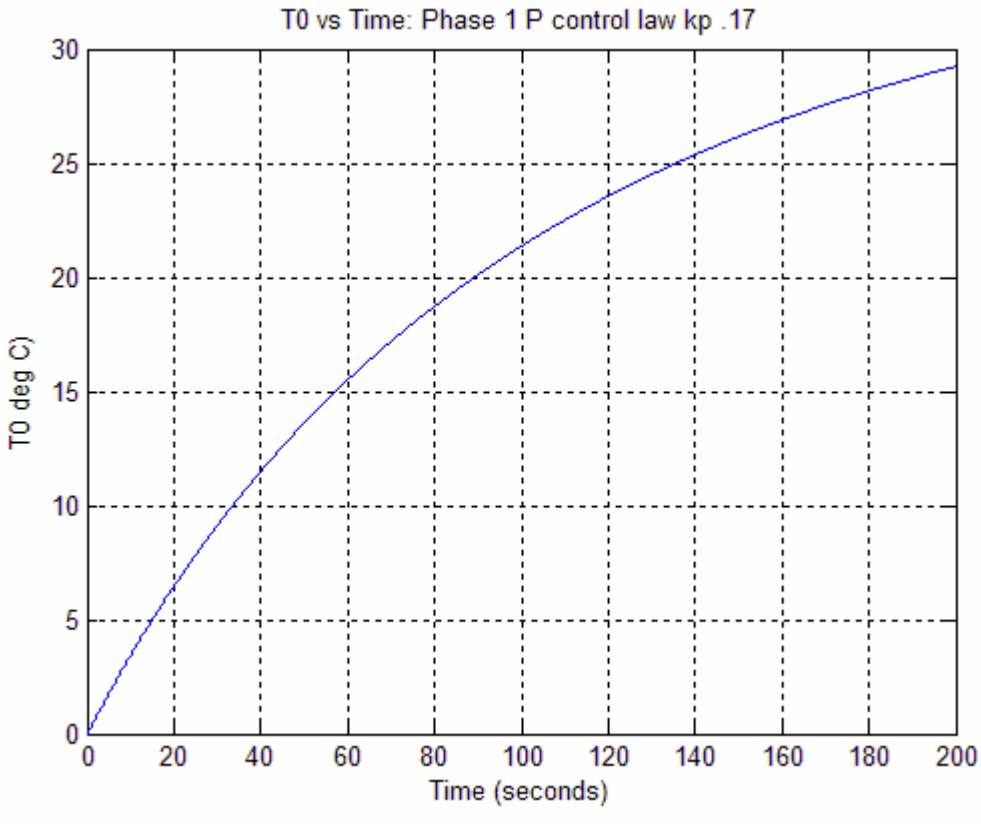

Figure 48: T_0 versus Time: Phase 1 Proportional Control Law k_p 0.17

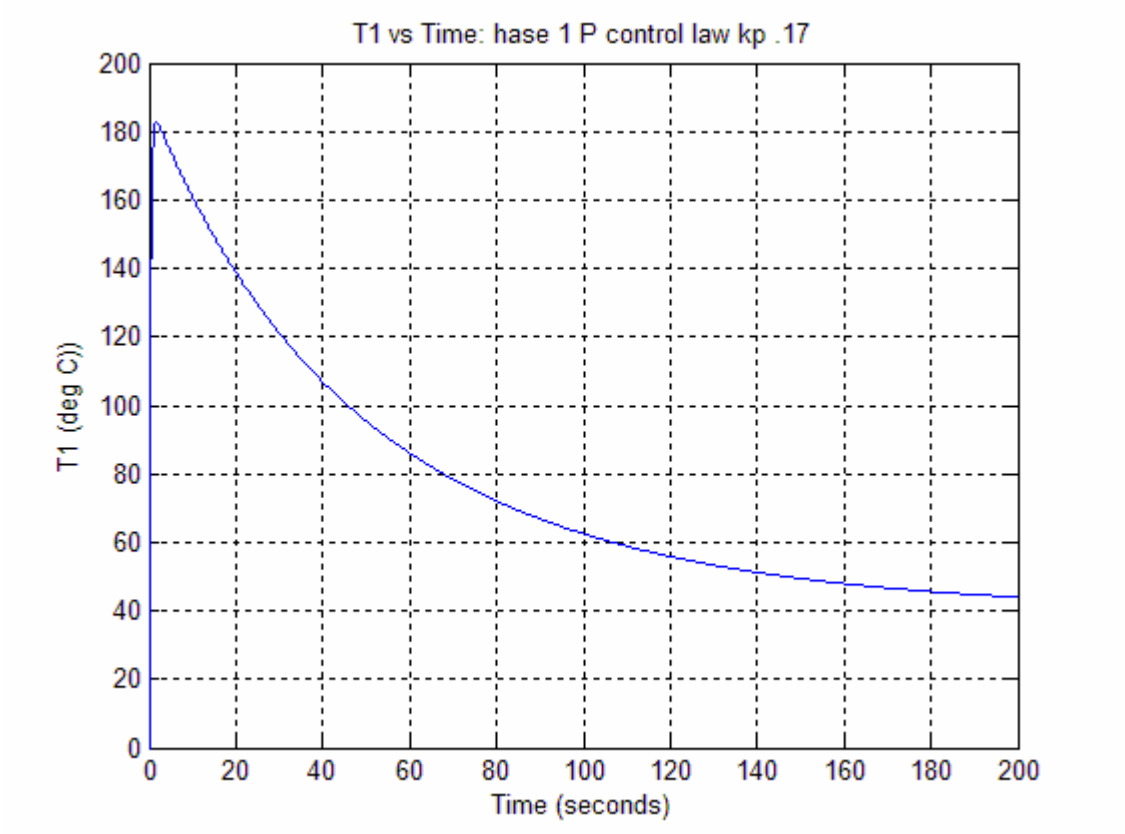

Figure 49: T_1 versus Time: Phase 1 Proportional Control Law k_p 0.17

As can be seen this new gain has had two effects. First, the T_0 response has slowed considerably and is not reaching steady state in the 200 seconds. Second, the initial spike in the temperature of T_1 is has been reduced greatly. This seems to be undesirable, however the other crucial data to look at is the current shown below.

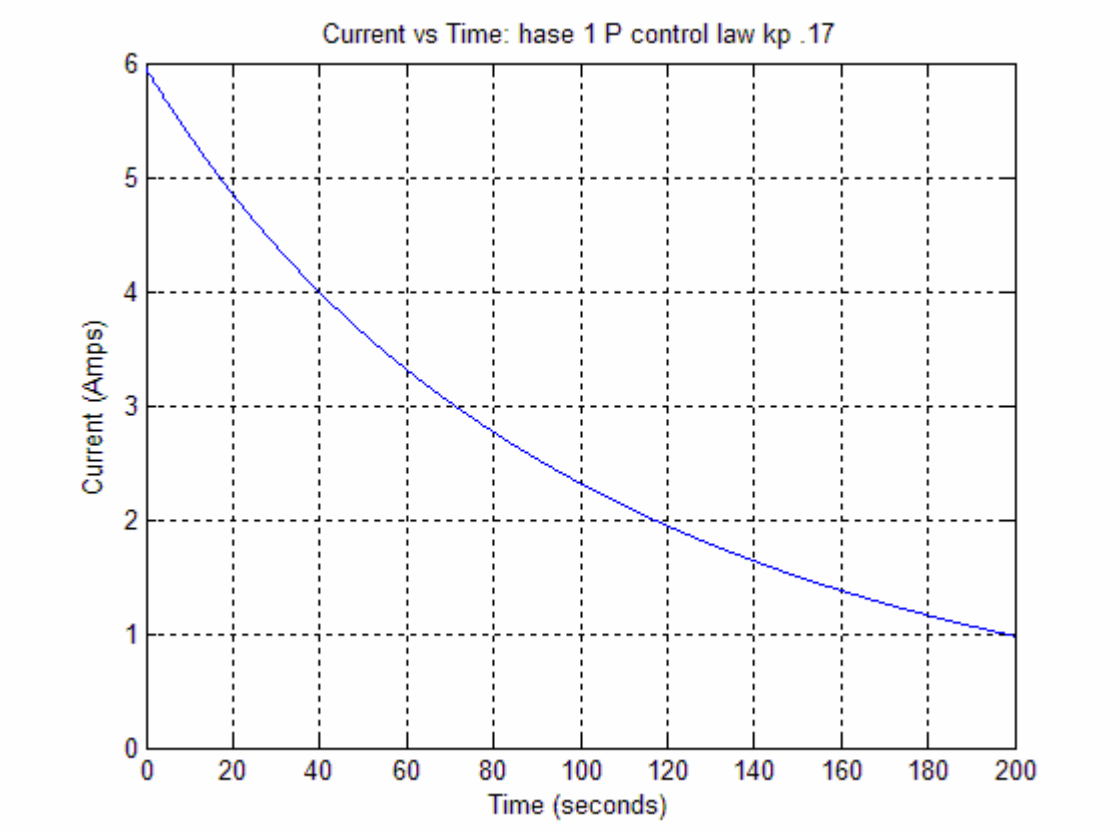

Figure 50: Current versus Time: Phase 1 Proportional Control Law k_p 0.17

As expected the current now begins at a maximum value of *6 amps*. This is an allowable value for the thermoelectric elements. As can be seen the control law allows a more detailed tuning between response speed and power supplied to the system. However, the system is not fully tunable. The solution is to utilize a more complex control law in an attempt to further improve performance and reduce total power consumption.

The next step in control law evolution is to add a new term to the control law. A proportional control law's signal is based only upon the error signal itself. A proportional integral control law has two parts, and is referred to as PI control. The first part is just the P control law from before. The second part adds a new gain called k_i

which is based on the integral of the error signal. The final current then is the sum of the proportional part of the control law and the integral portion of the control law. The model with PI is shown below.

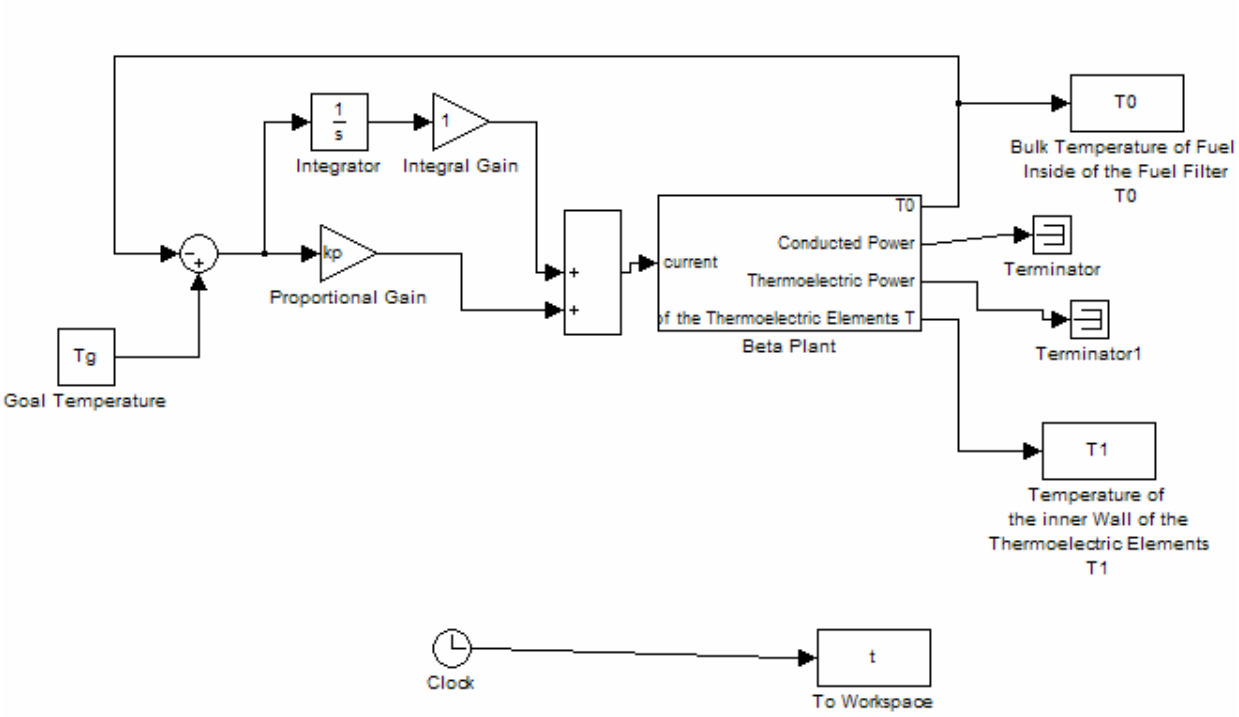

Figure 51: *Beta* Plant Phase 1 Proportional Integral Control Law

As can be seen this is almost exactly the same as the P control law model. Now there is an integral gain, which is hooked up to an integrator that is receiving the error signal as an input. The current supplied is the sum of the two control signals.

To examine how integral control works the gains k_p and k_i will both be set as *1*. The temperature graphs for T_0 and T_1 are shown in Figure 52 and Figure 53 and the graph for *current* is shown in Figure 54.

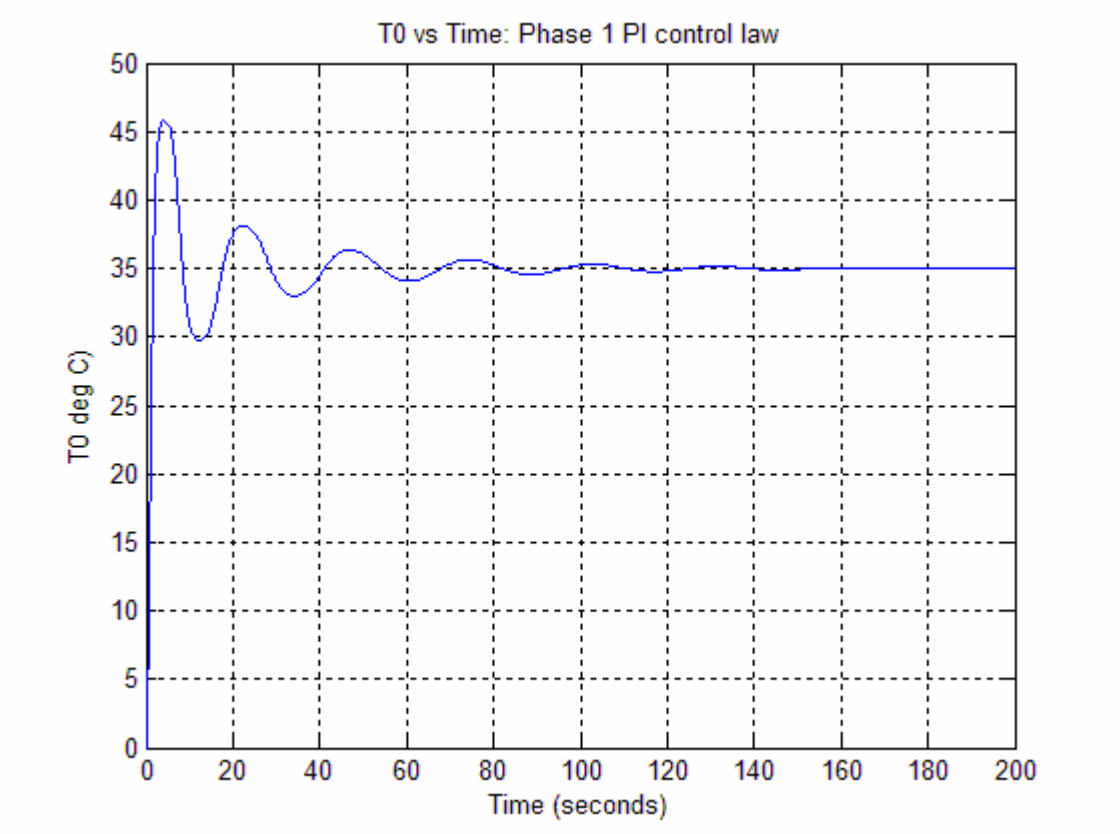

Figure 52: T_0 versus Time: Phase 1 Proportional Integral Control Law

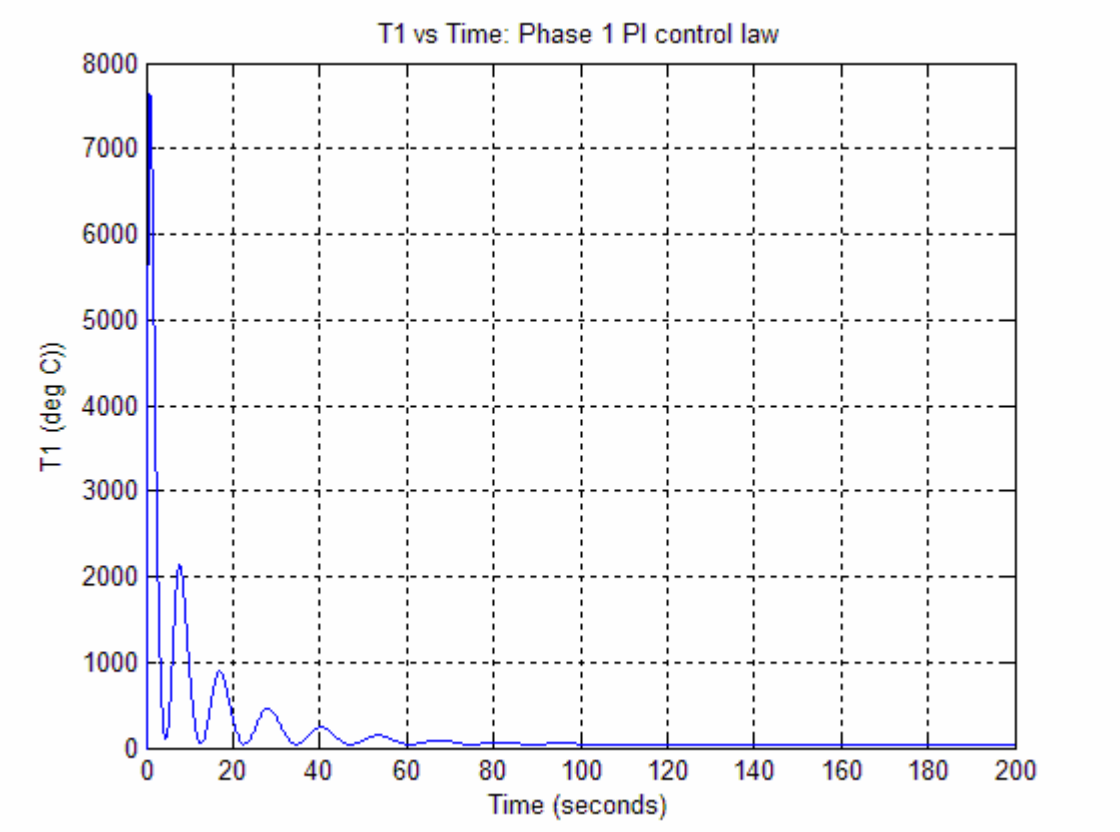

Figure 53: T_1 versus Time: Phase 1 Proportional Integral Control Law

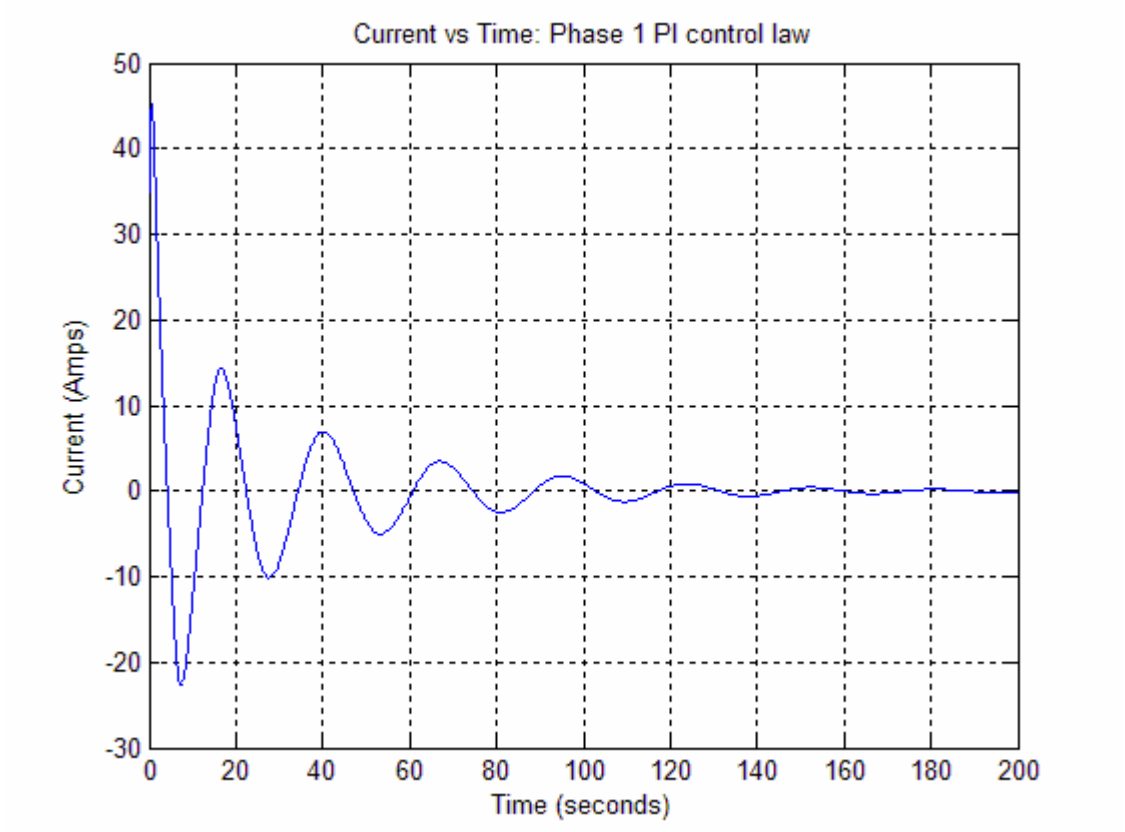

Figure 54: Current versus Time: Phase 1 Proportional Integral Control Law

As can be seen the temperature of the fuel slug quickly passes the goal temperature. In fact it oscillates about the goal temperature. T_1 also exhibits a shifted oscillatory behavior. The current is again far to large for implementation, and is oscillating, drifting into negative values to compensate for the overshoot. What can be seen however is that the control law hits the goal temperature much more quickly, by changing the shape of the response curve. This does come at the cost of an even higher current supplied, and undesirable oscillatory behavior.

To illustrate how the model reacts to changing values of k_i, the value of k_p is held constant and the value of k_i is reduced to *0.1*. The new temperature and current graphs are shown below.

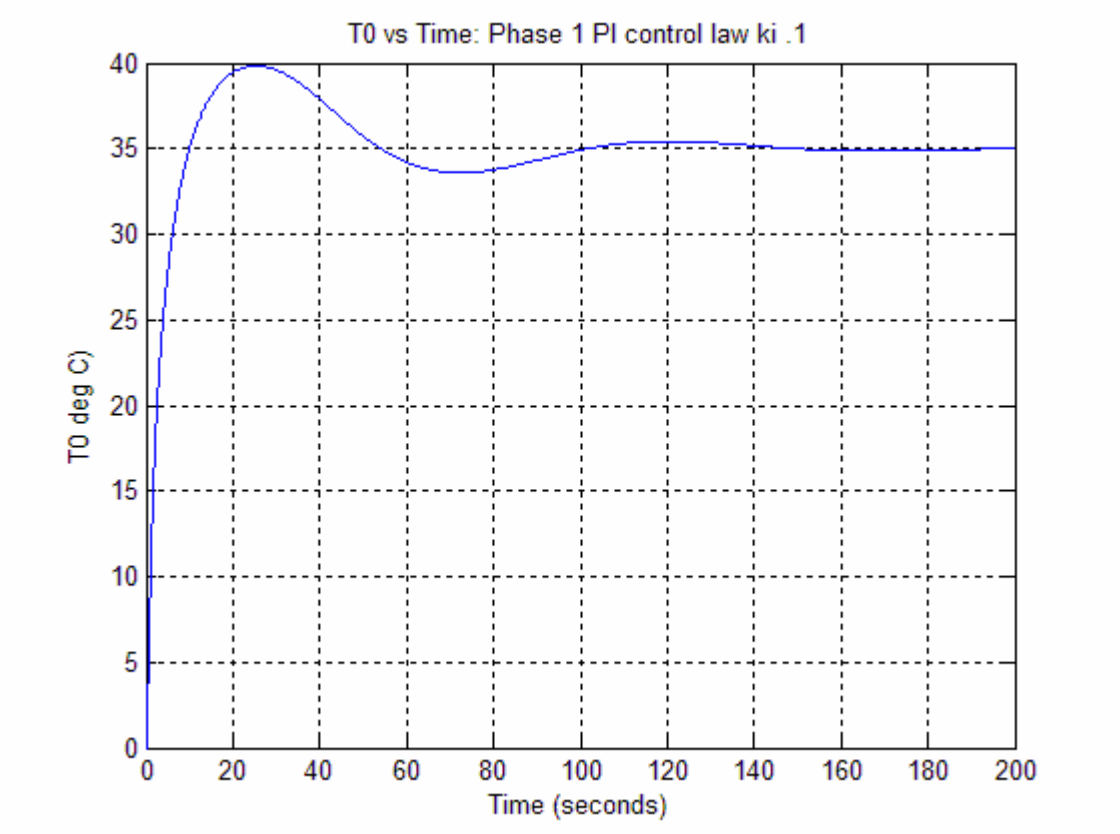

Figure 55: T_0 versus Time: Phase 1 Proportional Integral Control Law k_i 0.1

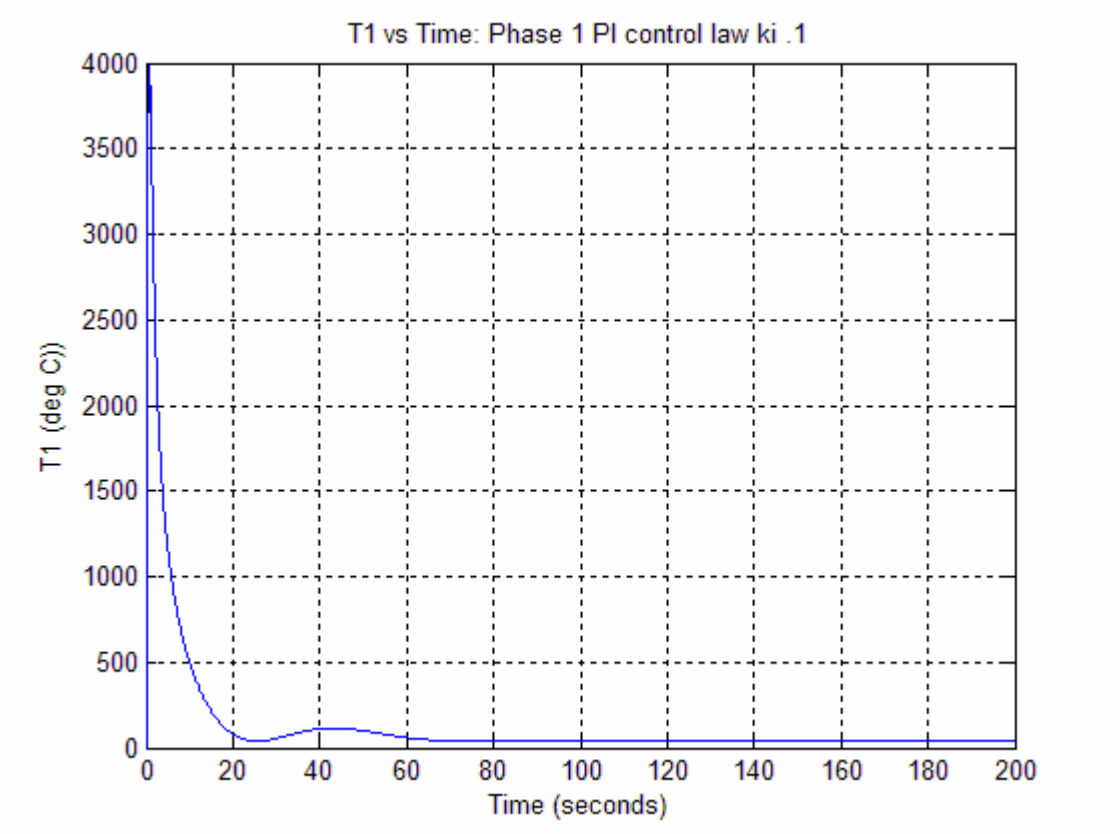

Figure 56: T_1 versus Time: Phase 1 Proportional Integral Control Law k_i 0.1

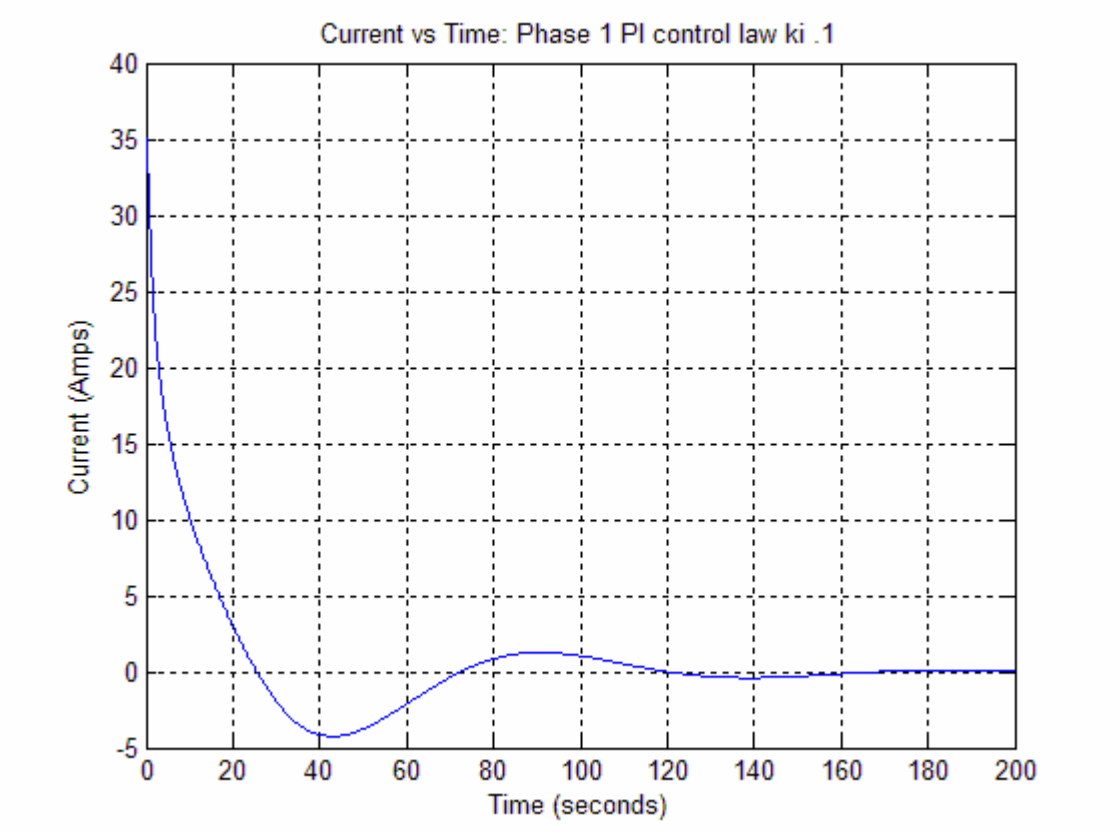

Figure 57: Current versus Time: Phase 1 Proportional Integral Control Law k_i 0.1

The smaller integral gain has had several effects. The most obvious are that the temperature T_1 has decreased, as has the current. T_0 is still overshooting the goal temperature as well, but the oscillatory behavior has been curtailed greatly. The model is still performing more quickly than the pure proportional control. The control law gains will not be optimized at all since the oscillatory behavior remains instead the control law will be refined.

The oscillatory behavior is problematic, but a solution exists in the form of derivative control. However, derivative control is not without its own problems. The reason it corrects oscillation is that it responds more quickly to changes in the error signal. This helps correct the oscillation, but also will magnify any noise in the system.

This is especially worrisome if plant variables are not known precisely. In addition, it tends to slow the system response down. Nevertheless it does help address oscillation. Thus, the next step is to implement PID control. PID control, as can be surmised, is the same as PI control with the addition of a gain based off of the derivative of the error signal. The model with PID control is shown in Figure 58.

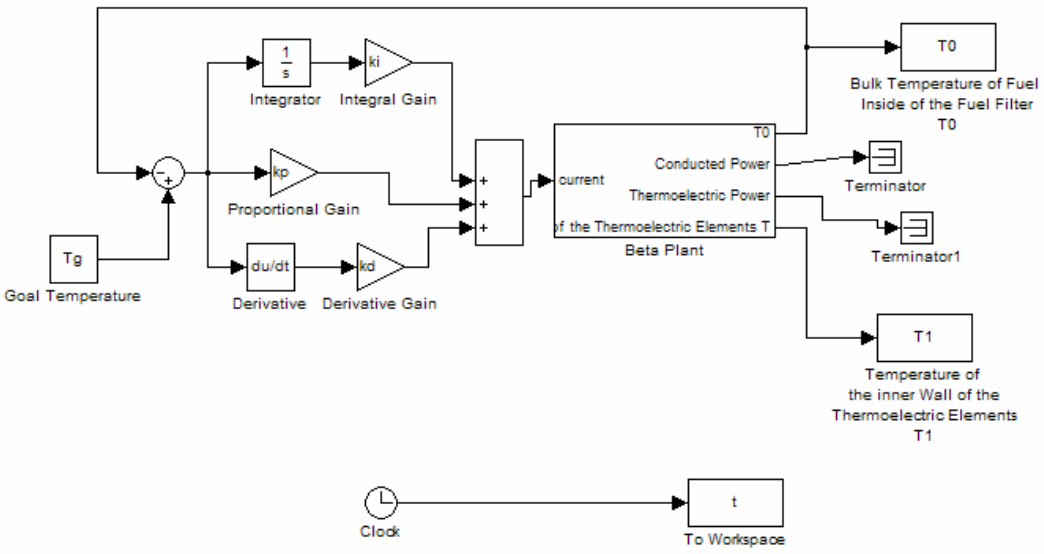

Figure 58: *Beta* Plant Phase 1 Proportional Integral Derivative Control Law

As can be seen the model is essentially the same as the PI model, but with the addition of a derivative block and a gain attached to it going into the summing block that outputs the current. The derivative block has the same basic logic as an integrator block it takes the input and takes the derivative of it and gives that as the output. It is worth noting that the *du/dt* derivative block is indeed the continuous derivative block, even though it may make more sense for the derivative block to show as just an s.

Now with a more robust control law the model was run with the gains again set at unity. The temperature graphs and the current graph are shown below.

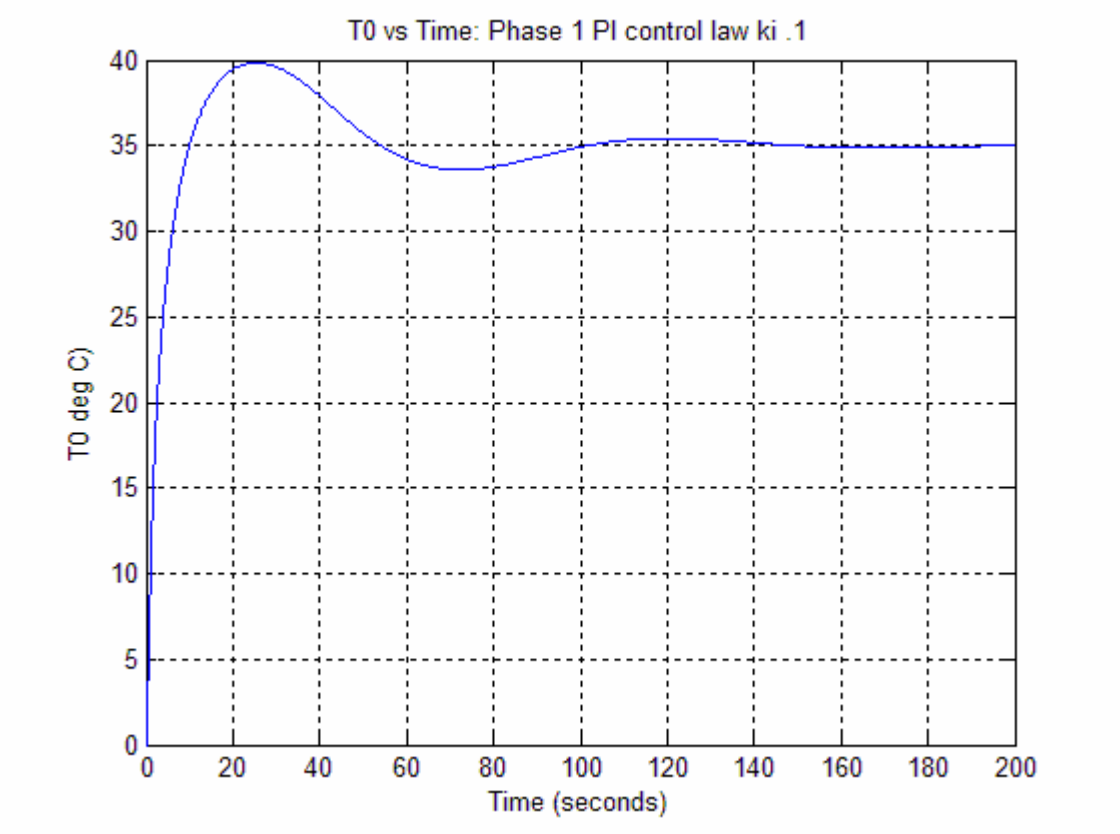

Figure 59: T_0 versus Time: Phase 1 Proportional Integral Derivative Control Law

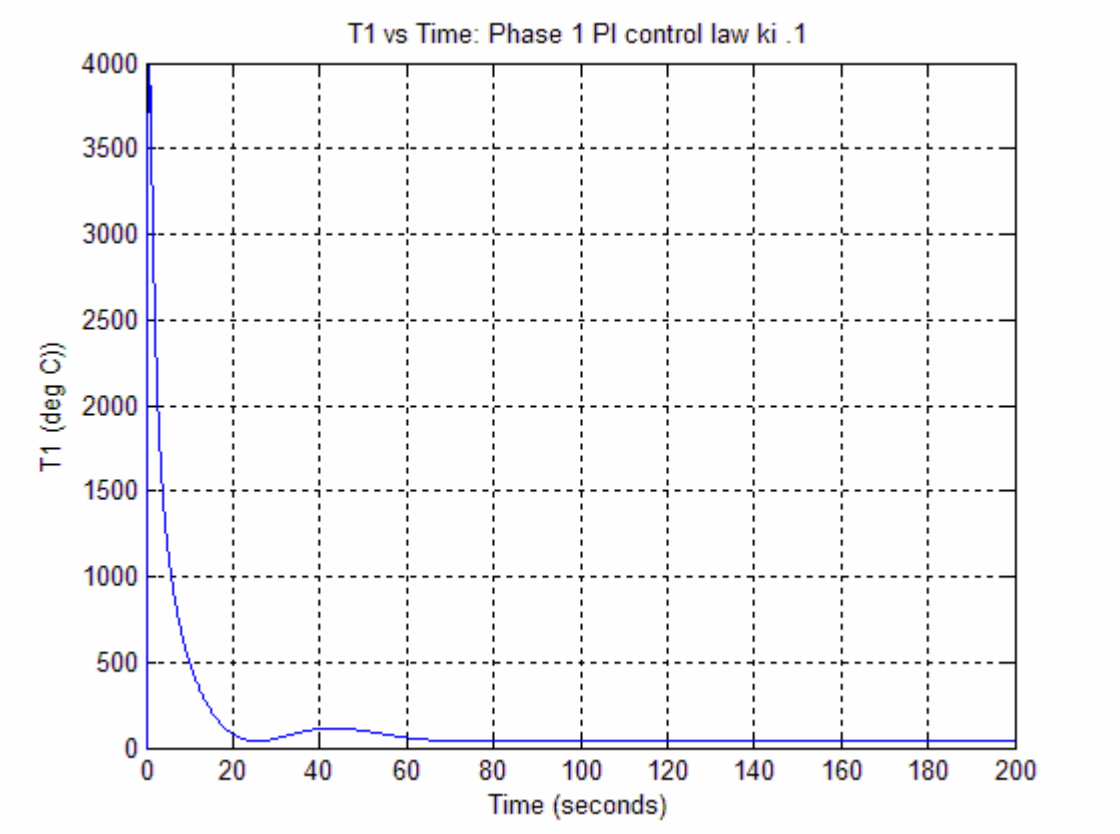

Figure 60: T_1 versus Time: Phase 1 Proportional Integral Derivative Control Law

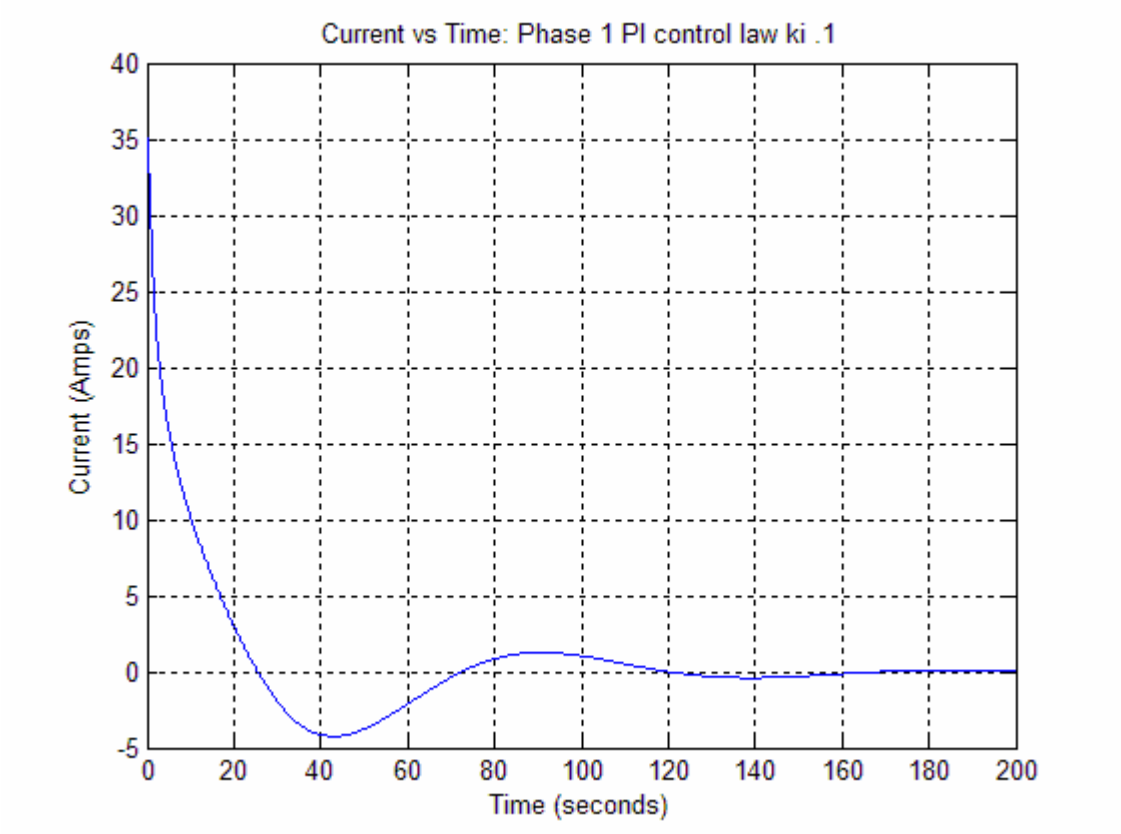

Figure 61: Current versus Time: Phase 1 Proportional Integral Derivative Control Law

The temperature graph again shows an increased temperature, but notice that it is considerably lower than the PI model with unity gains showed. Additionally, notice the T_0 response curve is still moving more quickly than with just P control, but is showing considerably less oscillation than the basic PI control law. As expected, the current is still too great, but is lower and less oscillatory than was seen in the PI control model. So in general it can be said that the PID control gives you the speed up of the PI control, but with the removal of oscillatory behavior.

2.8. Beta Plant Control Law Optimization

The system is now ready for a basic tuning. There are several methodologies for this process. However, there is an inherent problem with this system in regards to them. Most of the processes want the gains k_i and k_d set to zero initially, and the value of k_p increased until the system begins to oscillate. However, the gain on this system cannot reasonably be increased to a point to induce oscillation. What is more the value of k_p is then generally halved and the integral control and derivative control are added in one by one. Regardless of what the k_p term is, the output is still likely to be far too high of a current. Ergo, manual tuning will be used to get the system to a point where an optimization algorithm can be used to optimize the gains fully.

The tuning methodology is to first tune the proportional gain to a value that achieves a start-up current less than *6 amps*. This is easily accomplished, by selecting a gain of less than *0.17* as calculated above. Next, the integral gain will be set to a small number so that it doesn't dominate the control law. Finally, a modest derivative control gain will be set so the system overshoots the goal temperature, but does not oscillate. The first tune gains are $k_p = 0.15$, $k_i = 0.01$, and $k_d = 5$. Then the model should be ready for an optimization to be run. To perform the optimization, Matlab© and Simulink© software tools are utilized, namely the Optimization Toolbox for Matlab© and the Simulink© Response Optimization add in package. The Optimization Toolbox provides the functions necessary to run optimization code, and the Response Optimization add-in allows for a graphical optimization interface to be used. The first step in utilizing the optimization code is to add signal constraint blocks to the Simulink© *beta* plant PID control model. The new model is shown below in Figure 62

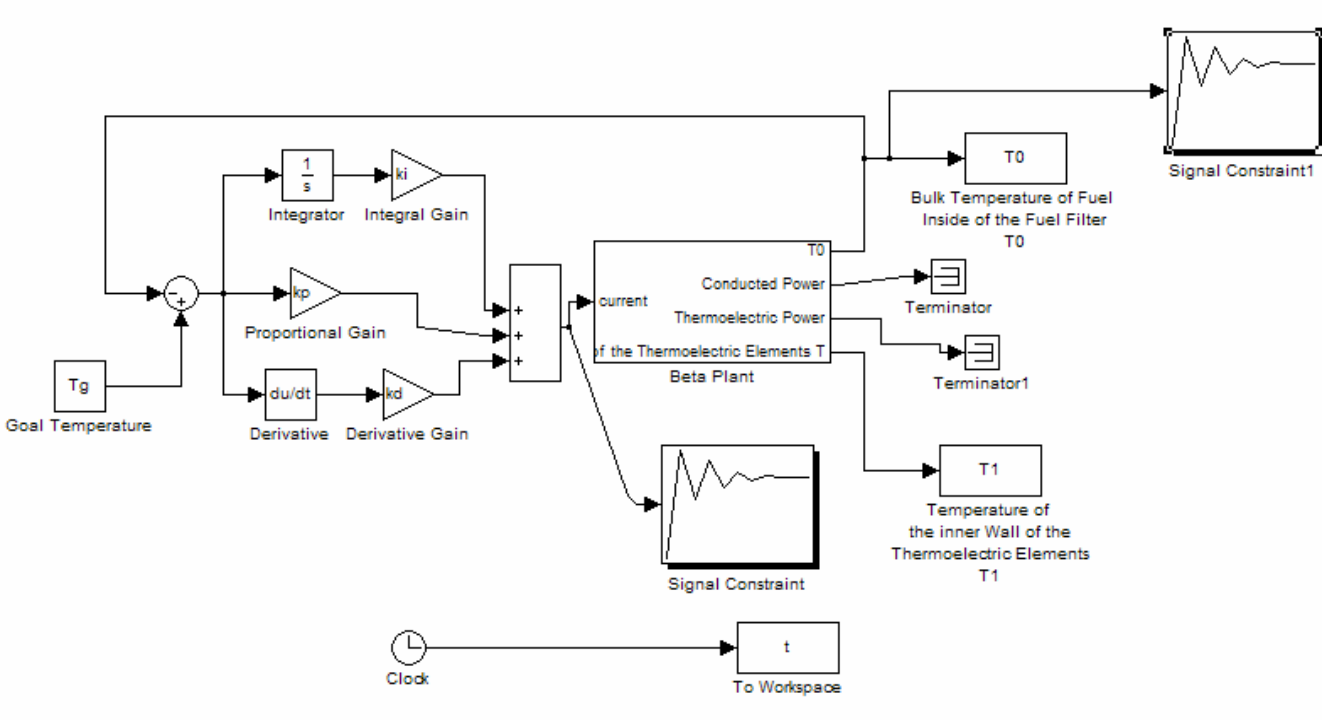

Figure 62: *Beta* Plant Phase 1 Proportional Integral Derivative Control Law Optimization Model

As can be seen there are now two signal constraint blocks. To use these blocks, a graphical interface is opened and the allowable values for the signals are input as a set of lines. This means that for this optimization, a constraint is being forced upon the bulk fuel temperature, T_0, and a constraint is also being applied to the supplied current. The constraints applied are shown below.

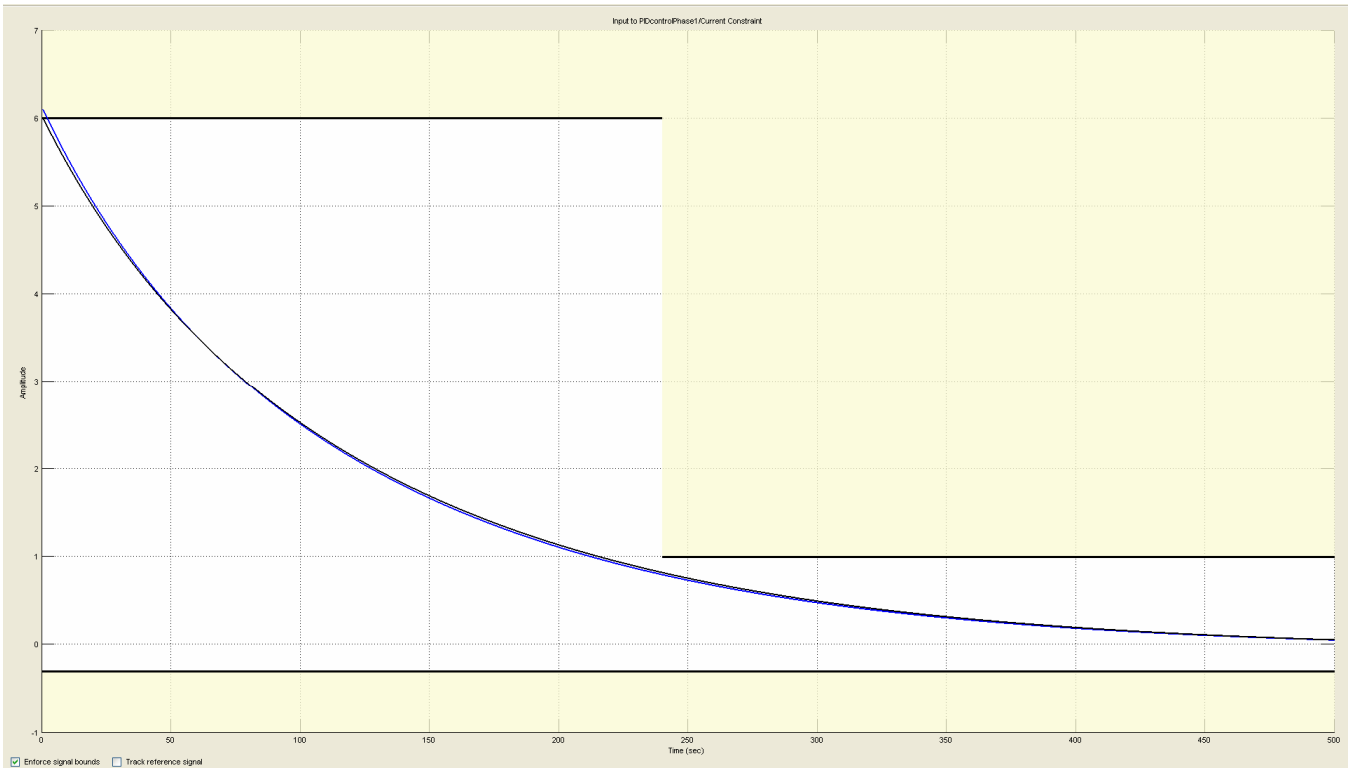

Figure 63: Current Constraint with Current versus Time (Showing constraint in the form of a step from 6 amps to 1 amp at 240 seconds)

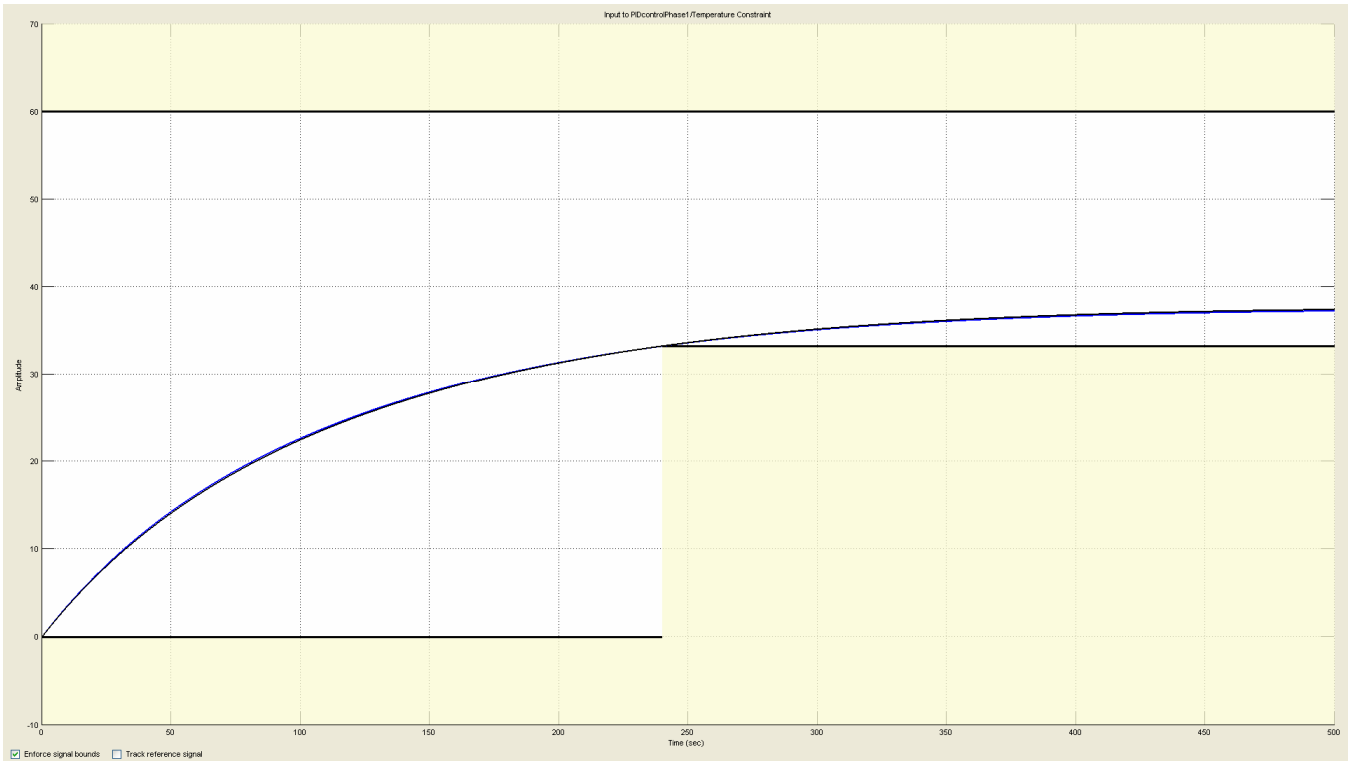

Figure 64: T_0 Temperature Constraint with Temperature versus Time (Showing constraint as a step from 0 °C to 33.25 °C at 240 seconds)

The temperature constraint consists of a single step, and an upper bound. This is based on the system to be benchmarked against. The only requirement is that the system reaches operating temperature in four minutes or 240 seconds. The upper bound limits the system to a maximum temperature of *60 °C*, which is the final operating temperature of the fuel. The current constraint consists of a single step. The maximum current is initially set at a current of *6 amperes*. The bottom current constraint is set at *-0.3 amps*. The step occurs at 240 seconds and requires that the current be less than *1 amp*. An easy way to interpret the constraint figures is that the white area is allowable values, while the shaded areas are unallowable values for the variable to take.

Once the constraints have been applied the next step is to tell the code which variables that may be varied to achieve the desired response. In this instance the variables that the model is allowed to change are the three control laws gains of k_p, k_i, and k_d. This is done in the dialog box shown below.

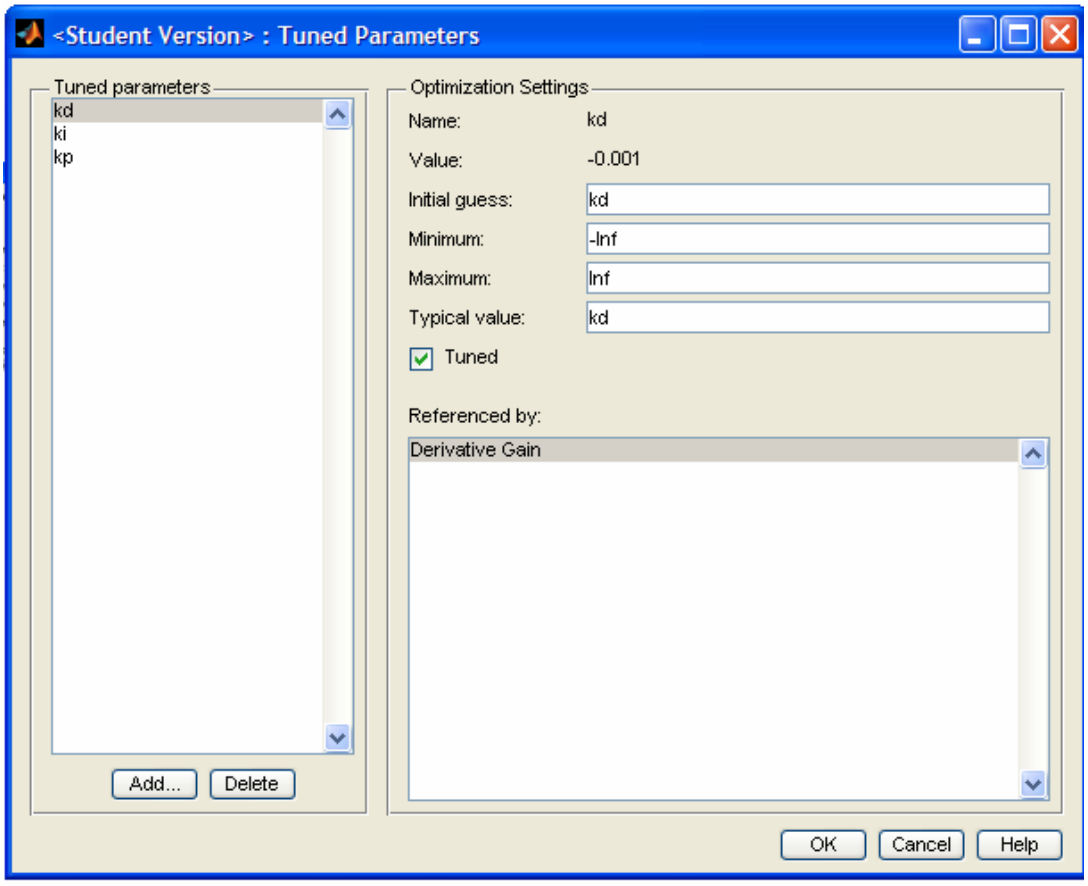

Figure 65: Tuned Parameters Dialog Box

Now the optimization can be run. The optimization runs in the window shown below, recording the values and other relevant optimization parameters.

```
                                  max                  Directional  First-order
 Iter  S-count         f(x)    constraint    Step-size   derivative   optimality  Procedure
    0        1            0      0.01616
    1       14            0   1.264e-006            1            0      0.00275
Successful termination.
Found a feasible or optimal solution within the specified tolerances.

kd =

   -0.3270


ki =

  1.6932e-004


kp =

    0.1687
```

Figure 66: Optimization Run Information (Showing the final values compromising a solution to the optimization, and data about each iteration of the optimization code)

As can be seen the code converged to a set of PID gains that would allow the model to operate within the constraints applied earlier. From Figure 66 it can be seen that the values of k_p, k_i, and k_d equal to *0.1687, 1.6932×10*$^{-4}$, and *-0.3270* respectively yield a satisfactory solution. With a set of optimized control law gains, the Phase 1 model was run to produce a set of temperature and current graphs shown below in Figure 67, Figure 68, and Figure 69.

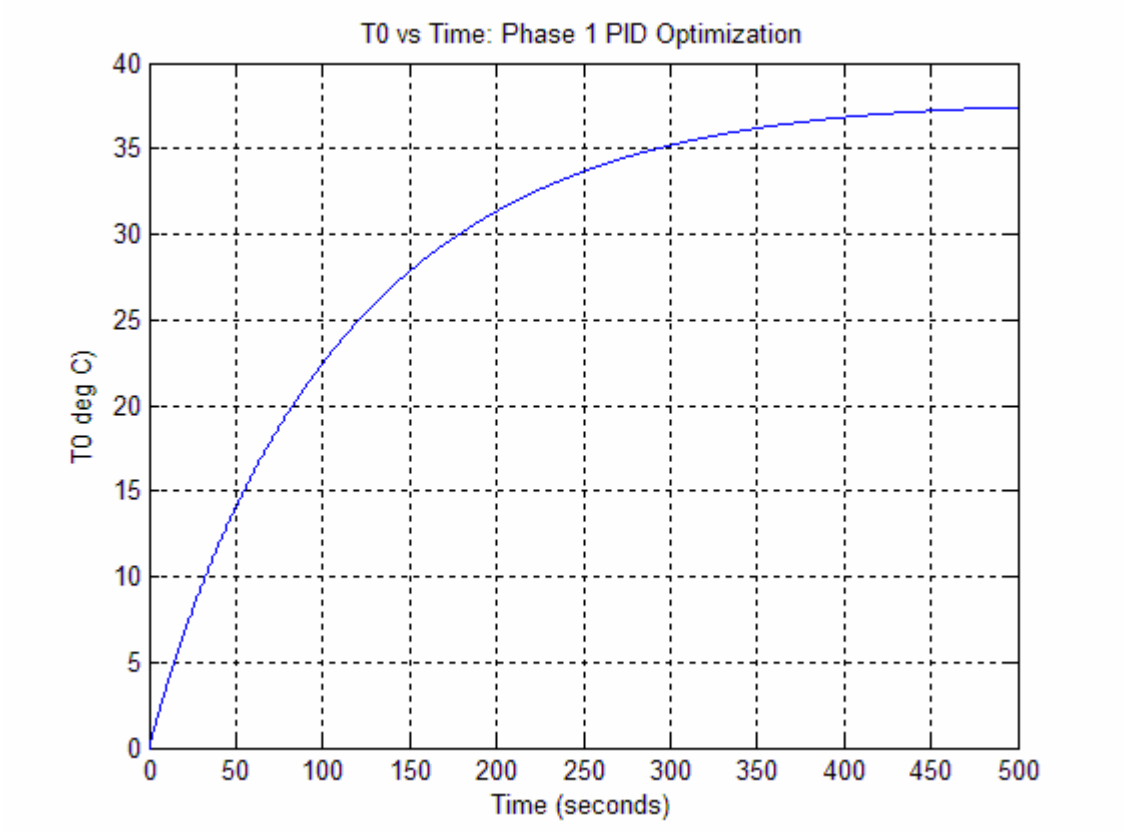

Figure 67: T_0 versus Time: Phase 1 Optimized Gains

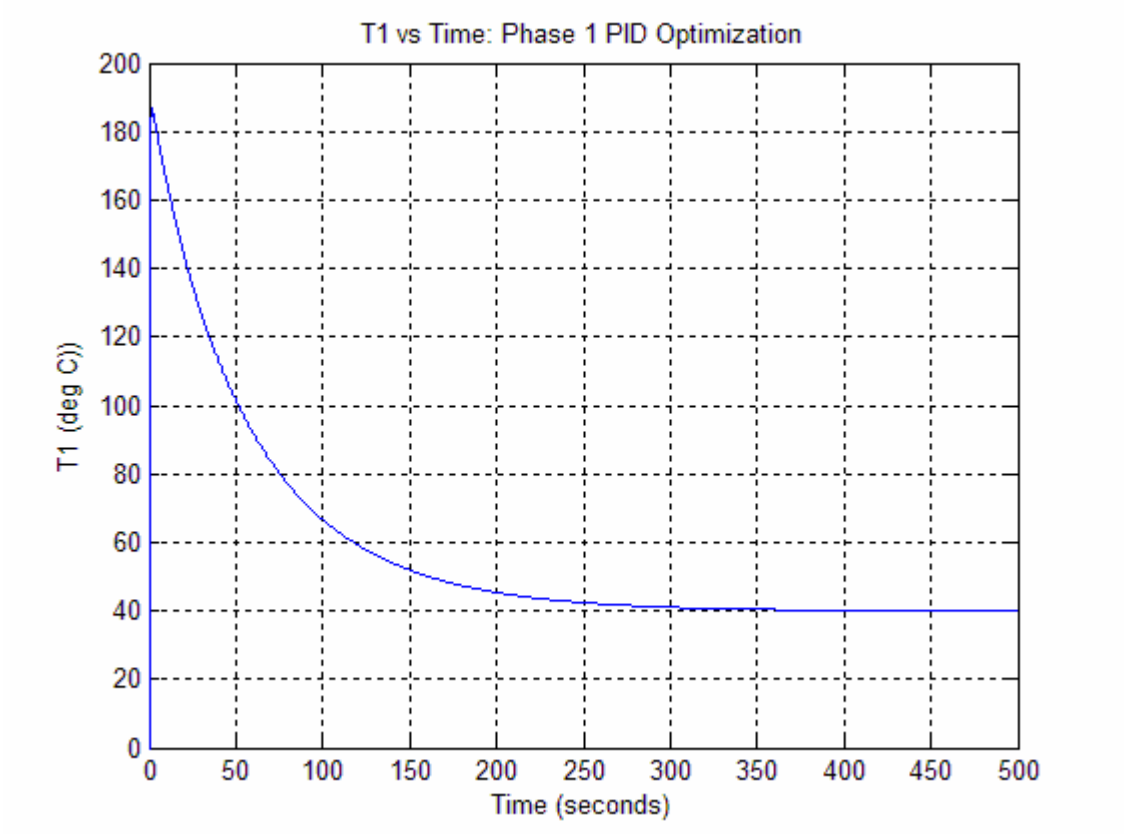

Figure 68: T_1 versus Time: Phase 1 Optimized Gains

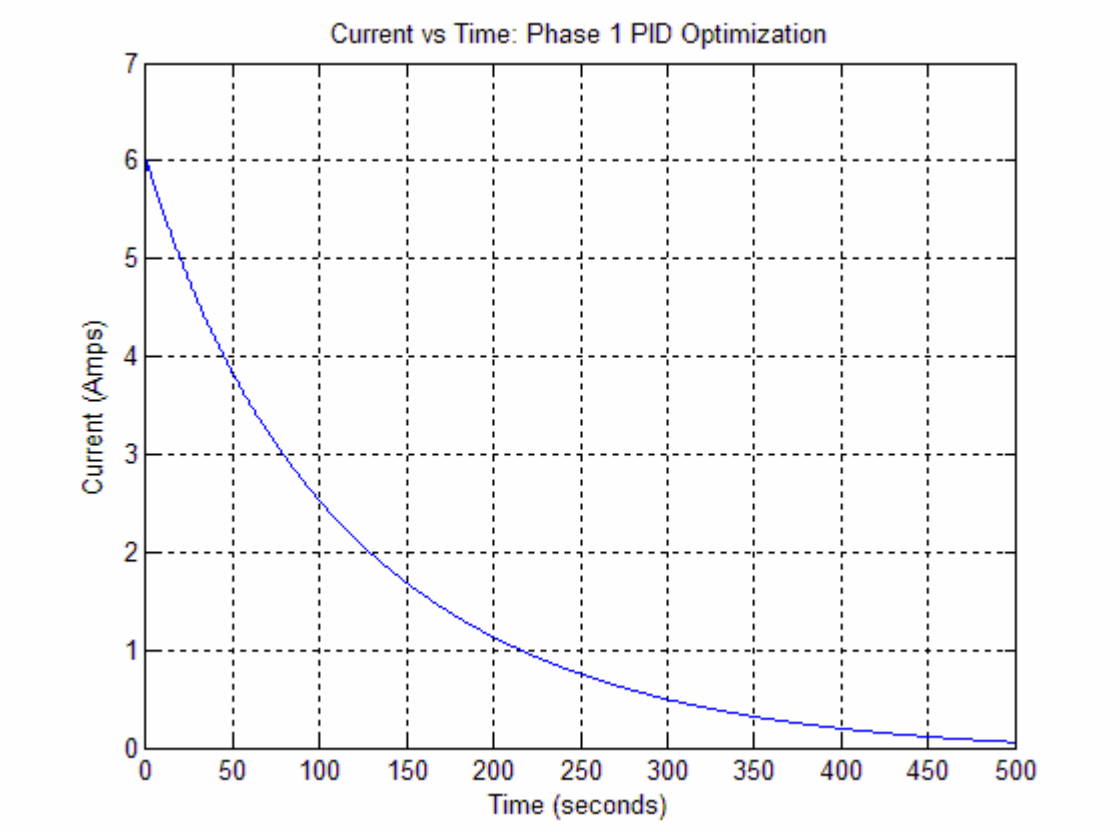

Figure 69: Current versus Time: Phase 1 Optimized Gains

T_0, as can be seen from Figure 67, is exhibiting acceptable behavior. The response is quickly ramping up passing through the required temperature range and eventually settling back toward the goal temperature as time pass *500 seconds*. This overshoot is expected as using a k_i to speed the response up leads to an overshoot such as this one. The T_1 response curve shows the expected peak at the beginning of operation as the joule heating raises the effective thermoelectric element's temperature and then the response settles down to a steady state value at the temperature of the eutectic reservoir. The current plot shows the system starting at a peak value of *6 amperes*, the maximum allowed for the elements, dropping to less than *1 ampere* just after 240 seconds.

2.9. Beta Plant Uncertainty

Now that an initial optimization has been run it is worthwhile to examine how well the control law gains can be tuned when the *beta* plant model has some uncertainty in the parameters. The Simulink© Response Optimization package allows for adding in plant uncertainty. The four plant variables, which are most likely to vary, are the specific heat of the fuel, C_f, the convection coefficient, h_0, the effective Seebeck coefficient, S_{eff}, and the resistance of the thermoelectric elements, R_{te}. A 5% variance will be placed on each one of these variables simultaneously and a new set of control law gains will be obtained. The simulation will be a Monte Carlo type of random values within the bounds of the plant uncertainty, with five samples. This means that five samples will be taken within the uncertainty bounds for each of the variables and the model then determines which set results in the maximum and minimum values. The graph is showing the run data from those two sets as well as the data from the nominal model parameters on the model constraint graphs. The uncertainty parameter input is shown below.

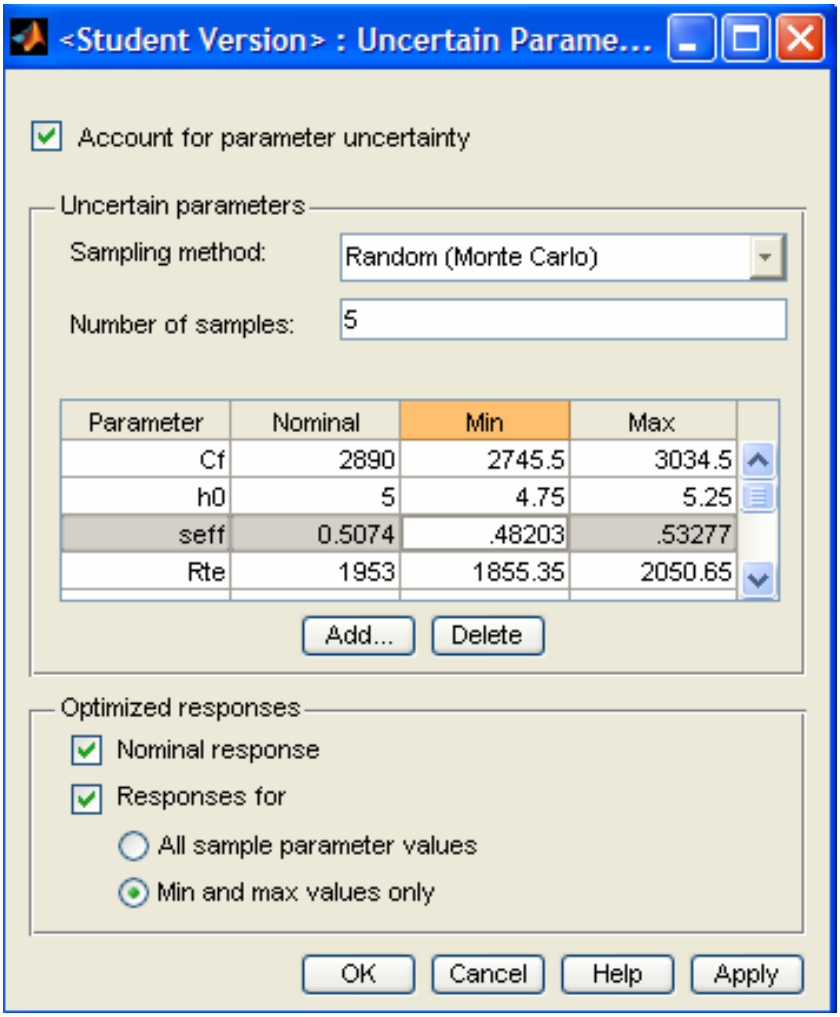

Figure 70: Plant Uncertainty Input Dialog

The input dialog shows the uncertainty sampling method, which as mentioned above, was chosen to be Monte Carlo. The number of samples is five. The parameters that uncertainty is applied to are shown in the table in the middle of the dialog box. Finally, the responses are plotted for the nominal values, as well as the values of the plant parameters that yield the minimum and maximum values for the response.

As with the optimization parameter, bounds must be input for the optimization to run. The temperature constraint was left exactly the same as for the optimization run

above, that is a step from a minimum value of T_0 to *33.25 °C* at 240 seconds. The current constraint unfortunately had to be relaxed for the model to obtain a successful solution. The current constraint still is a step occurring at 240 seconds, but the step has been increased from *1 ampere* to a value of *1.25 amperes*. The current and temperature constraint graphs are shown below as Figure 71 and Figure 72.

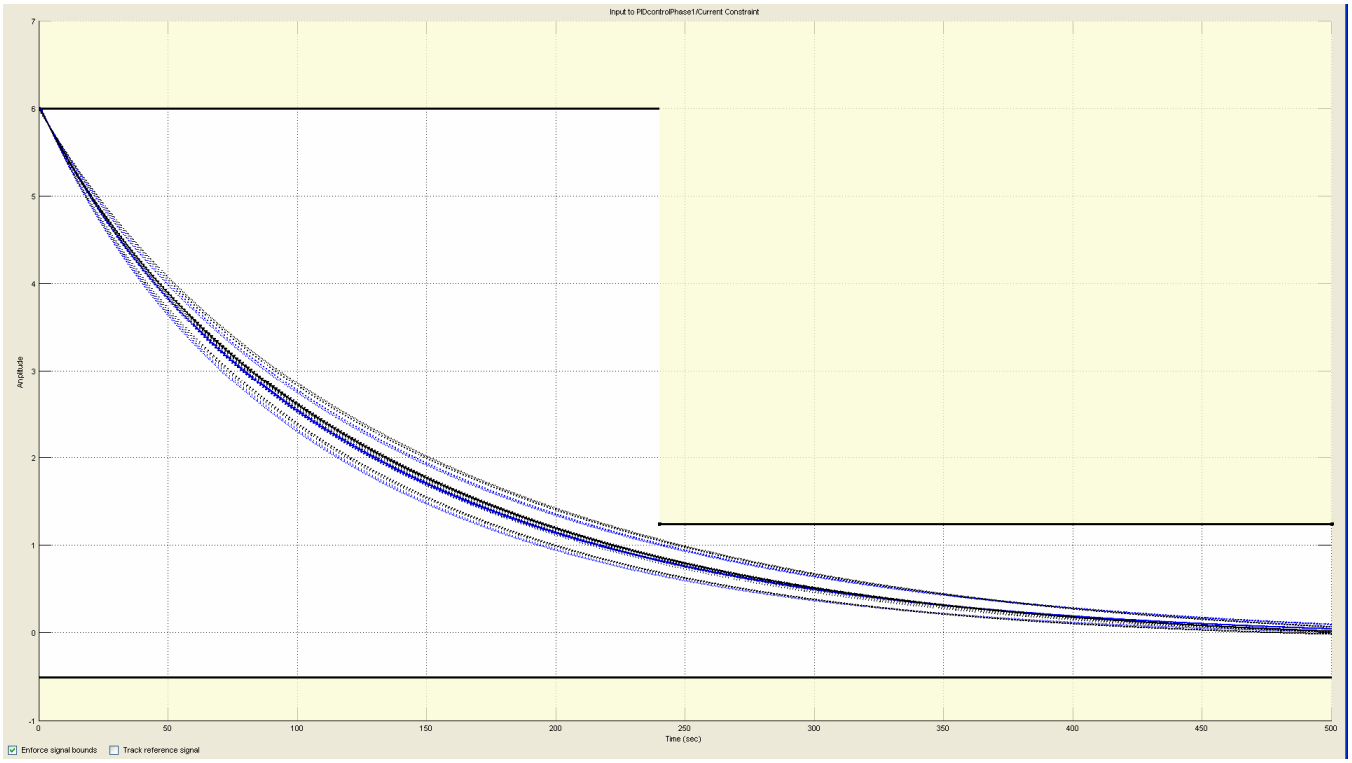

Figure 71: Current Constraint for Uncertainty (Showing step from 6 amps to 1.25 amp at 240 seconds)

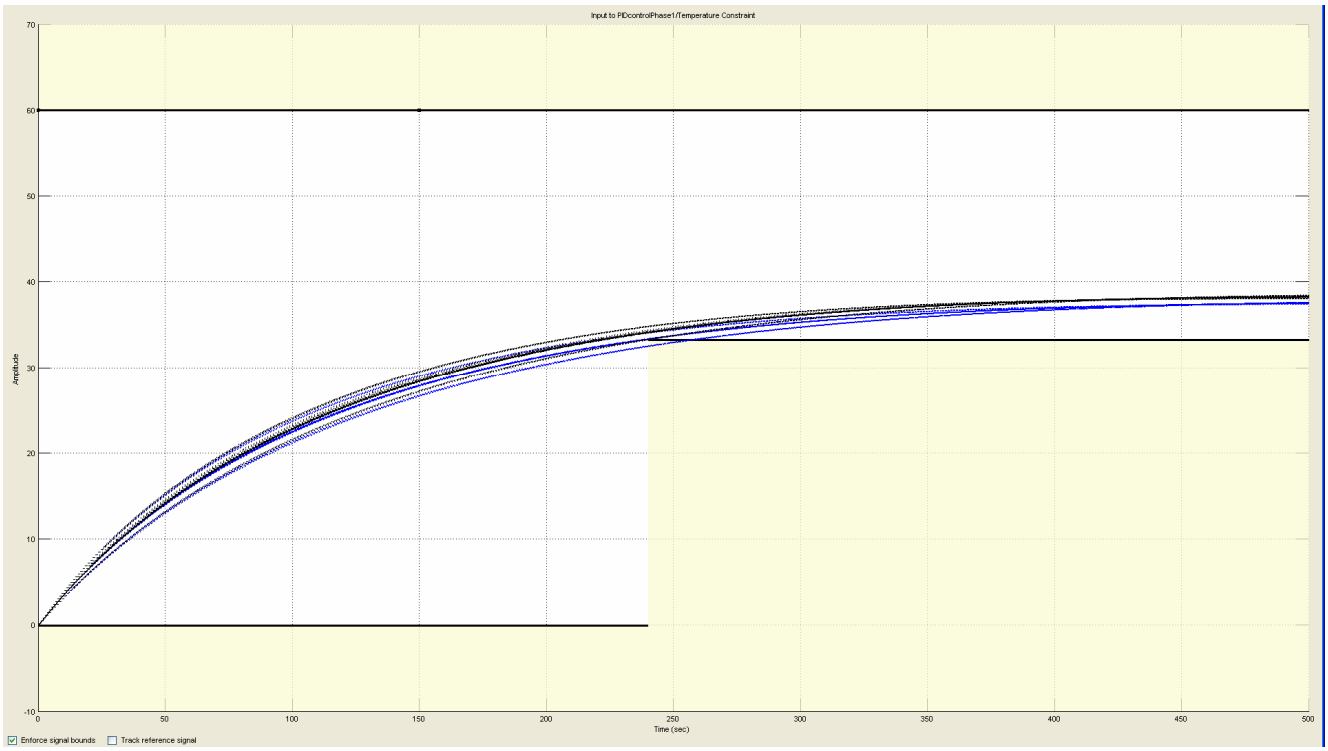

Figure 72: Temperature Constraint for Uncertainty (Showing step from 0 °C to 33.25 °C at 240 seconds)

The current and temperature constraint graphs show the minimum, nominal, and maximum response curves for each iteration. As can be seen on the second iteration (the black curves), the model was able to reach a satisfactory solution. The run information for the uncertainty optimization is shown below.

```
                                    max                  Directional  First-order
 Iter  S-count         f(x)    constraint    Step-size   derivative   optimality
    0        1            0         3.333
    1      280            0      0.000315            1            0     0.000439
Successful termination.
Found a feasible or optimal solution within the specified tolerances.

kd =

   -0.5929


ki =

  2.3888e-004


kp =

    0.1655
```

Figure 73: Uncertainty Run Information (Showing the final values compromising a solution to the optimization, and data about each iteration of the uncertainty optimization code)

As can be seen in Figure 73, a robust control law is provided by utilizing the gains: $k_p = 0.1655$, $k_i = 2.3888 \times 10^{-4}$, and $k_d = -0.5929$. That is to say that the model is able to handle the aforementioned uncertainty with the above gains.

While the model is fairly robust, it could be more robust if there was a greater amount of deviation allowed, or if more plant parameters were allowed to have uncertainty. However, computational limitations prevented this. As a useful note, the code was all run on a Dell© XPS 1710 series laptop containing an Intel Core 2 Duo T7400 running at 2.14 GHz, and 2 GB ram running at 667 MHz, and 15 Gb of free hard drive space. A typical Phase 1 model runs in less than 5 seconds, but an optimization run takes approximately 20 minutes. An uncertainty run if it does not fail to finish due to a lack of available memory runs in approximately an hour.

2.10. Beta Plant Phase 1 and Transition Supervisory Integration

With a robust Phase 1 control law obtained for the *beta* plant model it is now time to prepare it for integration into the supervisory control law to prepare for a full model run. To integrate the model, the Simulink© model must undergo several changes. The new Simulink© model is shown below.

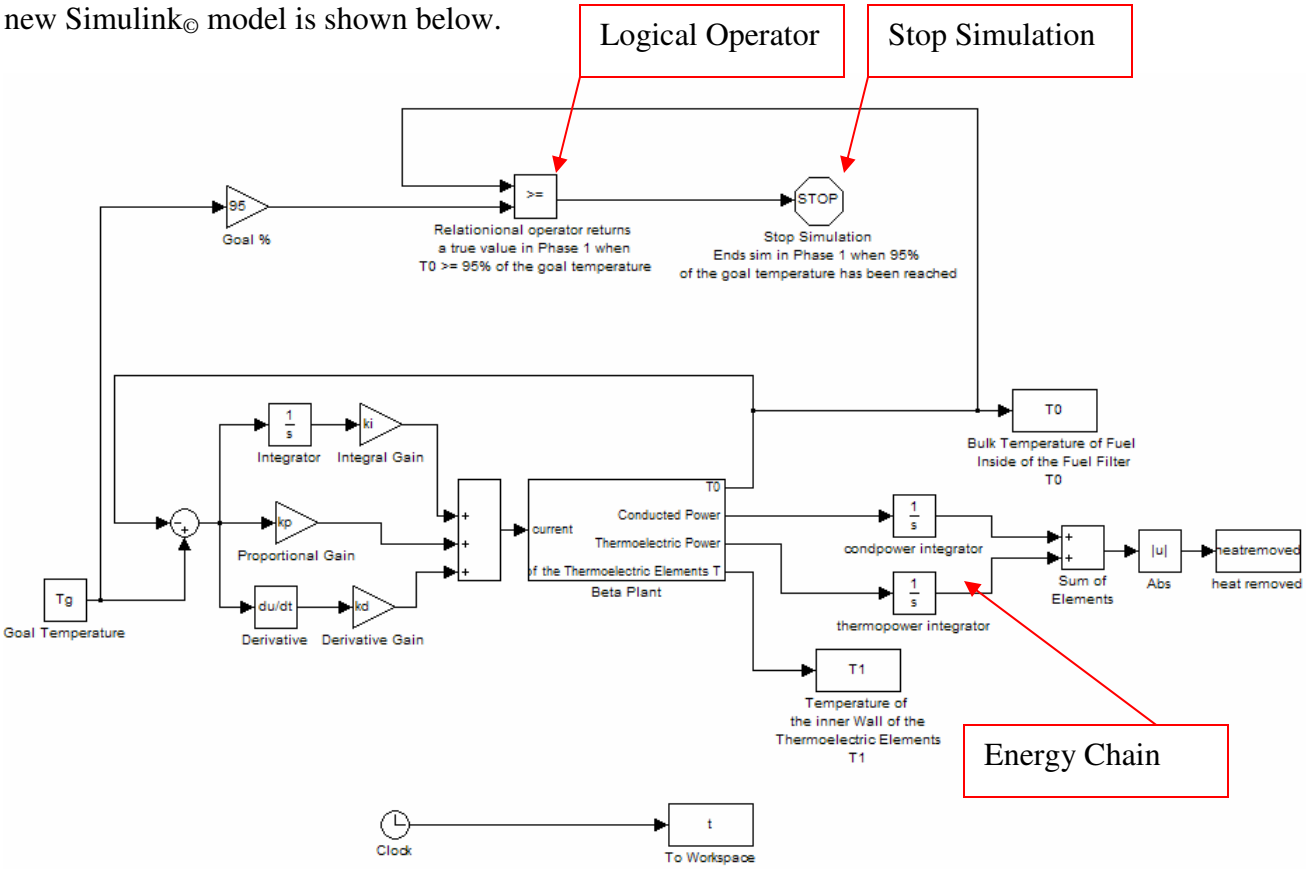

Figure 74: *Beta* Plant Phase 1 PID Integrated Model

The new integrated model has several additional items in it. First, the conducted power and thermoelectric power blocks no longer end in a terminator block. Both now proceed to an integrator block to transfer them into an energy removed term. Then the

signals proceed to a sum of elements block, which ends up outputting the final values from the integrators yielding a total energy removed during the Phase. This value then proceeds to an absolute value block to aide in the processing within the supervisory control law. Finally, the signal is output to the workspace using a "to workspace" block. This grouping of blocks is labeled as the energy chain in Figure 74. The model also no longer runs for a specified time, instead a stop simulation block and a logical operator block allow the model to compare back to its goal and end the simulation when 95% of the goal temperature, T_g, has been reached. The logical decision making is performed using the "Logical Operator" block and the stopping of the simulation is accomplished using the "Stop Simulation" block.

Next, the Transition Simulink© model must be created. It differs slightly from that of the Phase 1 model. The real difference at the Simulink© level is that the end condition is not logical in nature, rather it is time based. As mentioned above, the warm-up time for the engine is assumed to be five minutes and therefore the Transition model runs for 5 minutes. The Transition model is shown below in Figure 75.

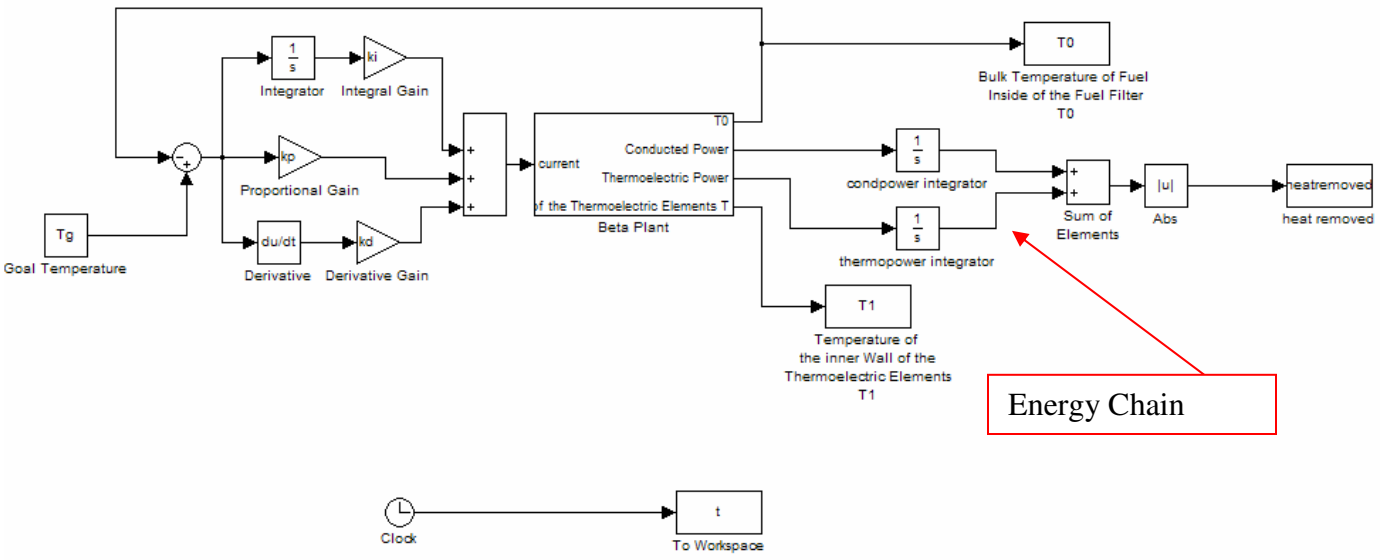

Figure 75: *Beta* Plant Transition Integrated Model

As can be seen, the model is essentially the same as the Phase 1 integrated model with the removal of the stop simulation block.

2.11. Beta Plant Phase 2 Model and Supervisory Integration

With integrated Phase 1 and Transition models obtained, the next step is to create a Phase 2 model. The Phase 2 model still utilizes the *beta* plant subsystem, but instead of a control law, the current supplied is at a constant value. The current supplied will be a constant *-1.0 amperes*, which will cause the model to force heat back into the eutectic reservoir from the fuel filter. The model will run until the heat forced back into the filter is equal to or greater than the heat removed during the Phase 1 and Transition operation. The Phase 2 Simulink© is shown in Figure 76.

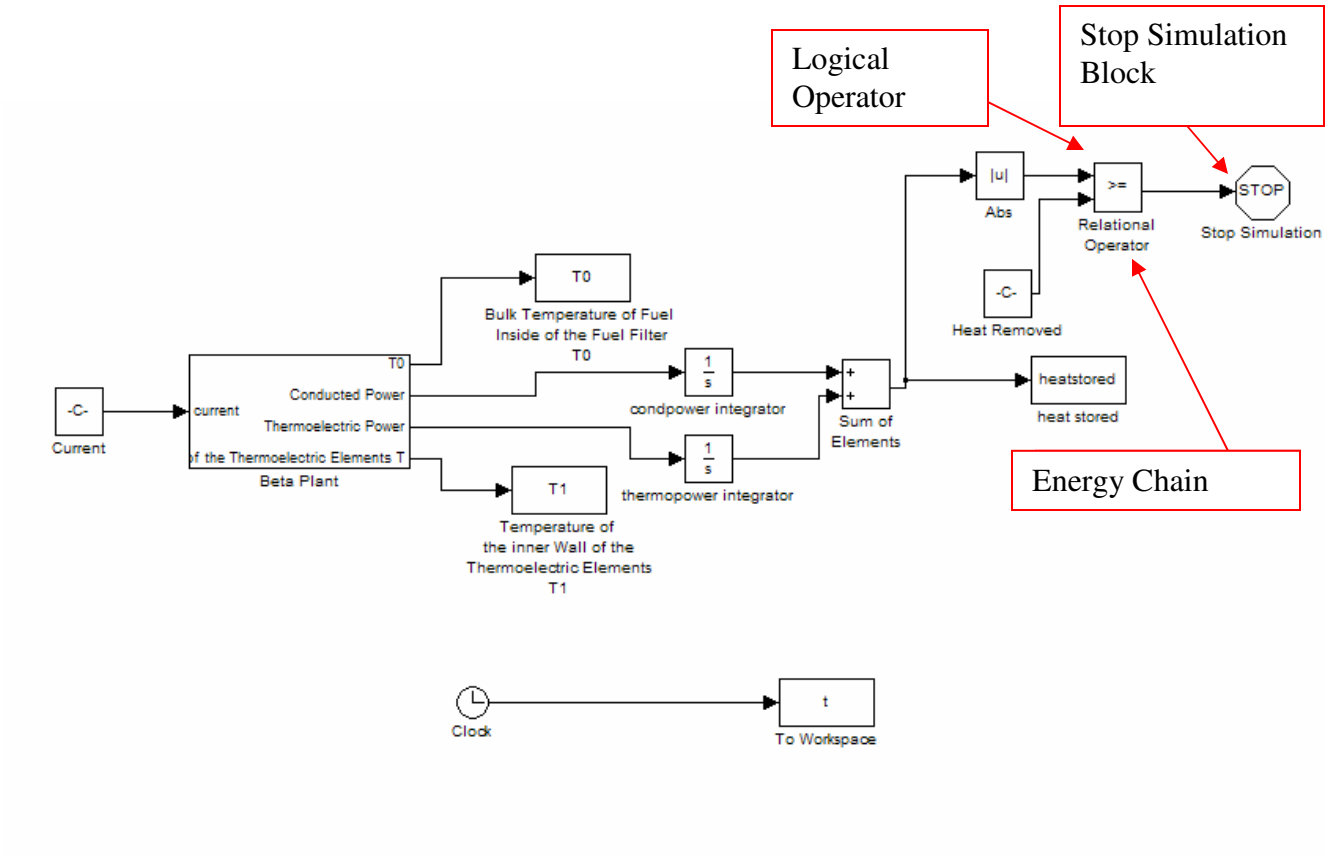

Figure 76: *Beta* Plant Phase 2 Integrated Model

As mentioned above the current supplied now is a constant value. Additionally the end condition is when the heat stored is greater than or equal to the heat removed during the Phase 1 and Transition operation. It can be seen that the "Logical Operator" block and the "Stop Simulation" block have been moved to the energy chain portion of the model showing that the model is checking to see the energy stored.

2.12. Beta Plant Phase 3 Model and Supervisory Integration

With the Phase 2 model now complete the Phase 3 model must be constructed. The Phase 3 model is very similar to the other models. The main difference is that there is no current supplied to the thermoelectric elements. The Phase 3 Simulink© model is shown below.

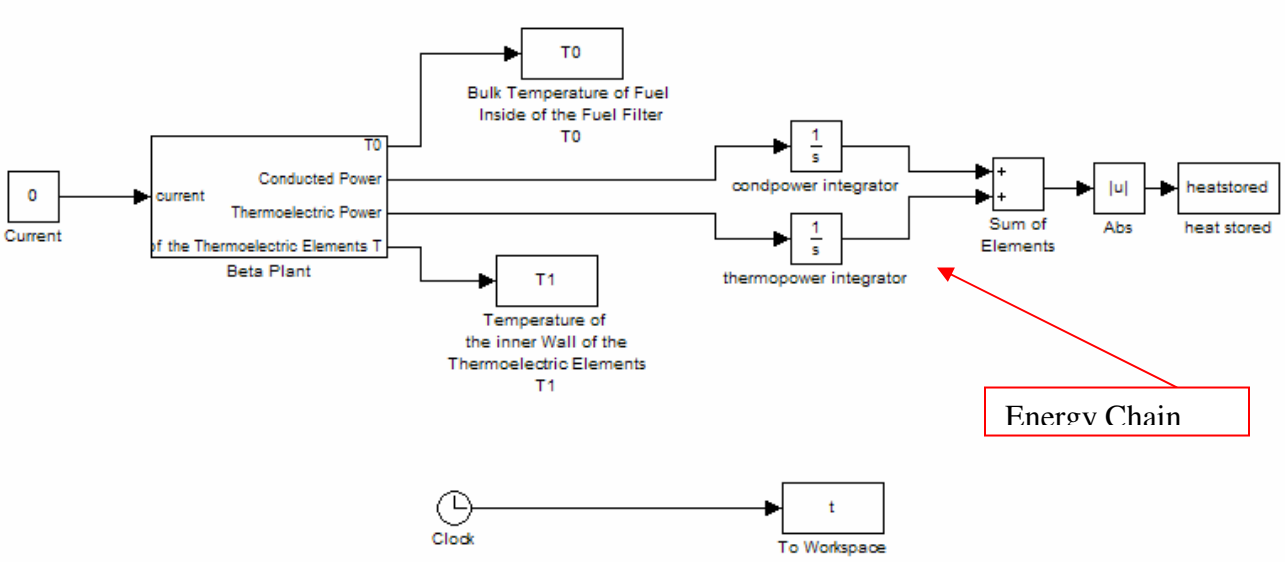

Figure 77: *Beta* Plant Phase 3 Integrated Model

The model has a current input of a constant value of *0 amperes*. The conducted power and thermoelectric power blocks are both present in the model, once again shown as a portion of the part of the model labeled the energy chain. The conducted power block serves two purposes. First, it allows for the heat stored in the filter to be tracked, additionally, it allows the electric power generated by the thermoelectric elements to be calculated. The thermoelectric power block is unnecessary as there should be no electrical power consumption, but it remains as a check to ensure that the model is performing as expected. Additionally, though not shown in the model above, the run time for the model is adjusted to be 2700 seconds or 45 minutes of driving.

2.13. Supervisory Control Law

With all Simulink© models created and prepared for integration into the overall supervisory control law, the supervisory control law itself must be constructed. The

supervisory control law as mentioned previously runs a level above the Simulink© models and is responsible for integrating the four Simulink© Phase models together. In addition the supervisory control law performs any additional calculations that are necessary for the Simulink© models to run. The supervisory control also plots the data. The supervisory control law exists as a .m Matlab© file. The supervisory control law is broken into several sections to aid in the understanding of the code. It should be noted that the Phase timing strategy number 2 shown in Figure 6 in Section 2.1 is being used in an attempt to minimize the power consumed. Phase change strategy 2 involves delaying Phase 2 operation until after the vehicle is shut down to allow for the Phase 3 heat transfer to occur first.

2.13.1. Variable Assignment

The first section in the supervisory control law is the variable assignment. This section initializes and assigns values to the variables the supervisory control law and the Simulink© models need to run. The code for this section is shown below in red text. Coding comments are preceded by a % sign.

```
h0 = 5;          %Convection coefficient between fuel filter wall and the
                 %Fuel slug matrix [W/m^2/K]
Ti = 60;         %Final fuel inlet temperature [deg C]
H = .1524;       %Height of the fuel filter [m]
r1 = .0508;      %Radius to the filter wall [m]
r2 = .05239;     %Radius to the outside of TE elements [m]
Rte = 1953.29;   %Total electrical resistance of the TE elements [ohms]
T2 = 40;         %Temperature of the TE elements at r2 [deg C]
kte = 15.056;    %Effective thermal conductivity of the TE elements [W/mK]
m0 = 1.1305;     %Mass of fuel slug [kg]
mte = .6374;     %Effective mass of thermoelectric elements [kg]
seff = .50743;   %Effective seebeck coefficient [V/K]
Cf = 2890;       %Specific heat of fuel [J/kgK]
Cte =477.27;   %Effective specific heat of thermoelectric elements [J/kgK]
T0i = 0;         %Initial temperature of the fuel in the filter [deg C]
kp = .1655;      %Control Law proportional gain [dimensionless]
ki = 2.3888E-4; %Control Law integral gain [dimensionless]
kd = -.5929;     %Control Law derivative gain [dimensionless]
Tg = 35;         %Goal Temperature [deg C]
```

```
powfact = 26.74E-4      %power factor from Zc equation = S^2*sigma
```

The variable assignment portion of the supervisory control law is very straightforward. The values for variables are the same as laid out in the sections above and Table 1

2.13.2. Phase 1

The code for the Phase 1 portion of the supervisory control law is shown below.

```
mdot = 0;   %set fuel mass flow rate to zero for Phase 1

sim('Phase1integrated');    %run the phase1 integrated model

T0phase1 = T0;  %Assign the run data to phase1 specific variables
T1phase1 = T1;
currentphase1 = current;
tphase1 = t;

lphase1 = length(t);

heatremovedtotal = heatremoved(lphase1); %store the total heat removed from
                                         %the eutectic reservoir
```

The Phase 1 portion of the code begins by laying out the additional parameters necessary for the model to run, namely setting the mass flow rate to *0 kg/s*. Next, the code calls for the Phase 1 integrated model to be run. After the model is run the code loads the T_0, T_1, *current,* and *time* variables into unique Phase1 versions. Then, the code calculates the length of those vectors using the "`length`" command. Finally, the `heatremovedtotal` variable is initialized and the value is set as the final value in the `heatremoved` variable vector.

2.13.3. Phase 1 Plotting

Shown below is the code for the Phase 1 Plotting portion of the supervisory control law

```
figure(1), plot(t,T0),grid on,
```

```
title('T0 vs Time: Phase 1'), xlabel('Time (seconds)'), ylabel('T0 deg C)')
figure(2), plot(t,T1), grid on, title('T1 vs Time: Phase 1'), xlabel('Time
(seconds)'),
ylabel('T1 (deg C))')
figure(3), plot(t,current), grid on,
title('Current vs Time: Phase 1'), xlabel('Time (seconds)'),
ylabel('Current (Amps)')
```

The Phase 1 Plotting portion of the supervisory control law is next. The code here is very basic and simply causes three figures to be created. The code then uses the plot commands to put data on the figures, labels the axes, labels the figure, and turns grid lines on for the figure.

2.13.4. Transition

The code for the Transition portion of the supervisory control law is shown below in red text.

```
mdot = .002352; %Mass flow of fuel when engine is on for transition [kg/s]
                  %set initial temperature for transition equal to final
T0i = T0(lphase1);
T1i = T1(lphase1);                    %temperature of phase 1
sim('Transitionintegrated');
T0trans = T0;  %Assign the run data to transition specific variables
T1trans = T1;
currenttrans = current;ttrans = t;

ltrans = length(t);
heatremovedtotal = heatremovedtotal + heatremoved(lphase1);
                              %store the total heat removed from
                              %the eutectic reservoir.
```

The Transition code is the next portion of the supervisory control law. The transition code first sets the mass flow rate. The code then sets the initial temperatures of T_0 and T_1 to be equal to their final values from Phase 1. The code calls for the model, creates the unique vectors, gets the length of those vectors, and updates the total heat removed next.

2.13.5. Transition Plotting

The Transition Plotting portion of the supervisory control law is shown below.

```
figure(4), plot(t,T0),grid on,
title('T0 vs Time: Transition'), xlabel('Time (seconds)'),
ylabel('T0 deg C)')
figure(5), plot(t,T1), grid on,
title('T1 vs Time: Transition'), xlabel('Time (seconds)'),
ylabel('T1 (deg C))')
figure(6), plot(t,current), grid on,
title('Current vs Time: Transition'), xlabel('Time (seconds)'),
ylabel('Current (Amps)')
```

The transition plotting code is essentially identical to the Phase 1 Plotting code.

2.13.6. Phase 3

The Phase 3 portion of the supervisory control law is shown below in red text.

```
T0i = T0(ltrans);  %set initial temperature for phase 3 equal to final
T1i = T1(ltrans);                    %temperature of the transition

sim('Phase3integrated');

T0phase3 = T0;  %Assign the run data to phase1 specific variables
T1phase3 = T1;
tphase3 = t;

lphase3 = length(t);

heatstoredtotal = heatstored(lphase3);

heatremovedtotal = heatremovedtotal - heatstoredtotal;
                %prepare remaining heat to be stored term for phase 2
```

The Phase 3 code follows the Transition Plotting code in the supervisory control law. The code sets the new initial temperatures. The Phase 3 code then calls the model. Then, the unique variables are created, and their length is computed. The `heatremovedtotal` value is adjusted by subtracting the heat stored during the Phase 3 operation.

2.13.7. Phase 3 Plotting

Shown below is the Phase 3 Plotting portion of the supervisory control law code.

```
figure(7), plot(t,T0),grid on,
title('T0 vs Time: Phase 3'), xlabel('Time (seconds)'),
ylabel('T0 deg C)')
figure(8), plot(t,T1), grid on,
title('T1 vs Time: Phase 3'), xlabel('Time (seconds)'),
ylabel('T1 (deg C))')
```

The Phase 3 plotting code again is nearly identical to the plotting code from Phase 1. The only notable difference is that the current is no longer plotted since there is no current supplied during Phase 3.

2.13.8. Phase 2

The Phase 2 portion of the supervisory control law is shown below.

```
mdot = 0;   %set fuel mass flow rate to zero for Phase 2
current = -1; %set constant current supplied to the TE elements for Phase 2

T0i = T0(lphase3); %set initial temperature for transition equal to final
T1i = T1(lphase3);                    %temperature of phase 1

sim('Phase2integrated');

T0phase2 = T0;  %Assign the run data to phase1 specific variables
T1phase2 = T1;
tphase2 = t;

lphase2 = length(t);
```

The code for Phase 2 begins by setting mass flow rate back to a value of 0 kg/s as the engine is off during Phase 2 for this mode of operation. The code also sets the *current* to be a steady *-1.0 amperes*. Then, the code sets the initial temperatures for the Phase 2 operation. Next, the model for Phase 2 is called and run. Finally, the code creates the unique temperature vectors, and computes the length.

2.13.9. Phase 2 Plotting

The code for Phase 2 Plotting portion of the supervisory control law is shown below.

```
figure(9), plot(t,T0),grid on,
title('T0 vs Time: Phase 2'), xlabel('Time (seconds)'),
ylabel('T0 deg C)')
figure(10), plot(t,T1), grid on,
title('T1 vs Time: Phase 2'), xlabel('Time (seconds)'),
ylabel('T1 (deg C))')
```

The Phase 2 Plotting portion of the code is again very similar to all the other plotting

2.13.10. Post Run Analysis

With all of the phase portions of the supervisory control law completed, the Post Run Analysis section is next. The Post Run Analysis section performs additional calculations necessary to better analyze the data from the runs. This includes the creation of phase spanning current and time variables. Additionally, the code calculates the total energy consumed during operation. Finally, the code calculates the energy generated by the system during Phase 3. The energy generated is calculated using several equations [1]. The maximum efficiency for the generation was used, and although the system is not ideal the value should vary less than 10% from the true value. The equation for the maximum efficiency is shown in Equation 40.

$$\phi_{\max} = \eta_c \gamma \tag{40}$$

The maximum efficiency is a product of the Carnot efficiency, η_c, and the material efficiency, γ. The Carnot efficiency and the material efficiency are shown below in Equations 41 and 42 respectively,

$$\eta_c = \frac{T_H - T_C}{T_H} = \frac{T_1 - T_2}{T_1} \tag{41}$$

$$\gamma = \frac{\sqrt{1+Z_c\overline{T}}-1}{\sqrt{1+Z_c\overline{T}}+\frac{T_H}{T_C}} = \frac{\sqrt{1+Z_c\overline{T}}-1}{\sqrt{1+Z_c\overline{T}}+\frac{T_1}{T_2}}$$

where (42)

$$\overline{T} = \frac{T_H + T_C}{2} = \frac{T_1 + T_2}{2}$$

The variable in Equation 42, Z_c, is a material driven thermoelectric figure of merit and is given by:

$$Z_c = \frac{S^2\sigma}{k_{te}} \tag{43}$$

The term $S^2\sigma$ is termed the power factor and is a model parameter given in Table 1.

The code for the Post Run Analysis is shown below:

```
currentphase3 =tphase3.*0;
currentphase2 =tphase2.*0.+-1;
currenttotal = [currentphase1;currenttrans;currentphase3;currentphase2];
totallength = lphase1+ltrans+lphase3+lphase2;
finaltime = .01*totallength-.01;
ttotal = [0:.01:finaltime]';
powerconsumed = currenttotal.*currenttotal*Rte;
totalenergyused = trapz(powerconsumed)*.01
Zc= powfact/kte;
etac = (T1phase3(lphase3)+T2)/T1phase3(lphase3);
gamma=((1+Zc((T1phase3(lphase3)+T2))/2)^.5-1)/((1+Zc...
    ((T1phase3(lphase3)+T2))/2)+(T1phase3(lphase3/T2);
energygenerated =heatstoredtotal*etac*gamma
```

The code begins by constructing a full matrix for the currents for both Phase 2 and Phase 3. Next the code concatenates the currents to create a total current variable.

The code then proceeds to construct a complete time variable. The power consumed by the system by squaring the current and multiplying it by the electrical resistance for each value of the vector. Finally the total energy used is computed by using the "`trapz`" trapezoidal integration function. The code then computes the variables required for the generation efficiency. This efficiency is then multiplied by the heat stored during Phase 3 to obtain the energy generated.

2.13.11. Post Run Plotting

The Post Run Plotting code from the supervisory control law is shown below.

```
figure(11), plot(ttotal,currenttotal),grid on,
title('Current vs Time: Complete Run'), xlabel('Time (seconds)'),
ylabel('Current (Amps)')
```

The code for the Post Run Plotting is very similar to the other plotting codes containing the plot command, and the labeling commands.

This concludes the development of the supervisory control law; the models are now ready for a full run.

3. Run Data

With the models complete the next step is to conduct a full run to retrieve the data to assess the system viability.

3.1. Benchmarking

To accurately assess the viability of the system a benchmark must first be established. The Racor Series C fuel filter and heater was chosen to benchmark against, as it is a typical commercially available fuel heater for an engine of approximately the same size. The heater in the filter is a *300W* electrical resistance heater and requires a four minute maximum time to allow for start up [40]. The heater runs continuously at its power for the four minutes. The total power consumed by the heater is *72000 J* To perform better, the E-TE system should maintain a four minute or less time, and utilize approximately the same, or less, energy. It should be noted that the initial temperature, for which data was provided, for the Racor heater was *0°C*. Thus for the run data the initial temperature will remain at *0°C*.

3.2. 0°C Starting Temperature

The data for the *0°C* starting temperature is presented in the order of system operation, beginning with Phase 1 through Phase 3. It is worth noting again that only Phase change strategy 2 was utilized. The performance of each Phase will be examined, and then the overall system run will be examined. Therefore the temperature data for

Phase 1 including T_0 and T_1 is shown below in Figure 78 and Figure 79 . The current graph for Phase 1 is shown in Figure 80.

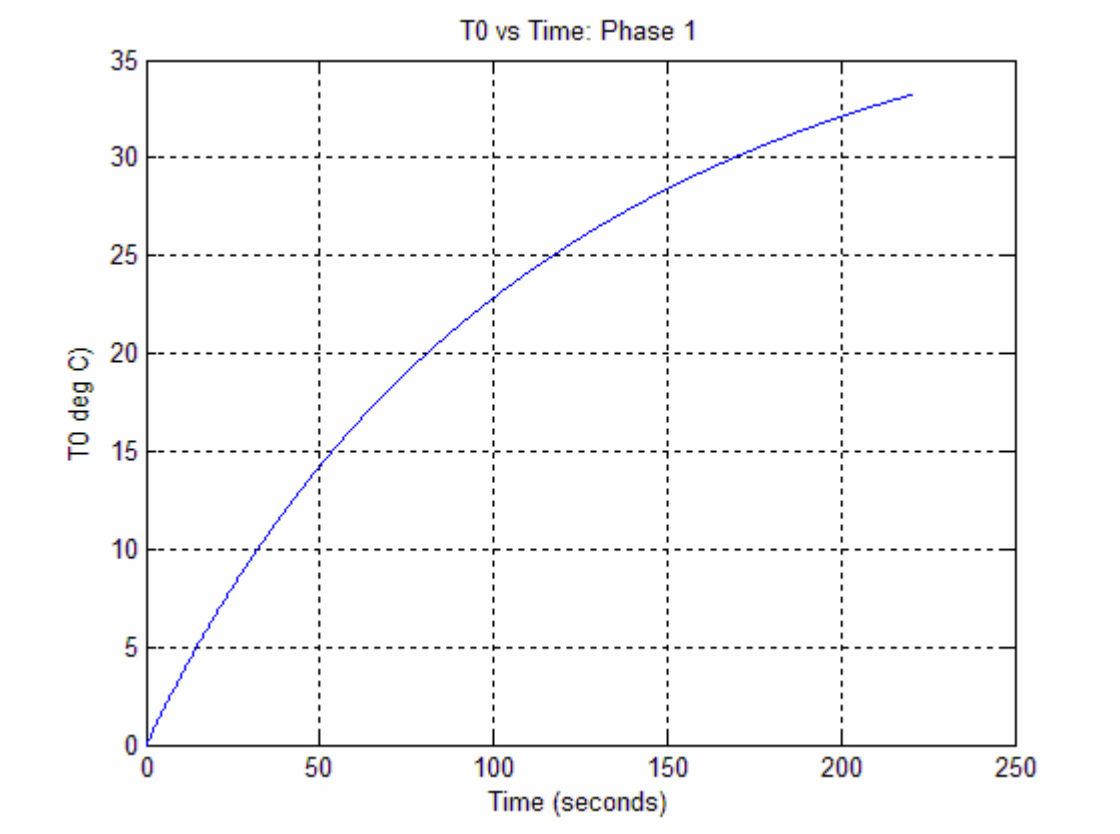

Figure 78: T_0 versus time: Phase 1

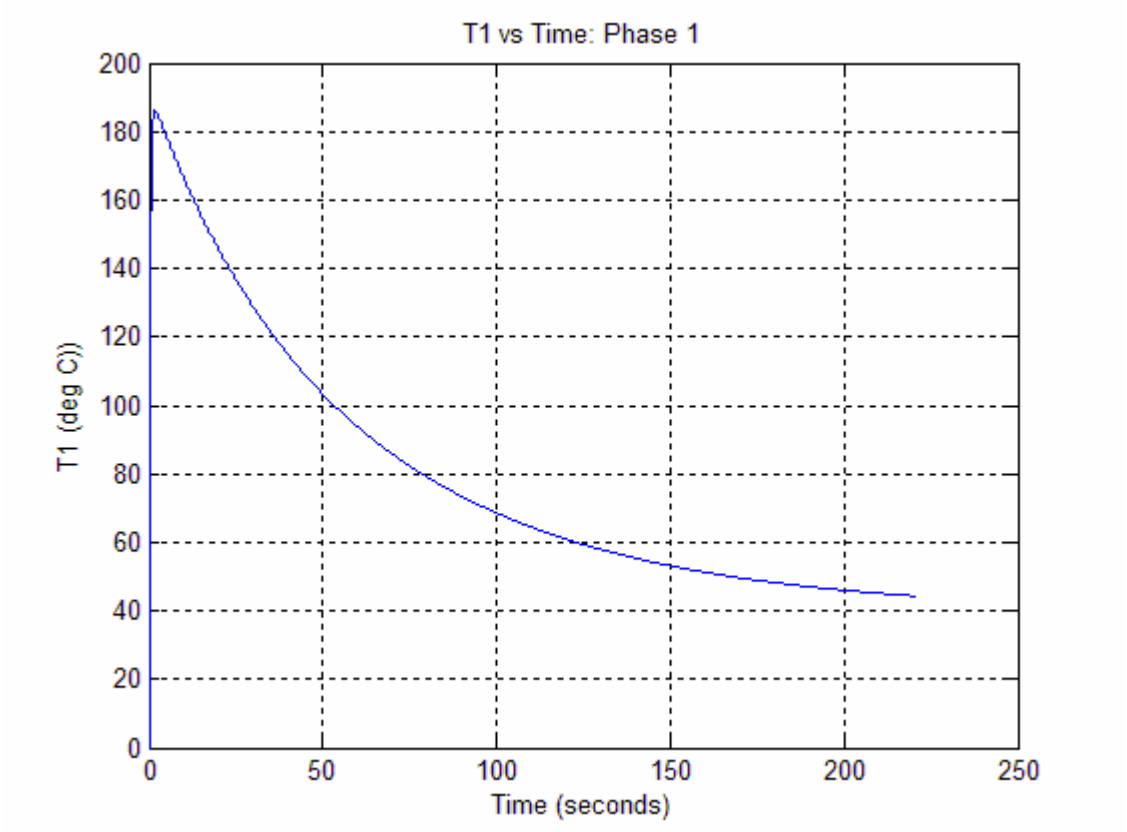

Figure 79: T_1 versus time: Phase 1

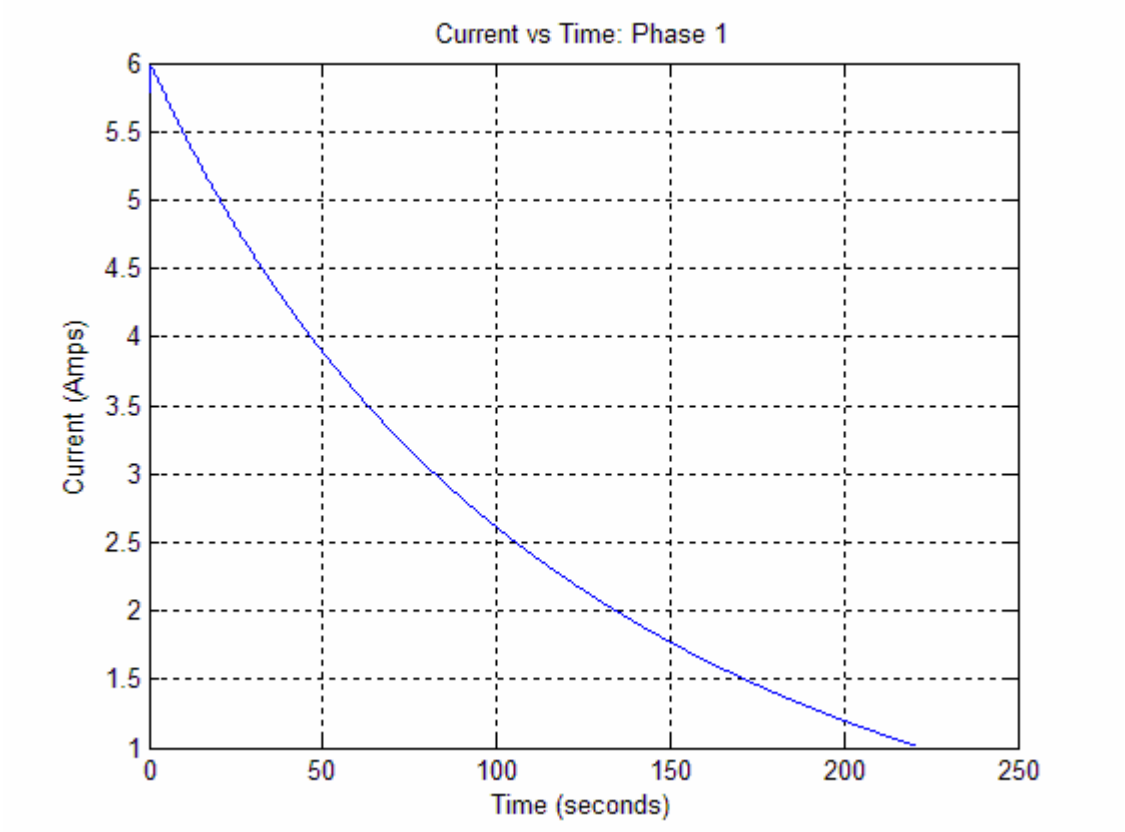

Figure 80: Current versus time: Phase 1

The T_0 temperature graph shows that the system is indeed performing adequately from a time perspective achieving a sufficient temperature to start the engine within 240 seconds and thus matching the benchmarked resistive heater. The system is actually performing slightly faster than 240 seconds, which is expected as the system is currently running with nominal plant parameters not the parameters associated with the worst case from the uncertainty study. The response shape as expected is typical of the system performance from the previous validation, optimization, and uncertainty cases. The T_1 temperature graph shows the typical decay toward the temperature of the eutectic reservoir as the resistive heating of the effective thermoelectric model declines with decreasing current supplied to the thermoelectric elements. The current as can be seen is

maintaining not exceeding the maximum allowable current of six amperes. However, as mentioned above it is still higher than ideal. While the current is decaying rather quickly, the modest electrical resistance of the thermoelectric elements combined with the dependence of power consumption on the square of the current means the system is likely consuming more power than the resistive heater. It should be noted that the fact the system exits Phase 1 at the point at which T_0 is equal to $33.25\ °C$ is an indication that the Phase 1 model is integrating correctly with the supervisory control law. There are a few reasons why this is likely the case, which will be discussed below.

The next portion of the model to run is the Transition. The temperature and current data for the Transition portion of the model is shown below.

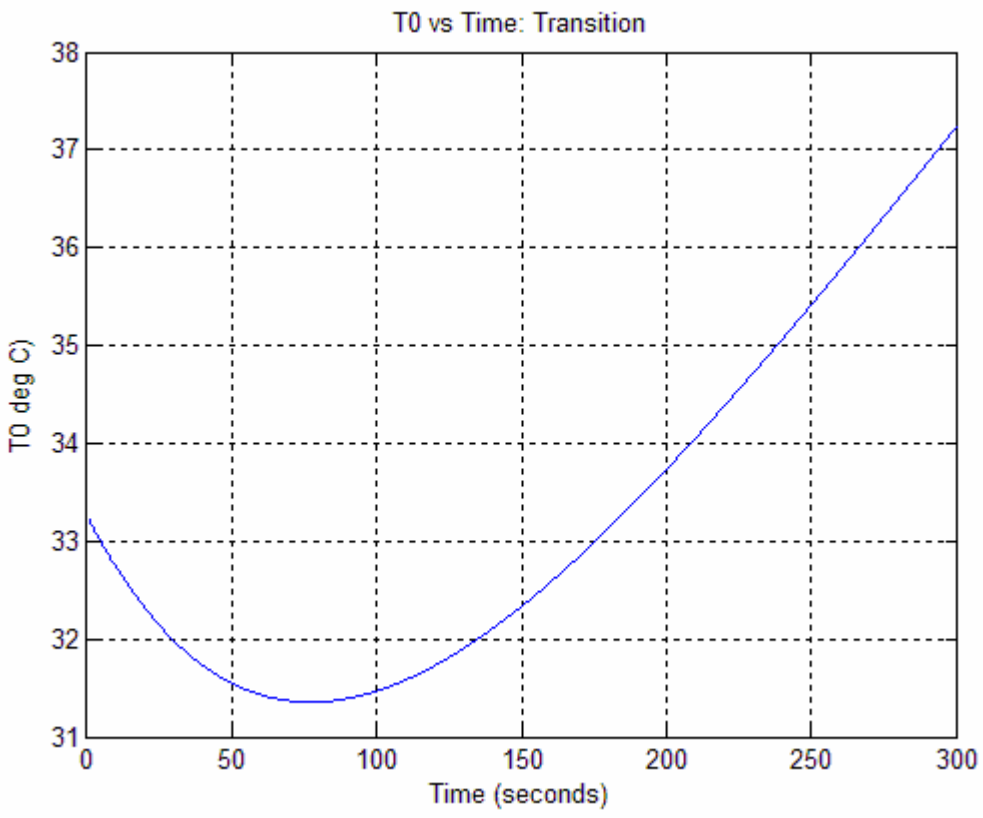

Figure 81: T_0 versus time: Transition

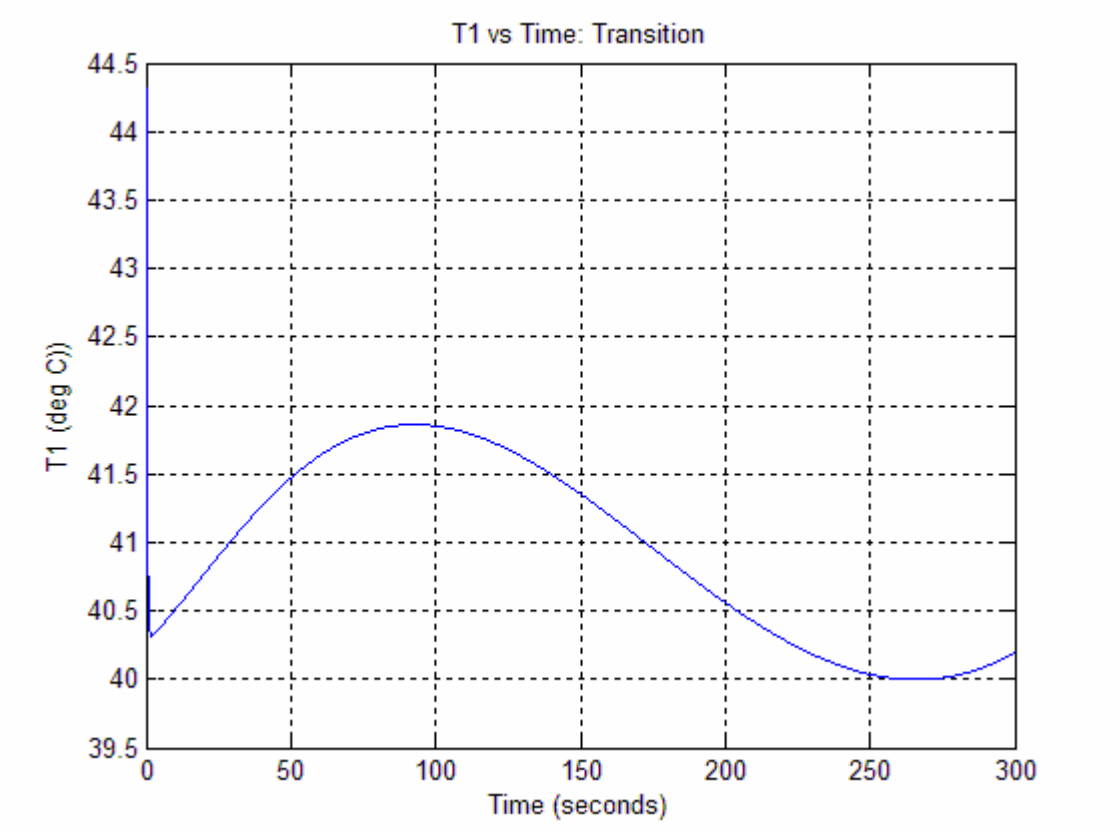

Figure 82: T_1 versus time: Transition

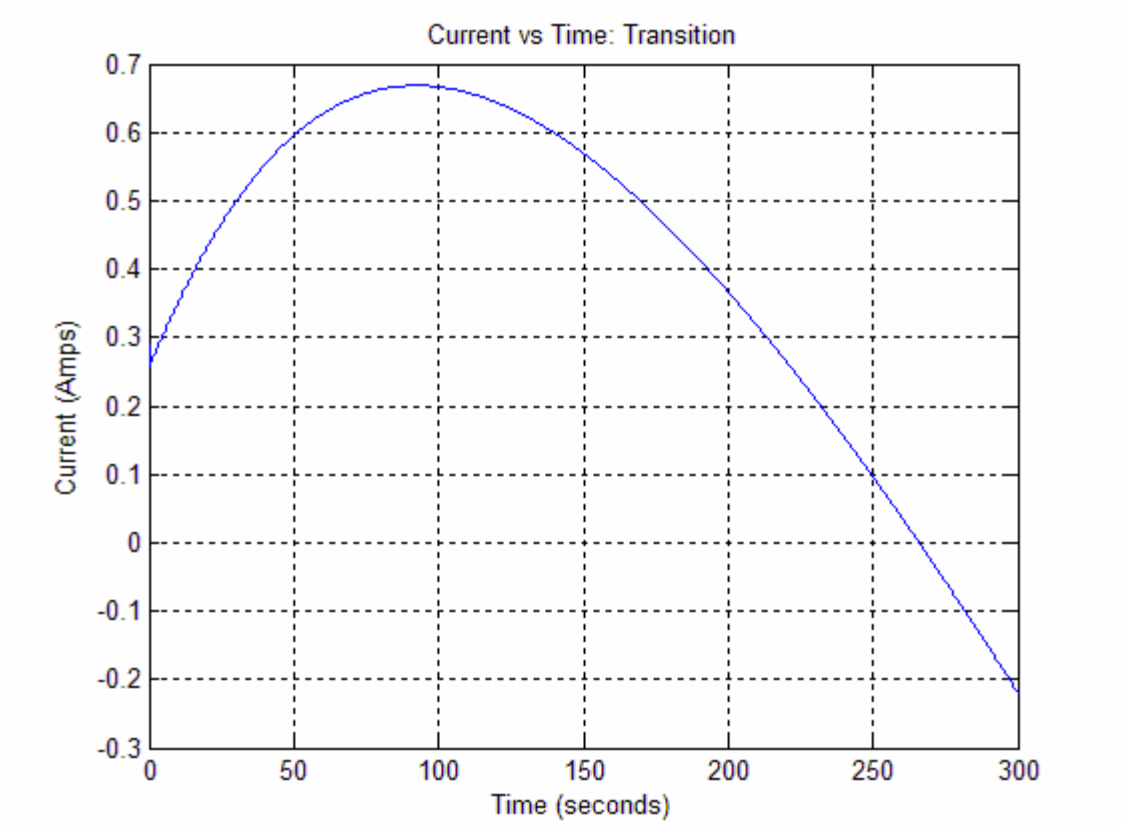

Figure 83: Current versus Time: Transition

The fuel slug temperature, T_0, initially starts at *33.25 °C*, where Phase 1 ended. The temperature then declines as initially cold fuel from the fuel tank flows in dropping the temperature to approximately *31.5 °C*. The temperature then begins to rise as the fuel entering the filter increases in temperature. The effective thermoelectric temperature, T_1, initially rises as the current supplied to the model increases, which increases the Joule heating. T_1 then declines as the current drops off as the fuel slug temperature rises along with the incoming fuel temperature. Finally, the temperature begins rising again as the fuel slug temperature surpasses the temperature of the eutectic reservoir. The current graph shows an upswing in the current followed by a decrease corresponding to increasing incoming fuel temperature. It should be noted that the current consumed throughout the Transition is significantly smaller than the current consumed during Phase

1. This is expected as the system is not heating the fuel so much as it is maintaining the temperature of the fuel.

The next phase of system operation is Phase 3. During Phase 3 there is no current supplied to the thermoelectric elements, and thus the current graph is omitted. The temperature graph for T_0 is shown in Figure 84 and the graph for T_1 is shown in Figure 85.

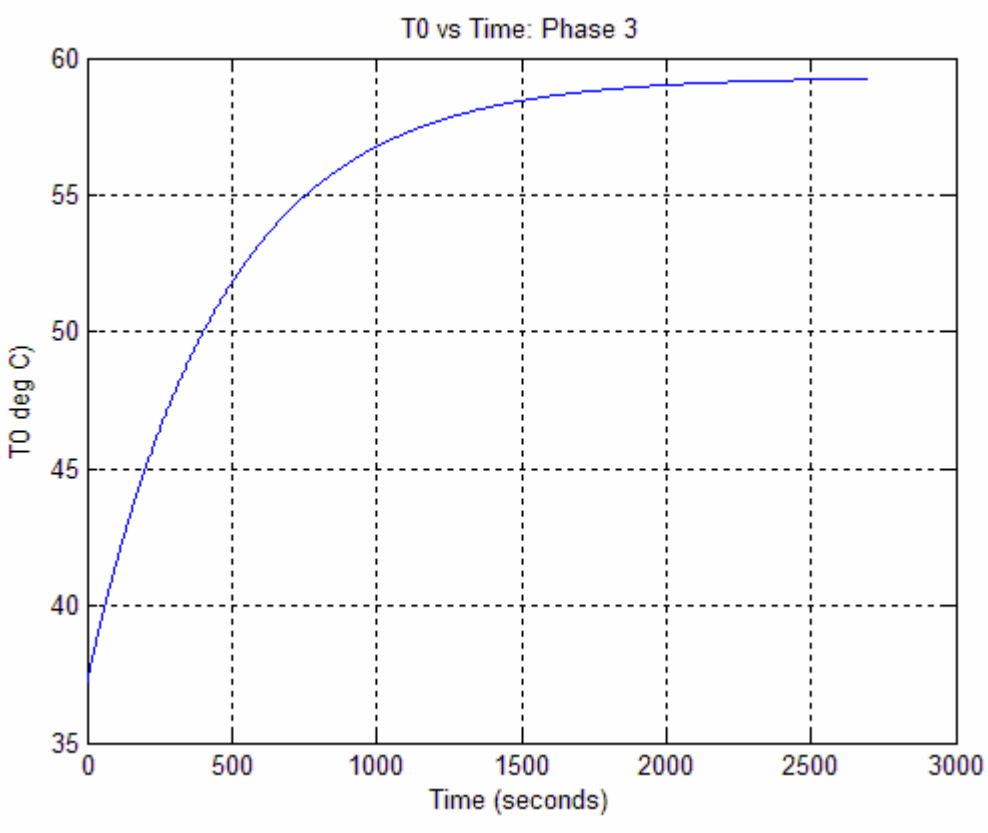

Figure 84: T_0 versus time: Phase 3

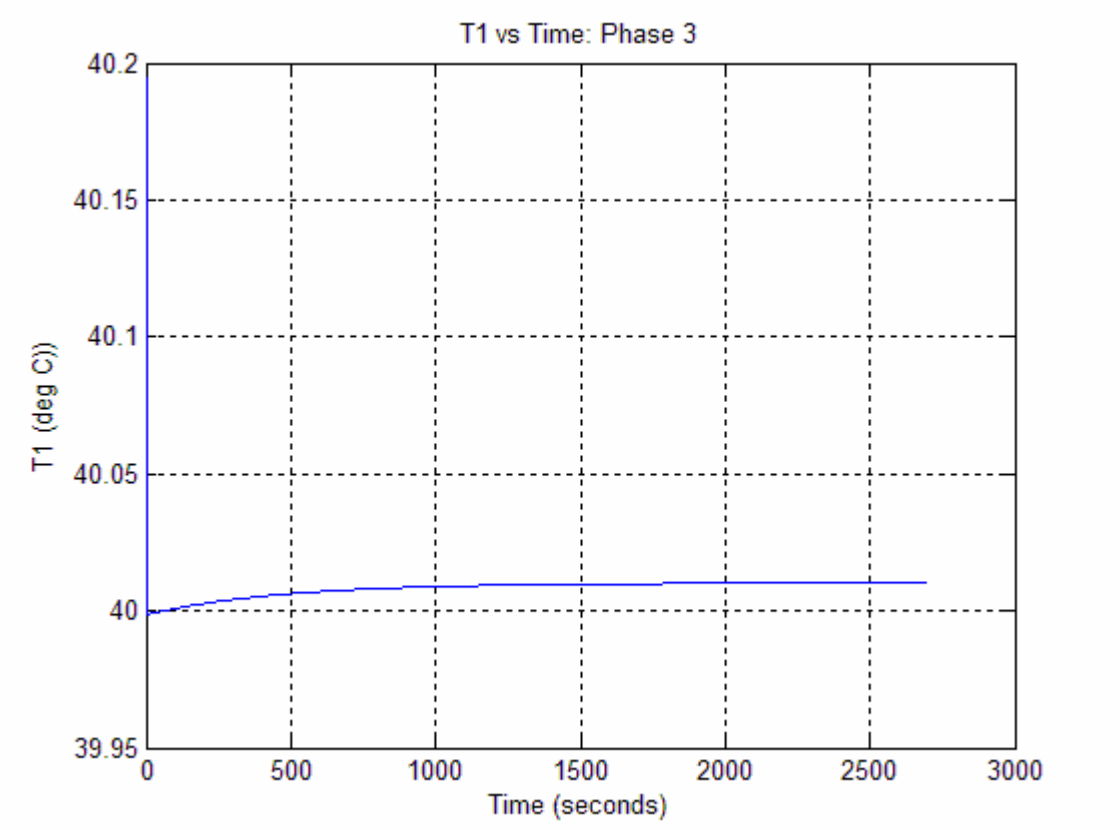

Figure 85: T_1 versus time: Phase 3

The T_0 temperature graph shows a steadily increasing T_0, which approaches *60 °C*, the final fuel inlet temperature. The final time of 2700 seconds as mentioned above corresponds to 45 minutes of driving time. The T_1 graph shows that the temperature is slowly approaching a steady state value wherein the conduction through the thermoelectric elements is balanced by the heat conveceted in from the now warm fuel.

The final phase of operation for the system is Phase 2, where the energy removed from the eutectic reservoir is replaced by applying a negative current of *-1.0 ampere* to the model. Phase 2 also has no current graph as the constant current renders such a graph redundant. The temperature graphs for Phase 2 are shown below.

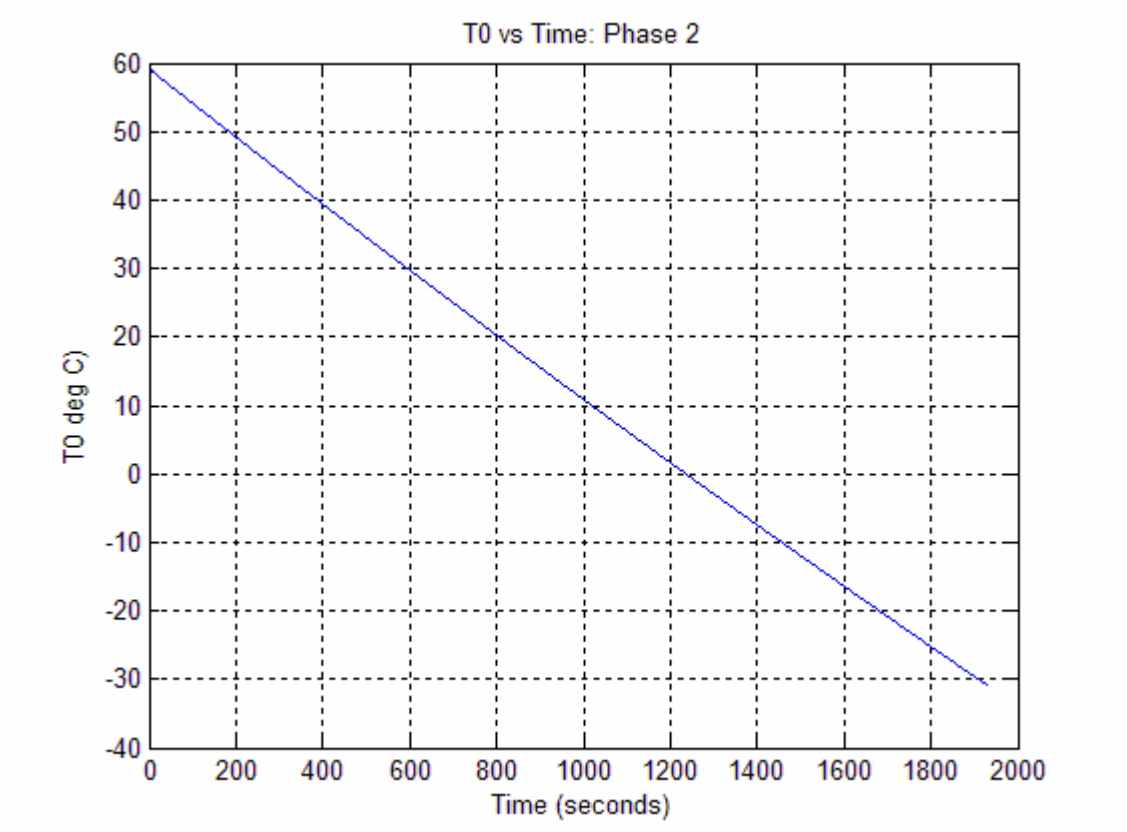

Figure 86: T_0 versus time: Phase 2

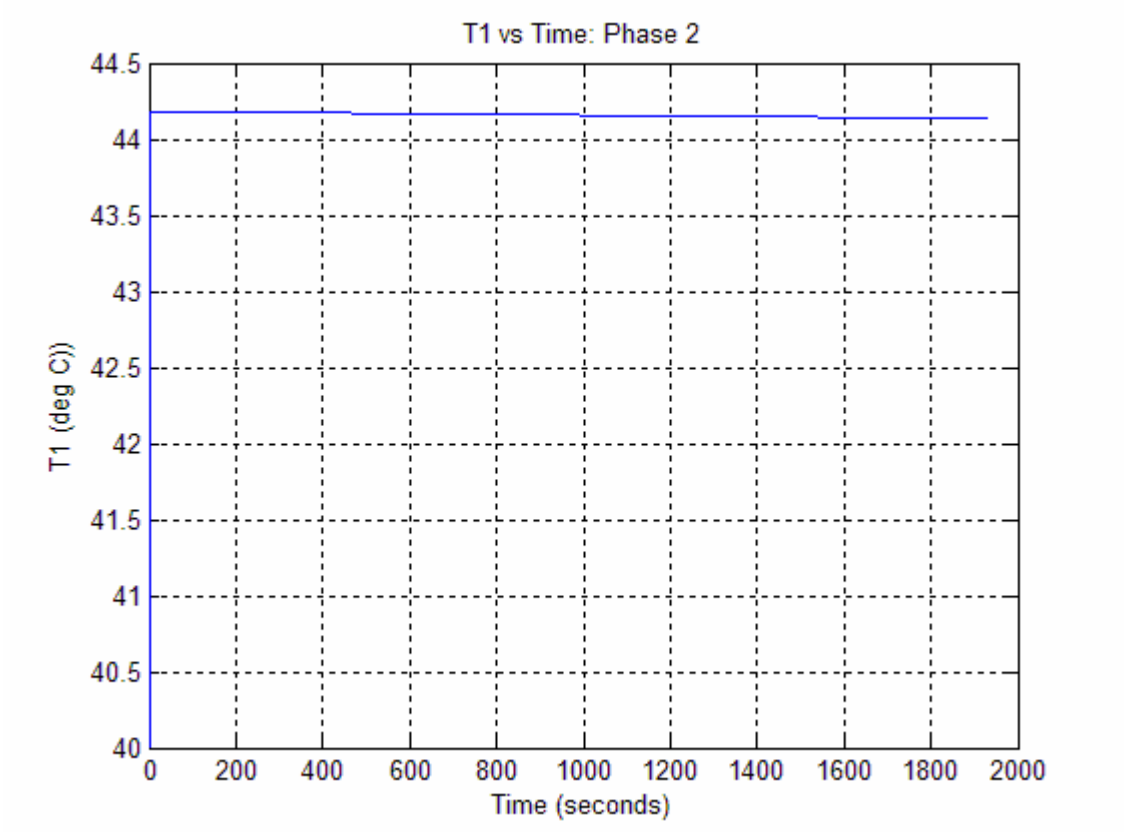

Figure 87: T_1 versus time: Phase 2

The fuel slug temperature, T_0, shows a linear decay from an initial temperature of approximately *60 °C* to approximately *-30 °C*. This temperature is lower than ideal and shows the model is not really being efficient with the energy that it uses. This is evident as the system removes more heat from the fuel than was initially taken to heat the fuel. This should be true to a certain extent as the cold fuel entering during the beginning of the Transition. The T_1 temperature graph shows a slow decay in temperature as the fuel temperature declines, increasing the heat convected out, which slowly is overwhelming the heat created by the resistive heating. It should be noted again that while utilizing Phase change strategy 2 the engine is off during Phase 2 operation meaning that the system is once again a closed system with no mass flow.

With all phases complete the Post Run Analysis portion executes. The code produces a complete current graph which is shown below in Figure 88.

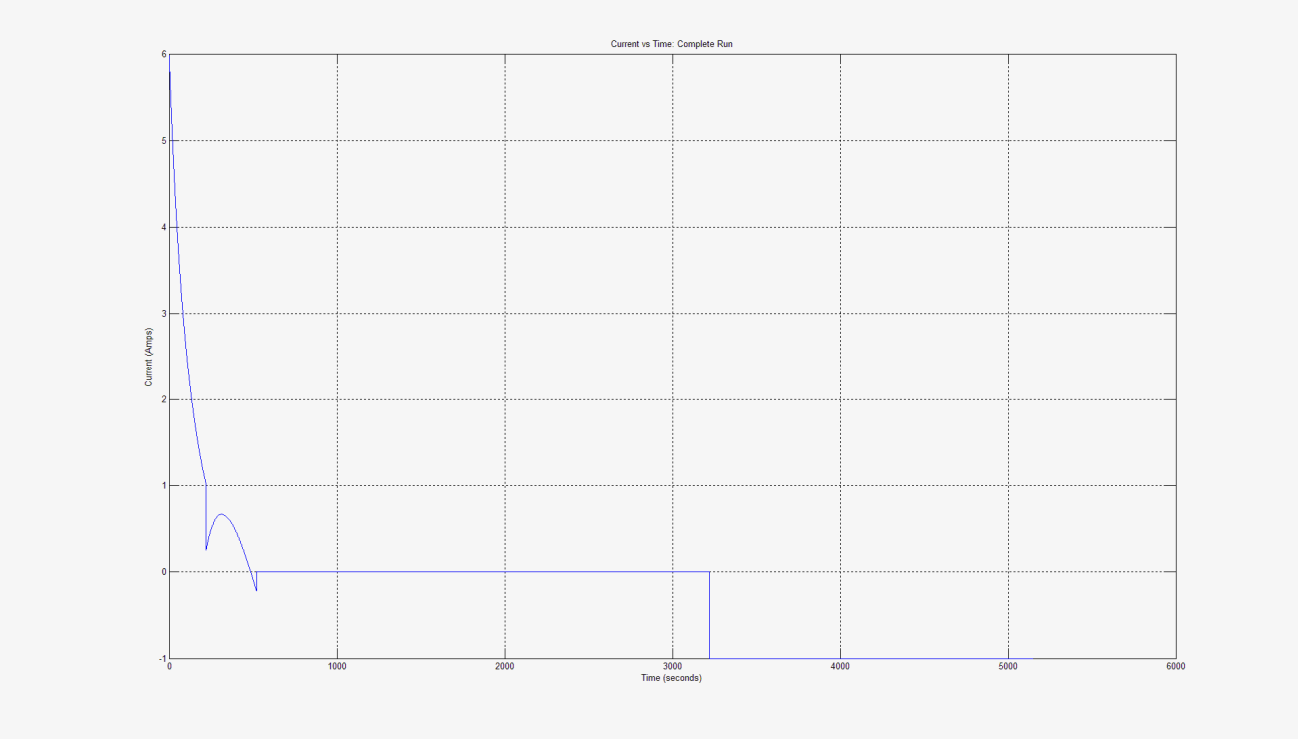

Figure 88: Current versus Time: Complete Run (showing supplied current starting at a maximum of 6 amperes, with a 1 ampere major gridline, over the approximately 6000 seconds of operation, with a 1000 second major gridline)

The current graph shown above demonstrates that the system is consuming a fairly minor amount of power during the majority of its operation, but the total amount of energy consumed is fairly large.

In addition to the graphs the supervisory control law produces, several other pieces of data are computed. The total energy used by the system is 7.99×10^{6} *joules*. The energy generated during Phase 3 is *36.73 joules*. The heat stored during Phase 3 is 1.04×10^{4} *joules*. The total amount of heat that needed to be stored during Phase 2 is 4.07×10^{4} *joules*. Several pieces of useful information can be gleaned from this data.

First, the amount of heat needing to be stored is significantly reduced by utilizing the alternative Phase timing strategy. This is evident by observing the total amount of heat needing to be stored in Phase 2 is of the same order of magnitude as the heat stored during Phase 3. This means that roughly one fifth of the heat needing to be stored was stored without using any power during Phase 3 operation. Also, the system generates almost no power during Phase 3, despite the fairly large amount of heat passing through the thermoelectric elements during the phase. This is due to the very low efficiency of the thermoelectric elements especially when operated at a low temperature and with a small temperature gradient. Finally, the total energy used when compared to the energy used by the benchmarked system, 0.072×10^6, is significantly greater. In actuality the energy consumed should be a bit greater than shown due to the need to maintain the eutectic reservoir during the hours the system is not in operation. While, this extra energy should be relatively minor, especially when compared to the already glaring discrepancy in energy consumption, it nonetheless would contribute if the systems were more closely matched.

Given that from a purely theoretical standpoint the E-TE system should outperform a purely resistive heating system, the large discrepancy in energy consumption is somewhat unexpected. The E-TE system should always outperform a resistive heating system since the system still generates the resistive heating power, but has the additional bonus of the Peliter effect heating. However, this ignores a very significant fact, which is the difference in system geometries. The resistive heater has a finned surface located in the center of the filter with a cartridge heater located inside of it. It should be obvious that such geometry is both much more conducive to efficiently

getting generated heat into the fuel filter, and is an unrealistic geometry for an E-TE system. The E-TE system requires that one side of the thermoelectric elements is in contact with the eutectic reservoir and if the reservoir were to be made in such a way as to flow up into the cylindrical cavity in the finned surface, any assumption of uniform reservoir temperature would be invalidated.

3.3. System Viability

Given that the E-TE system will cost more than a resistive heating system, and performs poorly when compared to the energy consumption of the resistive heating system it is not a viable option at this time. However, the system may be viable at a future point.

There are several things that could occur individually or in combination that would allow the system to be viable, at least in the performance aspect. A brief examination of the system yields several items that could be improved. First, the electrical resistance of the thermoelectric elements could be decreased. The power consumed is directly proportional to energy consumed during operation. Therefore if the electrical resistance were reduced more than three orders of magnitude, the energy consumption would be less for the E-TE system. Such a reduction is highly unlikely, but nevertheless any reduction would improve the E-TE system performance.

Secondly, the effective Seebeck coefficient could be improved. Any improvement in the Seebeck coefficient would improve the ratio between the thermoelectric heating and the resistive heating. Assuming all other parameter were constant, an increase in the order of magnitude of the Seebeck coefficient would lead to

the power consumption being cut to 5.41×10^5 *joules*. This is more than an order of magnitude in the reduction of power consumed, and the value for a fully optimized system is likely to be even larger. Additionally the energy generated increases substantially, though the level is still minor in relation to the order of the energy consumed. Thus an increase in the Seebeck coefficient by approximately three orders of magnitude would yield a performance viable system. This is also highly unlikely to occur.

Finally, and perhaps most practically the system would perform better if more of the resistive heating were to be transferred into the fuel. It would be very possible to make the inner surface of the fuel filter wall finned effectively increasing the surface area. By increasing the surface area by an order of magnitude, the energy consumed is reduced to 4.72×10^5 *joules*. This is a greater reduction in the energy consumption than any other method discussed. Additionally, the energy generated increases to 6.81×10^3 *joules*. This is a large increase in the energy generation to the point where it is likely important in the overall system scheme. Even with this substantial reduction, a significant increase in the order of magnitude of the filter wall interior surface area would be required, again approximately three orders of magnitude. However, increases in the fuel convection coefficient, h_0, also yield the exact same reductions in the power consumption. A combination of increased fuel convection coefficient and interior surface area should be fairly easy to achieve, although possibly not to the extent needed for system viability.

Thus it can be seen that a reduction in the thermoelectric resistance, R_{te}, or increases in the effective Seebeck coefficient, interior surface area, or fuel convection

coefficient all move the system closer to performance viability. A combination thereof could possibly be achievable thus yielding a system that can outperform a resistive heating system and moving the question of viability into a cost benefit analysis.

4. Conclusions and Recommendations for Future Work

This section of the document provides conclusions about the research and suggests some areas for future work on this subject.

4.1. Conclusions

The comparison showed that the E-TE system is not viable from a pure performance perspective, consuming approximately three orders of magnitude more energy than the benchmarked system to achieve similar performance. The reason for the poor performance was examined, as were ways in which the performance could be improved in order to make the system viable. The main reason for poor performance was a lack of interior filter surface area leading to an inefficient usage of energy spent on Joule heating. Other reasons mainly relate to poor material properties, mainly the high electrical resistance.

This document presents research into determining the viability of a eutectic thermoelectric fuel conditioning system for use in a Diesel engine utilizing biodiesel. To begin a literature review was conducted to become acquainted with previous work on eutectic thermoelectric fuel conditioning systems and other relevant technology including thermoelectrics, eutectic compounds, and biodiesel.

A system concept was developed leading to system models. First, a heat transfer based model was developed, which was termed the *alpha* plant model. When the heat transfer model proved insufficient, a new thermodynamic based model was developed, which was termed the *beta* plant model. The *beta* plant model was then implemented

into Simulink©. Once implemented into Simulink©, the *beta* plant model was validated using various limiting cases, and an analytical solution. The *beta* plant model's sensitivity to various model parameters was examined. After examining the model's sensitivity, an optimization was run on the model. Next, the *beta* plant model's robustness was examined using uncertainty in the plant parameters, and the optimization was rerun.

With a usable *beta* plant model, models for the Transition, Phase 2 and Phase 3 were developed, and integrated into a supervisory control law. With a complete system model, data was collected to compare the system performance in regards to a benchmarked system.

It should be noted that this work contradicts the work of IIT in the literature review section. The main reason is that the IIT authors found out how much electrical power was supplied to the fuel and then assumed that the same amount of heat power would equate to the same performance ignoring the differences in geometry.

4.2. Recommendations for Future Work

There are many avenues of future work available, including the application of E-TE system technology to catalytic converter and to other alternative fuels, both of which are applications that should be well suited to this type of system. Additionally, the models for the system should be validated experimentally. However, none of that work should take place until such a point where the system model that is in place now indicates that the system is viable. Thus, the only truly available research lies in making a E-TE system viable from a performance perspective. As mentioned above, there are several things that could change in order for this to happen; however only one of the factors

mentioned above is a direct continuation of this work. That is a redesign of the conceptual system to a more sophisticated geometry in an attempt to increase the product of the convection coefficient and the interior surface area. Further research in that vein would allow for a better assessment of the system's viability at this point in current material's research. This would then allow the new examiner to determine if the system is viable and ready for experimentation, or alternatively set a much more precise set of materials' requirements that would allow the system to reach viability.

5. References:

[1] Rowe, D. M. "General Principles and Basic Considerations", Thermoelectric Handbook. 2006. Taylor and Francis Group. Edited: Rowe, D. M.

[2] http://www.its.caltech.edu/~jsnyder/thermoelectrics/images/typicalte.jpg Visited June 2007

[3] http://en.wikipedia.org/wiki/Thermoelectric_effect Visited October 2006

[4] http://en.wikipedia.org/wiki/Alternative_fuels Visited October 2006

[5] http://www.mda.state.mn.us/ethanol/balance.html Visited October 2006

[6] Tickell, Joshua. (2003). From the Fryer to the Fuel Tank. Joshua Tickell Media Productions, New Orleans, Louisiana.

[7] Sheehann, J., Dunahaay, T., Benemann, J. & Roessler, P. "A Look back at the US Department of Energy's Aquatic Species Program: Biodiesel from Algae" National Renewable Energy Laboratory, July 1998.

[8]Korbitz, K., "The Technical, Energy, and Environmental Properties of Biodiesel" Korbitz Consulting, Vienna, Austria, 1993.

[9] Dunn, R. O., Bagby, M. O. "Low-Temperature Filterability Properties of Alternative Diesel Fuels from Vegetable Oils" http://www.biodiesel.org/resources/reportsdatabase/reports/gen/19960801_gen-150.pdf Visited October 2006

[10] http://en.wikipedia.org/wiki/Phase_Change_Material Visited October 2006

[11] Palm III, W. J. "Modeling and Analysis of Control Systems" System Dynamics. 2005. McGraw Hill.

[12] Slotine, Jean-Jacques E. Li, Weiping. (1991). Applied Nonlinear Control. Prentice-Hall. Upper Saddle River, New Jersey.

[13] Bobi, Dr. Miguel Angel Sanz. "Applications of Thermoelectricity in the Automobile Industry". Instituto de Investigacion (Universidad Pontificia Comillas), Santa Cruz de Marcenado, Madrid.

[14] Morelli, Donald T. (1996). "Potential Applications of Advanced Thermoelectrics in the Automobile Industry". 15th International Conference on Thermoelectrics (1996).

[15] Luo, Q. et al Jingwei. (2005). "A novel water heater integrating thermoelectric heat pump with separating thermosiphon". Applied Thermal Engineering 25 (2005) 2193–2203.

[16] Vazquez, Jorge, et al. (2000). "Thermoelectricity Applied to Heating of a Fuel Filter of a Car in Cold Starting". XIX International Conference on Thermoelectrics. Cardiff, Wales, United Kingdom. 20-24th August, 2000.

[17] Vazquez, Jorge and Bobi, Dr. Miguel. (2002) "Thermoelectric device to allow diesel engine start-up at cold weather conditions". Proceedings of the 7th European Workshop on Thermoelectrics, Poster #2, Oct 2002, Pamplona.

[18] Chien, R. and Huang, G. "Thermoelectric cooler application in electronic cooling". 2004. Applied Thermal Engineering 24 (2004) 2207–2217

[19] Wijngaards, D. D. L. "Single-chip micro-thermostat applying both active heating and active cooling". 2004. Sensors and Actuators A 110 (2004) 187–195.

[20] Palacios, Rafael, Li, Ming Zhu. (1998) "Electrical Properties of Commercial Thermoelectric Modules". Fourth European Workshop on Thermoelectrics, ETS'98. September 1998. Madrid, Spain. Pag. 159-162.

[21] Bell, Lon E. (2003). “Alternate Thermoelectric Thermodynamic Cycles with Improved Power Generation Efficiencies”. 22nd International Conference on Thermoelectrics (2003).

[22] Crane, Douglas T., Jackson, Gregory S. (2002). “Systems level optimization of low temperature thermoelectric waste heat recovery”. 2002 37th lntersociety Energy Conversion Engineering Conference (IECEC).

[23] Furue, T. et al. (1998). “Case Study on Thermoelectric Generation System Utilizing the Exhaust Gas of Internal Combustion Power Plant”. 17th International Conference on Thermoelectrics (1998).

[24] Ikoma, K., et al. (1998). “Thermoelectric Module and Generator for Gasoline Engine Vehicles”. 17th International Conference on Thermoelectrics (1998).

[25] Tsuyoshi A., Matsuura K., Yamamoto M., Tsutsumida K. (1998), “Effective Thermoelectric Generation by Use of Heat Stored in a Thermal Accumulator”. 17th lntemational Conference on Thermoelectrics (1998).

[26] Vázquez, Jorge, et al. (2002). “State of the Art of Thermoelectric Generators Based on Heat Recovered from the Exhaust Gases of Automobiles”. Proceedings of the 7th European Workshop on Thermoelectrics, Paper #17, Oct 2002, Pamplona, Spain.

[27] Yang, J. (2005). “Potential Applications of Thermoelectric Waste Heat Recovery in the Automotive Industry”. 2005 International Conference on Thermoelectrics.

[28] Tuncbilek, Kadir, et al. (2003). “Lauric and palmitic acids eutectic mixture as latent heat storage material for low temperature heating applications”. Energy 30 (2005) 677–692.

[29] Longfei, Lin, Fengpingn, Xiao. (2004). “Phase diagram of the ternary system lauric acid–capric acid–naphthalene”. Thermochimica Acta 424 (2004) 1–5.

[30] Sarı, A. et. al. “Thermal properties and thermal reliability of eutectic mixtures of some fatty acids as latent heat storage materials”. Energy Conversion and Management 45 (2004) 365–376.

[31] Knothe, Gerhard. “Dependence of biodiesel fuel properties on the structure of fatty acid alkyl esters”. Fuel Processing Technology 86 (2005) 1059– 1070.

[32] Chiu, Chuang-Wei, Schumacher, Leon G., Suppes, Galen J. (2004). Impact of cold flow improvers on soybean biodiesel blend. Biomass and Bioenergy 27 (2004) 485–491.

[33] Soriano Jr. N. et. al. “Ozonized vegetable oil as pour point depressant for neat biodiesel”. Fuel 85 (2006) 25–3.

[34] Tan, J., Kalantar-zadeh1, K., Wlodarski,, W., Bhargava, S., Akolekar, D., Holland, A., Rosengarten, G., “Thermoelectric properties of bismuth telluride thin films deposited by radio frequency magnetron sputtering.”, (2005) Smart Sensors, Actuators, and MEMS II, Proc. of SPIE Vol. 5836.

[35] http://www.chanco.unima.mw/physics/biodieselanaly.html visited 4/27/2008 Visited March 2008

[36] http://en.wikipedia.org/wiki/Corporate_Average_Fuel_Economy Visited March 2008

[37]Ineropera, F. P. and DeWitt, D. P. Fundatmentals of Heat and Mass Transfer 2002. John Wiley and Sons

[38] Takashiri, M., Shirakawa, T., Miyazaki, K., Tsukamoto, H., "Fabrication and characterization of bismuth–telluride-based alloy thin film thermoelectric generators by flash evaporation method" Sensors and Actuators A 138, (2007), pg 329-334

[39] Takashiri, M., Tanaka, M., Miyazaki, K., Tsukamoto, H., "Thermoelectric properties of *n*-type nanocrystalline bismuth-telluride-based thin films deposited by flash evaporation" Journal of Applied Physics 101, (2007)

[40] http://www.maesco.com/products/racor/r_c_intro/r_c_intro.html Visited June (2007)

Appendix A: Preliminary Design Work

Several pieces of preliminary design modeling work on the *alpha* plant model are presented below. The Phase 1 and Transition model for the *alpha* plant is shown below in Figure 89. The Phase 2 model for the *alpha* plant is shown in Figure 90. The Phase 3 model for the *alpha* plant is shown below in

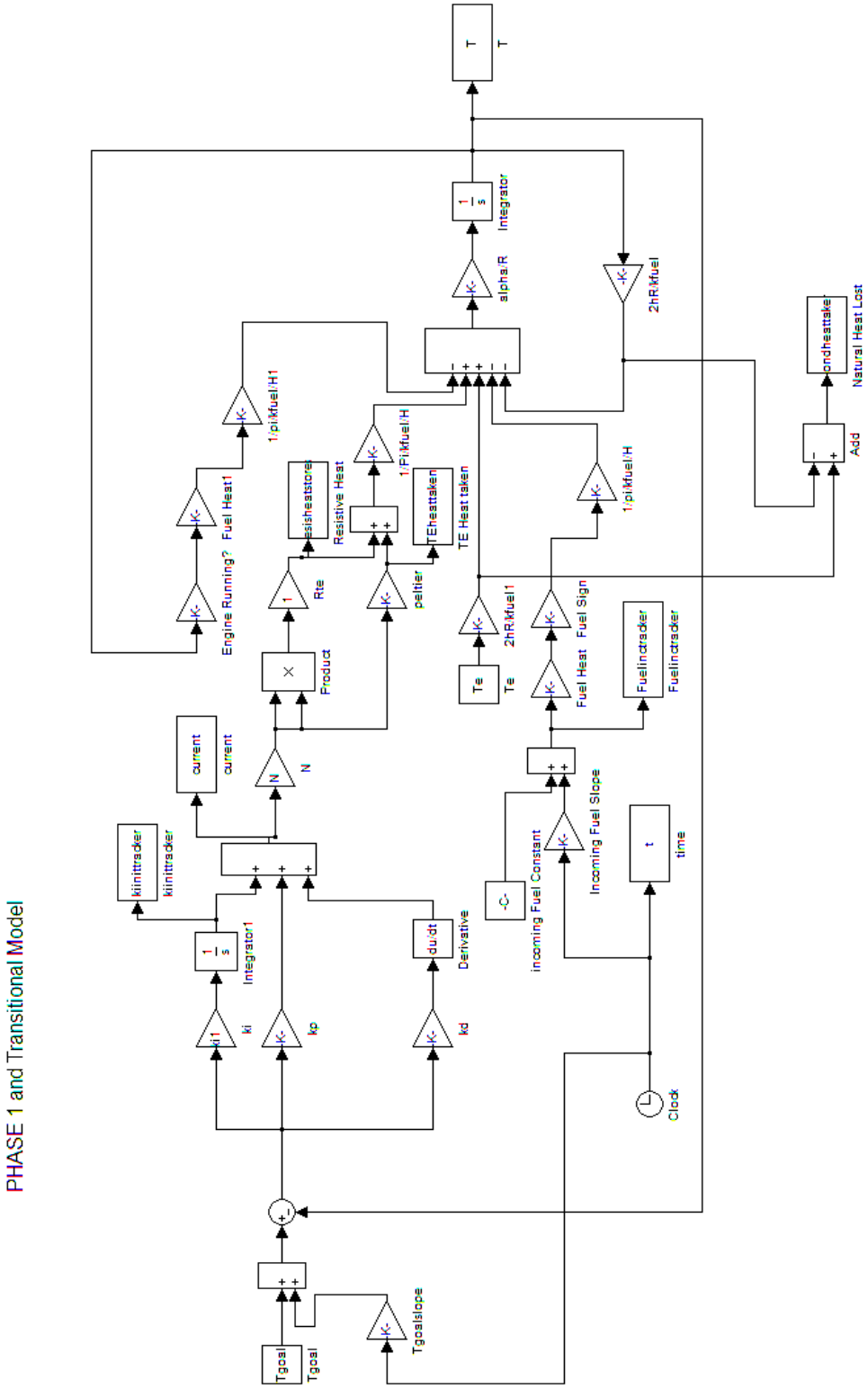

Figure 89: *Alpha* Plant Phase 1 and Transition Model

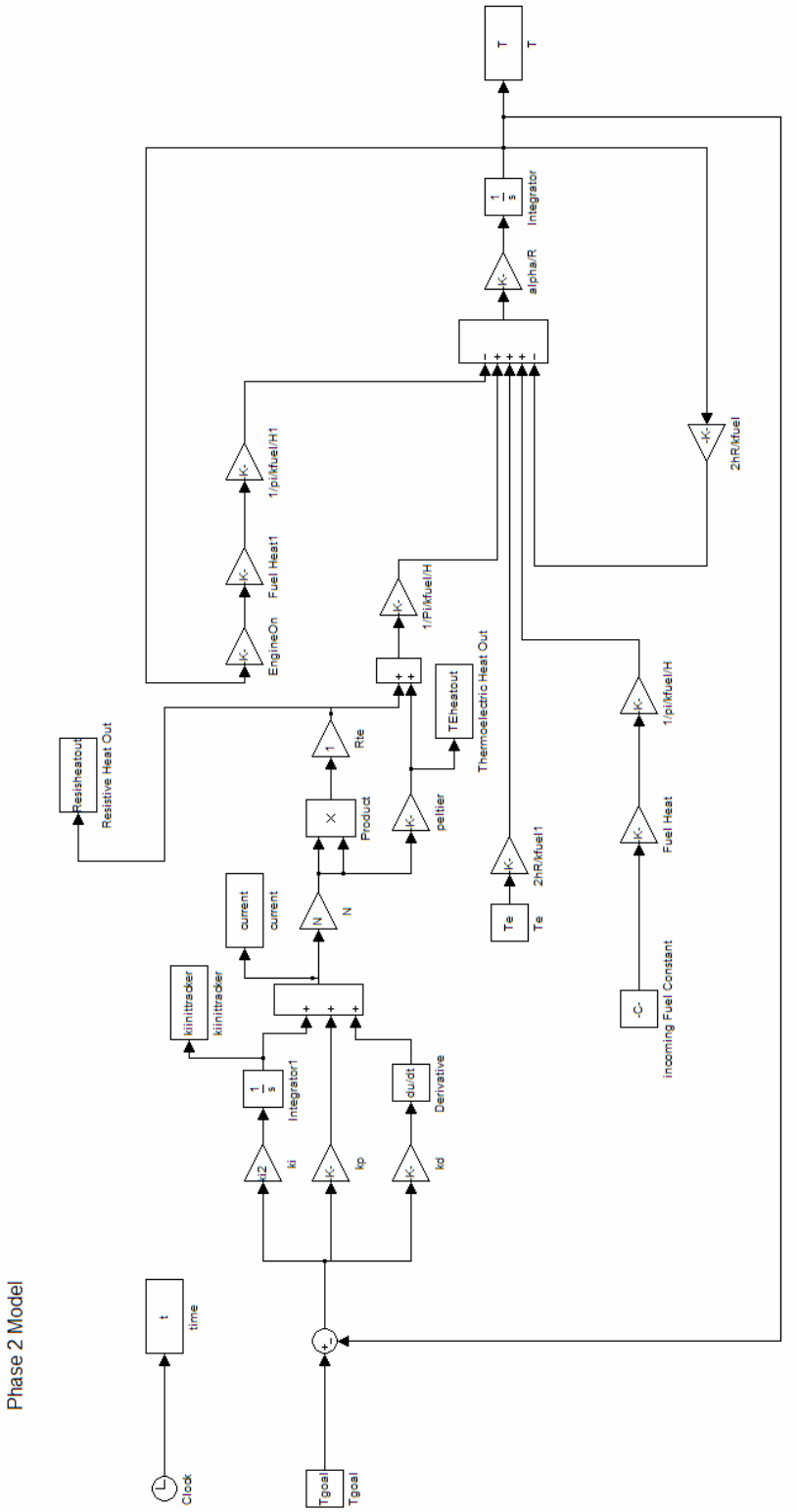

Figure 90: *Alpha* Plant Phase 2 Model

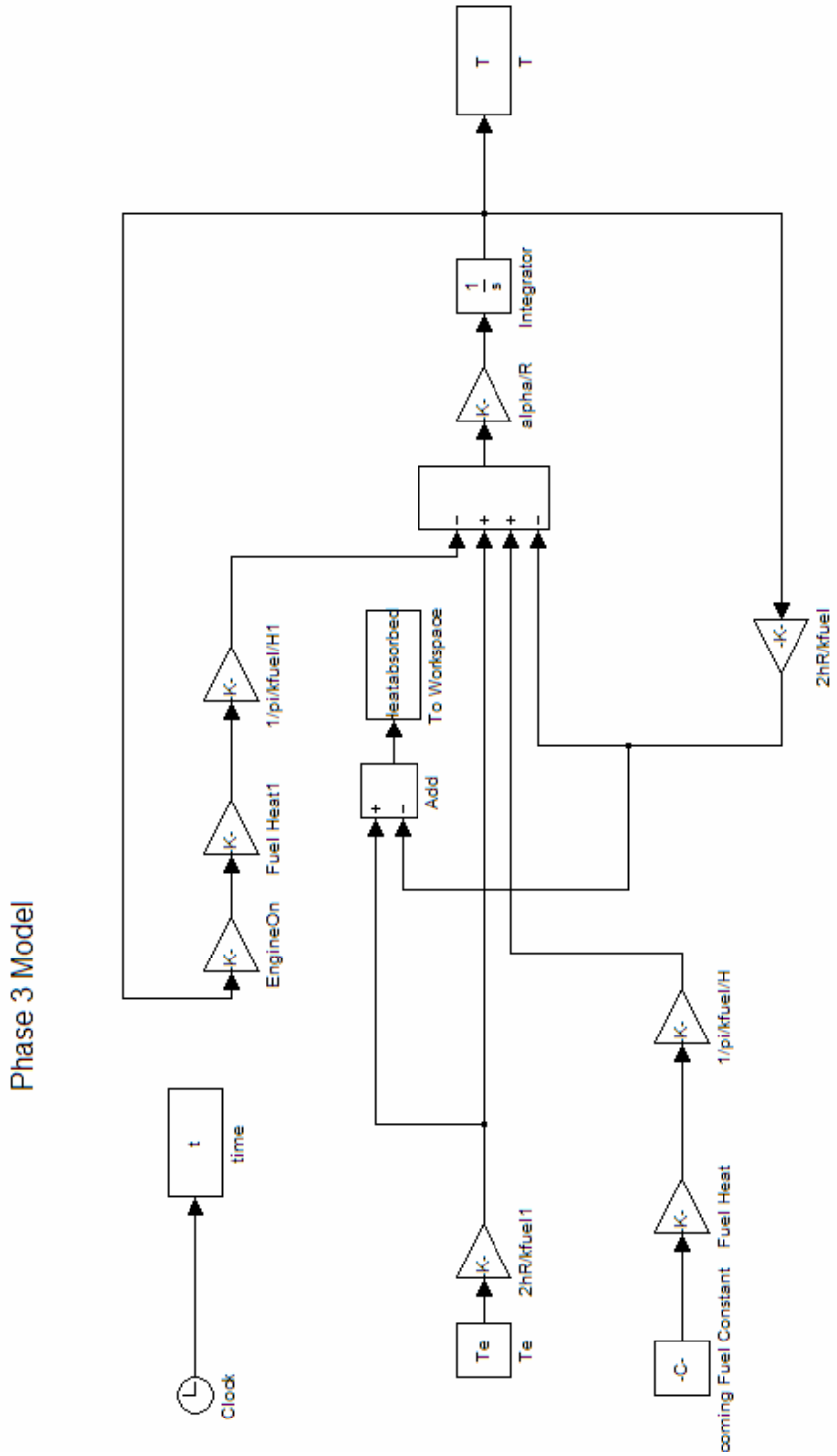

Figure 91: *Alpha* Plant Phase 3 Model

The supervisory control law for the *alpha* plant model is shown below. As within the main body of the thesis a % symbol denotes coding comments. The parameters for the model were preliminary and are not nearly as valid as the values used above. Additionally, it should be noted that the *alpha* supervisory control law was based upon Phase change strategy 1. Another important distinction is that the *alpha* plant supervisory control law exhibits a much more invasive control of the three models. This caused several problems regarding the models actually being able to be run. Finally, it should be noted that the Phase 2 portion of the supervisory control law is based not upon a steady negative current as it is in the main body of the thesis, but rather upon changing the value of the goal temperature to cause the PID controller to apply a negative current in an attempt to bring the temperature back down to the new goal temperature. This is problematic for two reasons, namely it is not a very logical way of achieving the desired result, and it causes the T_0 and current responses during Phase 2 to have asymptotic behavior as large supplied currents caused the temperature to rise despite the negative heat transfer action from the negative applied current. This was due to the greater importance within the *alpha* plant of the resistive heating term.

```
%%%%%%%%%%%%%%%%%%%%%%%%%%%%%%%%%%%%%%%%%%%%%%%%%%%%%%%%%%%%%%%%%%%%%%%%%%%%
%%%%%%%%%%%%%%%%%%%%%%%%%INTRODUCTION%%%%%%%%%%%%%%%%%%%%%%%%%%%%%%%%%%%%%%%
%%%%%%%%%%%%%%%%%%%%%%%%%%%%%%%%%%%%%%%%%%%%%%%%%%%%%%%%%%%%%%%%%%%%%%%%%%%%

%This .m file is the supervisory control law to manage the three phase
%models.  It also contains the constant sets.
%Timothy Schriefer July 10, 2007 Rochester Institute of Technology

%%%%%%%%%%%%%%%%%%%%%%%%%%%%%%%%%%%%%%%%%%%%%%%%%%%%%%%%%%%%%%%%%%%%%%%%%%%%
%%%%%%%%%%%%%%%%%%%%%%%%VARIABLE ASSIGNMENT%%%%%%%%%%%%%%%%%%%%%%%%%%%%%%%%%%
%%%%%%%%%%%%%%%%%%%%%%%%%%%%%%%%%%%%%%%%%%%%%%%%%%%%%%%%%%%%%%%%%%%%%%%%%%%%


h = 1.125; %Thermal "convection" coefficient takes care of
           %natural conduction through model
alpha = 6.1E-8; %Thermal diffusivity of the fuel (m^2/s)
R = .0762; %Radius of the fuel filter (meters)
```

```
Rte = 1.667; %Electrical Resistance of the Thermoelectric elements (ohms)
H = .18; %Height of fuel filter (meters)
kfuel = .134; %thermal conductivity of the fuel (W/mK)
peltier = 10.33; %Peltier coefficient (Volts)
Te = 40; %Temperature of eutectic compound (deg C)
Tgoal = 35; %Temperature goal for CLAW to try and attain (deg C)
kp1 = .173; %proportional gain constant phase 1 and transition
ki1 = 0; %integral gain phase 1 and transition
kd1 = 0; %derivitave gain phase 1 and transition
kp2 = .1; %proportional gain constant phase 2
ki2 = 0; %integral gain phase 2
kd2 = 0; %derivitave gain phase 2
timerun = 1000; %time for the vehicle to be running (seconds)
Tphase1 =[0]; %temperature variable for phase 1 (deg c)
N = 96; %number of TE elements
T = zeros(201,1); %temporary temperature variable (deg C)
Tinit = 0; %initial temperature also used for passing new initial condition
           %to model during iterations (deg C)
current = zeros(201,1); %temporary temperature variable (amps)
cphase1 = 0; %current variable for phase 1 (amps)
tphase1 = 0; %time variable for phase 1 (s)
check1 = 0; %secondary check variable
check = 0; %primary check variable
i = 0;
j = 0;
k = 0;
l = 0;
m = 0;
n = 0;
o = 0;
kiinit = 0; %tracking variable for ki initial condition
kiinittracker = zeros(201,1); %tracking variable for ki initial condition
delT = 60-Tinit; %Temperature difference used for transitional phase (deg C)
Fuelinc = Tinit; %Temperature used for transional phase (deg C)
twarmup = 500; %time in second for engine to reach operating temp (sec)
Fuelincslope = 0; %slope for model to scale incoming fuel temp
FuelHeat = .00013456; %fuel heat (J/deg C)
Fuelinctracker = zeros(201,1); %tracking variable for incoming fuel temp
                               %condition
Tgoalslope = 0; %set modification of temp goal equal to zero initially
Ttrans = [0]; %Temperature variable for transition phase (deg C)
ttrans = 0; %time variable for transition phase (sec)
ctrans = 0; %current variable for transition phase (amps)
EngineOn = 0; %variable to track whether fuel is flowing
Natcond = 1; %determines the direction of the natural conduction through
             %thermoelectric element
Heatstored = 0; %variable tracking heat storage to the reservoir (J)
Heattaken = 0; %variable tracking heat taken from the reservoir (J) note
               %should be a positive number
Tphase2 = [0];
cphase2 = 0; %current variable for phase 1 (amps)
tphase2 = 0; %time variable for phase 1 (s)
Tgoalprime = Tgoal; %variable to track initial Tgoal (deg C)
Fuelsign = 1; %variable that tracks whether incoming fuel is decreasing or
              %increasing temperature
Tphase3 = [0]; %Temperature variable for phase 3 (deg C)
tphase3 = 0; %time variable for phase 3 (sec)
```

```
Zc = 3E-3;  %term for finding maximum generator power efficiency
Eenergy = 0; %variable that tracks the amount of electrical energy (joules)
tenergy = 0; %time variable for phase 3 energy (sec)
ttotal = 0; %time variable for phase 1-2 (sec)

%%%%%%%%%%%%%%%%%%%%%%%%%%%%%%%%%%%%%%%%%%%%%%%%%%%%%%%%%%%%%%%%%%%%%%%%%%%%%%%
%%%%%%%%%%%%%%%%%%%%%%%%%%PHASE 1 PORTION%%%%%%%%%%%%%%%%%%%%%%%%%%%%%%%%%%%%%
%%%%%%%%%%%%%%%%%%%%%%%%%%%%%%%%%%%%%%%%%%%%%%%%%%%%%%%%%%%%%%%%%%%%%%%%%%%%%%%


while check == 0;

    sim('thesismodelphase1'); %run phase 1 model

    [rowsize,colszie]=size(T);

    if check1 == 1 %check to see if ready to move to transitory phase

        if T (rowsize,1)> .95*Tgoal
            check=1;
        end %check if

    end %check1 if

    Tphase1=[Tphase1;T]; %Store data
    cphase1=[cphase1;current];%Store data
    Tinit =T(rowsize,1); %Reset model initial conditons to end condition
    kiinit=kiinittracker(rowsize,1); %Reset model initial conditons

    Heattaken = Heattaken - trapz(t,TEheattaken) + ...
        trapz(t,Resisheatstored) - trapz(t,Condheattaken);

    if T (rowsize,1)> .95*Tgoal %check to see if ready to move to transitory
phase
        check1 =1;
    end %check1 if

end %while

[row,col]=size(Tphase1);

for i= 0:1:(row-2)
    tphase1(i+2,1)=tphase1(i+1,1)+.1;
end %for


%%%%%%%%%%%%%%%%%%%%%%%%%%%%%%%%%%%%%%%%%%%%%%%%%%%%%%%%%%%%%%%%%%%%%%%%%%%%%%%
%%%%%%%%%%%%%%%%%%PHASE 1 PLOTTING%%%%%%%%%%%%%%%%%%%%%%%%%%%%%%%%%%%%%%%%%%%%
%%%%%%%%%%%%%%%%%%%%%%%%%%%%%%%%%%%%%%%%%%%%%%%%%%%%%%%%%%%%%%%%%%%%%%%%%%%%%%%

figure(1), plot(tphase1,Tphase1),grid on,
title('Temperature vs Time: Phase 1'), xlabel('Time (seconds)'),
ylabel('Temperature (deg C)')
figure(2), plot(tphase1,cphase1), grid on,
title('Current Supplied vs Time: Phase 1'), xlabel('Time (seconds)'),
ylabel('Current (amps)')
```

```
%%%%%%%%%%%%%%%%%%%%%%%%%%%%%%%%%%%%%%%%%%%%%%%%%%%%%%%%%%%%%%%%%%%%%%%%%%%%%%%
%%%%%%%%%%%%%%%%%TRANSITION PORTION%%%%%%%%%%%%%%%%%%%%%%%%%%%%%%%%%%%%%%%%%%%%
%%%%%%%%%%%%%%%%%%%%%%%%%%%%%%%%%%%%%%%%%%%%%%%%%%%%%%%%%%%%%%%%%%%%%%%%%%%%%%%

Tinit =T(rowsize,1); %Reset model initial conditons to end condition
EngineOn = 1;
Fuelincslope = delT/twarmup;

while check ==1

    sim('thesismodelphase1');

    [rowsize,colszie]=size(T);

    if check1 == 2 %check to see if ready to move to phase 2
        check = 2;
    end %check if


    Fuelinc = Fuelinctracker(rowsize,1);
    Ttrans=[Ttrans;T]; %Store data
    ctrans=[ctrans;current];%Store data
    Tinit =T(rowsize,1); %Reset model initial conditons to end condition
    kiinit=kiinittracker(rowsize,1); %Reset model initial conditons

    Heattaken = Heattaken + trapz(t,TEheattaken) - ...
        trapz(t,Resisheatstored) + trapz(t,Condheattaken);

    if Fuelinctracker(rowsize,1) > T(rowsize,1)
        Fuelsign = -1;
    end %if

    if Fuelinctracker(rowsize,1) > Tgoal
        Tgoal = Fuelinctracker(rowsize,1);
        tincfuelgoal=(Tgoal-Tinit)/Fuelincslope;
        tTgoalmod = twarmup-tincfuelgoal;
        Tgoalslope = (Te - Tgoal)/tTgoalmod;
    end %goal change if

    if  Fuelinctracker(rowsize,1) > Te
        check1 = 2;
    end %check1 if

end %while

   [row1,col1]=size(Ttrans);

for j= 0:1:(row1-2)
    ttrans(j+2,1)=ttrans(j+1,1)+.1;
end %for

%%%%%%%%%%%%%%%%%%%%%%%%%%%%%%%%%%%%%%%%%%%%%%%%%%%%%%%%%%%%%%%%%%%%%%%%%%%%%%%
%%%%%%%%%%%%%%%%%TRANSITION PLOTTING%%%%%%%%%%%%%%%%%%%%%%%%%%%%%%%%%%%%%%%%%%%
%%%%%%%%%%%%%%%%%%%%%%%%%%%%%%%%%%%%%%%%%%%%%%%%%%%%%%%%%%%%%%%%%%%%%%%%%%%%%%%

figure(3), plot(ttrans,Ttrans),grid on,
title('Temperature vs Time: Transition'), xlabel('Time (seconds)'),
```

```
ylabel('Temperature (deg C)')
figure(4), plot(ttrans,ctrans), grid on,
title('Current Supplied vs Time: Transition'), xlabel('Time (seconds)'),
ylabel('Current (amps)')

%%%%%%%%%%%%%%%%%%%%%%%%%%%%%%%%%%%%%%%%%%%%%%%%%%%%%%%%%%%%%%%%%%%%%%%%%%%%%%%
%%%%%%%%%%%%%%%%%%PHASE 2 PORTION%%%%%%%%%%%%%%%%%%%%%%%%%%%%%%%%%%%%%%%%%%%%
%%%%%%%%%%%%%%%%%%%%%%%%%%%%%%%%%%%%%%%%%%%%%%%%%%%%%%%%%%%%%%%%%%%%%%%%%%%%%%%

Tinit =T(rowsize,1); %Reset model initial conditons to end condition
Tgoal = Tgoalprime;

while check == 2

    sim('thesismodelphase2')

    [rowsize,colszie]=size(T);


    Heatstored= Heatstored - trapz(t,TEheatout)+trapz(t,Resisheatout);

    Tphase2=[Tphase2;T]; %Store data
    cphase2=[cphase2;current];%Store data
    Tinit =T(rowsize,1); %Reset model initial conditons to end condition
    kiinit=kiinittracker(rowsize,1); %Reset model initial conditons


    if Heatstored > Heattaken
        check = 3;
    end %if

end %while

[row2,col2]=size(Tphase2);

for l= 0:1:(row2-2)
    tphase2(l+2,1)=tphase2(l+1,1)+.1;
end %for


%%%%%%%%%%%%%%%%%%%%%%%%%%%%%%%%%%%%%%%%%%%%%%%%%%%%%%%%%%%%%%%%%%%%%%%%%%%%%%%
%%%%%%%%%%%%%%%%%%PHASE 2 PLOTTING%%%%%%%%%%%%%%%%%%%%%%%%%%%%%%%%%%%%%%%%%%%%
%%%%%%%%%%%%%%%%%%%%%%%%%%%%%%%%%%%%%%%%%%%%%%%%%%%%%%%%%%%%%%%%%%%%%%%%%%%%%%%

figure(5), plot(tphase2,Tphase2),grid on,
title('Temperature vs Time: Phase 2'), xlabel('Time (seconds)'),
ylabel('Temperature (deg C)')
figure(6), plot(tphase2,cphase2), grid on,
title('Current Supplied vs Time: Phase 2'), xlabel('Time (seconds)'),
ylabel('Current (amps)')

%%%%%%%%%%%%%%%%%%%%%%%%%%%%%%%%%%%%%%%%%%%%%%%%%%%%%%%%%%%%%%%%%%%%%%%%%%%%%%%
%%%%%%%%%%%%%%%%%%PHASE 3 PORTION%%%%%%%%%%%%%%%%%%%%%%%%%%%%%%%%%%%%%%%%%%%%
%%%%%%%%%%%%%%%%%%%%%%%%%%%%%%%%%%%%%%%%%%%%%%%%%%%%%%%%%%%%%%%%%%%%%%%%%%%%%%%

Tinit =T(rowsize,1); %Reset model initial conditons to end condition
Heataddedinitial = Heatstored - Heattaken;
```

```
tempchange = Heataddedinitial / 1770 / 2.58745;
Te = Te+tempchange;

r=0;

while check ==3

    sim('thesismodelphase3')
    [rowsize,colszie] = size(T);
    Tphase3 = [Tphase3;T]; %Store data
    Tinit = T(rowsize,1); %Reset model initial conditons to end condition
    Th = mean(T);
    Tc = Te;
    Tmean = (Th + Tc)/2;
    ceff = (Th-Tc)/Th;
    mateff = [(1+Zc*Tmean)^.5 -1]/[(1+Zc*Tmean)^.5 +Tc/Th];
    Heatadded = -trapz(t,Heatabsorbed);
    tempchange = Heatadded / 1770 / 2.58745;
    Te = Te+tempchange;
    Eenergy = [Eenergy; ceff * mateff* Heatadded * N/H/(2*pi*R)*.0298^2];

r=r+1;
    if r ==100
        check =4;
    end

% if Te>T(rowsize,1)
%     check = 4;
% end %if

end %while

[row3,col3]=size(Tphase3);

for m= 0:1:(row3-2)
    tphase3(m+2,1)=tphase3(m+1,1)+.1;
end %for

[row4,col4]=size(Eenergy);

for n= 0:1:(row4-2)
    tenergy(n+2,1)=tenergy(n+1,1)+10;
end %for

%%%%%%%%%%%%%%%%%%%%%%%%%%%%%%%%%%%%%%%%%%%%%%%%%%%%%%%%%%%%%%%%%%%%%%%%%%%%%%%
%%%%%%%%%%%%%%%%%PHASE 3 PLOTTING%%%%%%%%%%%%%%%%%%%%%%%%%%%%%%%%%%%%%%%%%%%%%
%%%%%%%%%%%%%%%%%%%%%%%%%%%%%%%%%%%%%%%%%%%%%%%%%%%%%%%%%%%%%%%%%%%%%%%%%%%%%%%
figure(7), plot(tphase3,Tphase3),grid on,
title('Temperature vs Time: Phase 3'), xlabel('Time (seconds)'),
ylabel('Temperature (deg C)')
figure(8), plot(tenergy,Eenergy/10),grid on,
title('Power Generation vs Time: Phase 3'), xlabel('Time (seconds)'),
ylabel('Power (Watts)')


%%%%%%%%%%%%%%%%%%%%%%%%%%%%%%%%%%%%%%%%%%%%%%%%%%%%%%%%%%%%%%%%%%%%%%%%%%%%%%%
%%%%%%%%%%%%%%%%%POST RUN ANALYSIS%%%%%%%%%%%%%%%%%%%%%%%%%%%%%%%%%%%%%%%%%%%%
```

```
%%%%%%%%%%%%%%%%%%%%%%%%%%%%%%%%%%%%%%%%%%%%%%%%%%%%%%%%%%%%%%%%%%%%%%%%%%%%%%%

currenttotal = [cphase1;ctrans;cphase2];
ttotallen =[tphase1;ttrans;tphase2];
[row5,col5]=size(ttotallen);

for p= 0:1:(row5-2)
    ttotal(p+2,1)=ttotal(p+1,1)+.1;
end %for

power = currenttotal.*currenttotal.*Rte;


%%%%%%%%%%%%%%%%%%%%%%%%%%%%%%%%%%%%%%%%%%%%%%%%%%%%%%%%%%%%%%%%%%%%%%%%%%%%%%%
%%%%%%%%%%%%%%%%%%POST RUN PLOTTING%%%%%%%%%%%%%%%%%%%%%%%%%%%%%%%%%%%%%%%%%%%
%%%%%%%%%%%%%%%%%%%%%%%%%%%%%%%%%%%%%%%%%%%%%%%%%%%%%%%%%%%%%%%%%%%%%%%%%%%%%%%

figure(9), plot(ttotal,power),grid on,
title('Power Consumption vs Time: Total'), xlabel('Time (seconds)'),
ylabel('Power (Watts)')
```